“CFD ANALYSIS OF MICROCHANNEL HEAT SINK WITH PILLARS”

A DISSERTATION

SUBMITTED IN PARTIAL FULFILLMENT OF THE REQUIREMENTS FOR THE AWARD OF THE DEGREE OF

MASTER OF TECHNOLOGY

IN

[THERMAL ENGINEERING]

Submitted by:

[MAYANK KUMAR GUPTA]

(2K16/THE/13)

Under the supervision of

[Dr. M. ZUNAID]

ASSISTANT PROFESSOR

DEPARTMENT OF MECHANICAL ENGINEERING

DELHI TECHNOLOGICAL UNIVERSITY

(Formerly Delhi College of Engineering)

Bawana Road, Delhi-110042

JULY, 2018

DECLARATION

I, (MAYANK KUMAR GUPTA), Roll No. 2K16/THE/13 student of M.Tech (Thermal Engineering), hereby declare that the project Dissertation titled "CFD ANALYSIS OF MICROCHANNEL HEAT SINK WITH PILLARS" which is submitted by me to the Department of Mechanical Engineering, Delhi Technological University, Delhi in partial fulfillment of the requirement for the award of the degree of Master of Technology, is original and not copied from any source without proper citation. This work has not previously formed the basis for the award of any Degree, Diploma, Associateship, Fellowship or other similar title or recognition.

Place: Delhi **(MAYANK KUMAR GUPTA)**

Date:

CERTIFICATE

I hereby certify that the project Dissertation titled "CFD ANALYSIS OF MICROCHANNEL HEAT SINK WITH PILLARS" which is submitted by MAYANK KUMAR GUPTA, Roll No. 2K16/THE/13, Department of Mechanical Engineering, Delhi Technological University, Delhi in partial fulfillment of the requirement for the award of degree of Master of Technology, is a record of the project work carried out by the student under my supervision. To the best of my knowledge this work has not been submitted in part or full for any Degree or Diploma to this University or elsewhere.

Place: Delhi

Date:

(Dr. M. ZUNAID)

SUPERVISOR

ASSISTANT PROFESSOR

DEPARTMENT OF MECHANICAL ENGINEERING

DTU, DELHI

ACKNOWLEDGEMENT

First of all, I would like to express my gratitude to God for giving me ideas and strengths to make my dreams true and accomplish this thesis. To achieve success in any work, guidance plays an important role. It makes us put right amount of energy in the right direction and at right time to obtain the desired result. Express my sincere gratitude to my guide, **Dr. M. ZUNAID**, Assistant Professor, Mechanical Engineering Department for giving valuable guidance during the course of this work, for his ever encouraging and timely moral support.

I am greatly thankful to **Dr. VIPIN**, Professor and Head, Mechanical Engineering Department, Delhi Technological University, for his encouragement and inspiration for execution of the this work. I express my feelings of thanks to the entire faculty and staff, Department of Mechanical Engineering, Delhi Technological University, and Delhi for their help, inspiration and moral support, which went a long way in the successful completion of my report work.

MAYANK KUMAR GUPTA

(Roll No-2K16/THE/13)

ABSTRACT

In the present study fluid flow, heat transfer characteristics and pressure drop channel heat sinks have been analyzed using computational fluid dynamics. One of them is a single phase straight rectangular micro-channel heat sink on which validation is done. Water is taken as the working fluid for the simulation. The material for heat sink is copper. The micro-channels have a width of 0.226mm and height of 0.71mm. The validation for the straight rectangular microchannel heat sink will be done for five values of Reynolds number 390, 590, 790, 990, and 1190. The input flux to the sink will be taken as 100 W/cm^2 and 200 W/cm^2 during the simulation .The simulations is done on CFX after modelling in the SOLID WORKS. The work will be extended to include the heat augmented surfaces pillar like structures of cylindrical cross section of length 0.60mm and diameter 0.02602 mm along the flow direction to enhance the thermal performance of heat sink for a given length. Five values of Reynolds number will be used i.e.390, 590, 790, 990, 1190.Four heat flux values are used i.e.100 W/cm^2, 125 W/cm^2, 200 W/cm^2 and 225 W/cm^2. The modelling will be done in solid works and its analysis will be done using ANSYS CFX using the same set of five Reynolds number. It was found after the analysis that for constant properties of fluid, there was a linear relationship between Reynolds number and pressure drop. For constant heat flux to the base of the heat sink and inlet temperature of water, the outlet temperature is decreasing with increase in Reynolds number which in turn increases the water viscosity and hence the pressure losses along the flow. Hence pressure losses were more pronounced at higher Reynolds number. The outlet temperature at the channel with pillars was found to be more than that of channel without pillars for

same inlet temperature of water and power input. The pressure losses were on a higher side due to the presence of the obstruction in the form of pillars.

CONTENTS

LIST OF FIGURES

LIST OF TABLES

NOMENCLATURE

A	Area of cross section of channel (mm^2)
a	Width of channel (mm)
b	Thickness of channel (mm)
D	Hydraulic Diameter (mm)
H	Thickness of micro-channel heat sink (µm)
H_{s1}	Substrate thickness on insulated side of micro-channel heat sink (µm)
H_{s2}	Substrate thickness on heated side of micro-channel heat sink (µm)
L	Length of micro-channel heat sink (mm)
q	Heat flux (W/cm^2)
Re	Reynolds number based on channel hydraulic diameter
R_{th}	Thermal resistance (W/K)
T	Temperature (K)
W	Width of micro-channel heat sink unit cell (µm)
W_{w1}, W_{w2}	Half-thickness of wall separating micro-channels (µm)
V	Velocity of flow (m/s)
C	Specific heat of fluid at constant pressure (J/kg-K)
Q	Volumetric flow rate (m^3/s)
p	Static pressure (bar)
Δp	Pressure drop (bar)
T	Temperature (K)
ΔT	Temperature rise (K)
h	Heat transfer coefficient (W/m^2-K)
k	Thermal conductivity (W/m-K)

Greek symbols

µ	Dynamic viscosity (Pa-s)
ρ	Density (kg/m^3)

Subscripts

i	Inlet
o	Outlet
c	Channel
s	Substrate
f	Fluid
w	Wall
th	Thermal
max	Maximum
avg	Average

CHAPTER 1

INTRODUCTION

1.1 Microchannel Heat Sink

The challenge of heat removal has been a challenge for most of the engineering applications irrespective the kind of application whether it is electronics, microelectronics, thermal plants etc. whether the application is micro or macro the heat removal was always challenging for the engineers as the heat removal comes with a cost i.e. increasing the surface area thereby increasing the space. One such technique of increasing heat dissipation rate from microelectronics is the provision of microchannels heat sink. The microchannel heat sink can be single phase or two phases depending upon the amount of heat to be dissipated.

The microchannels were introduced in early 1980s which were able to enhance heat transfer than conventional channels as they had good surface area to volume ratio and high heat transfer coefficient. Microchannels could easily handle heat flux of about 100 W/cm^2. The microchannels generally have hydraulic diameter below 1mm. The heat sink is usually made of materials which have high thermal conductivity viz copper. The miniaturisation of electronic gadgets is the trend of the day and more miniaturisation has led to the overheating of devices due to accumulation of high heat fluxes in a small space which demands of a device to remove high heat fluxes within a confined space without compromising the thermal performance. The cross section of the heat sink serves as a passage for the liquid so that heat transfer can occur between the source of heat flux and fluid. The study of microchannel is gaining importance due to the necessity of dissipating large amount of heat with space as a great constraint.

However dissipation of increased heat load has been a problem for simple microchannel heat sink due to high pressure penalty and temperature gradient along the flow. Various studies have been done on graded microchannel heat sinks to overcome the difficulties encountered in simple microchannel heat sink. For example, heat sink with pillars of various shapes , heat sink involving flow boiling(two phase) heat sink with pillars with jet impingement etc. are some of the graded microchannel heat sink that are the hot topics in the study of microchannels.

1.2 Requirement of Microchannels

The microchannel heat sink are gaining importance due to two main reasons

1. Enhancement in heat transfer rate.
2. High heat flux removal required for microelectronics.

Increase in heat generation rates from micro electronic systems demand smart cooling techniques. The development of such thermal systems has been a challenge to micro fluidic industries and academicians. Microchannel coolers have number of coolant channels through which fluid is passed. Depending upon the thermo physical properties of fluid and amount of heat to be dissipated , the appropriate fluid with suitable dimension of heat sink is selected. Many studies had been done on microchannel coolers with different dimensions and with different coolants with varying thermo physical properties. The studies had demonstrated the pros of single phase microchannel heat sink like handling of large heat load with small surface area, large heat transfer coefficient and minimum cooling inventory. The only purpose of these studies were to optimise the geometry of the heat sink.

1.3 Coolants and Material of Heat Sink

There are many options for the selection of coolants depending upon the kind of heat load. The coolant with better thermo physical properties can be selected for maximum overall thermal performance. The commonly used coolant is water which is readily available. The nano fluids performance cannot go undiscussed. The thermal performance is enhanced if the nano

fluids are used in conjunction with graded microchannels. As far as material of heat sink is concerned, copper is widely used due to its good thermal conductivity. Besides copper, there are many other options like aluminium, silver etc.

1.4 Solid Works

Solid works is parametric and modeller software made by Dassault systems of France. It is one of the commonly used software across wide spectrum of industries from needle making to aerospace for the modelling purpose. It deals with complex assemblies by being parametric to deal with subassemblies, parts and models. Parameters can be either numeric or geometric.

1.5 ANSYS CFX

It is a high end performing software when it comes to solving complex fluid problems and heat transfer. It is being widely used in many industries for last two decades. Applications mainly include:

(i) Heat transfer problems

(ii) Fluid flow problems

(iii) Problems involving both heat transfer and fluid flow.

(iv) Problems involving heat transfer between solid and fluid.

The CFX solver uses finite elements to discretize the domain under consideration similar in nature to that of mechanical analysis. The advantage of using CFX package is seen in conjugate heat transfer problems where it readily creates a default interface between a solid and fluid. This automatic creation of interface is not there in other modules of ANSYS where the user has to manually create the boundary between solid and fluid.

1.6 CFD

CFD is a strong tool based on physics and mathematical formulations in the form of in built coding. It is mainly used to visualise gas and liquid flows. The CFD is governed by Navier-Stokes equations. We can visualise the fields of

velocity, temperature, pressure and density of fluid in motion through these equations. It has found great use in for the analysis of thermal properties and modelling of air flow around any obstruction. One can analyse the interaction of fluid with the obstruction through the CFD. Recent researches are going on to improve the accuracy of the tool when it comes to analyse the turbulent or transonic flows.

1.7 Conjugate Heat Transfer

The process which involves the variations in temperature in solids and fluids comes under the ambit of conjugate heat transfer. The term usually defines the thermal interaction between solid and fluid. Microchannel heat sink is the best example of conjugate heat transfer.

The overall criteria in judging the effectiveness of conjugate heat transfer is convective heat transfer. Forced convection helps to achieve high heat transfer rate. Conjugate heat transfer plays a crucial role in the designing of heat transfers, heat dissipating units, coolers etc. In some cases the overall thermal performance is improved by providing the heat transfer augmenting surfaces like pillars, fins etc combined with phase change.

1.8 Applications

(i) Aerospace

(ii) Gas turbine blades

(iii) Microelectronic mechanical systems (MEMS)

(iv) Process and power industries

(v) Bioengineering

(vi) Superconductors

CHAPTER 2

LITERATURE REVIEW

Peng and Peterson (1996) investigated the heat transfer in forced convective mode in micro-channel structures having small rectangular channels. The rectangular channels had hydraulic diameters from 0.133–0.367 mm. The results showed heat transfer and flow characteristics. The laminar heat transfer was dependent upon the aspect ratio which is the ratio of hydraulic diameter of the channel to the centre to centre distance of micro-channels.

Kambiz Vafai (1999) introduced new concept of double layered microchannel heat sink which had a counter flow arrangement for the cooling purpose of electronic components. The thermal aspects of this arrangement were studied and temperature distribution were analysed. Geometry optimisation parameters were also introduced. Through his study it was found out that pressure drop for double layered microchannel was significantly lower than single layered which was a substantial improvement.

Fedorov and Viskanta (2000) worked on a 3-D model to investigate the conjugate heat transfer in microchannel heat sinks. The study went on to show that the average wall temperature in the flow direction was uniform except at the channel inlet, where large temperature gradients were observed.

Liu and Garimella (2004) have studied numerically on fluid flow and heat transfer in micro channels and confirmed that the behaviour of micro channels is quite similar to that of conventional channels. And their analysis showed that conventional correlations offer reliable predictions for the laminar flow characteristics in rectangular micro channels over a hydraulic diameter in the range of 244–974 μm.

Roy et al. (2004) has studied a steady, laminar flow and heat transfer of a nanofluid flowing inside a radial channel between two coaxial and parallel discs. The non-dimensional governing equations of mass, momentum and energy were solved by computational fluid dynamics method. Results have shown that the inclusion of

nanoparticles in a traditional coolant can provide considerable improvement in heat transfer rates, even at small particle volume fractions. Increases in the resulting wall shear stresses were also noticed

W.A. Khan (2005) introduced optimisation of thermodynamic losses in pin fins using entropy generation minimisation technique. This technique allowed to study temperature drop and pressure losses. This technique allowed to study the combined effect of thermal resistance and pressure drop through simultaneous interaction with heat sink. An equation for entropy generation rate was obtained by taking heat sink as control volume and applying the conservation equations for mass and energy with the entropy balance. Pin fin diameter was taken as the characteristic length and reference velocity used in Reynolds number and pressure drop is based on the minimum free area available for the fluid flow. Inline and staggered arrangements of pin fins were studied.

D. Liu (2005) provided the modelling approaches with increasing complexities of convective heat transfer in microchannels giving an idea on the thermal performance of microchannels. His work allowed for easier manipulations of the geometries of microchannel heat sinks for design optimisations. The models were in complete agreement with the practical models.

Jun Yao (2006) Numerical simulation has been conducted for the investigation of heat transfer in a rectangular, high–aspect ratio microchannel with heat sinks, similar to an experimental study. Water at ambient temperature is used as working fluid and the heating power of 180 W is introduced via electronic cartridges in the solids. Three channel heights of 0.3 mm, 0.6 mm and 1 mm are considered and the Reynolds number is in the range of 300 to 2360, based on the hydraulic diameter. The study is mainly focused on the Reynolds number and channel height effects on microchannel thermal performance. Validation study shows that Nusselt number variations agree with the theory and other predictions very well, but the numerical predicted Poiseuille number has shown some deficits compared to the theory, same as observed by other researchers. It is found that the scaling effect only appears at small channel height of 0.3 mm, for both the friction factors and the thermal resistance. The thermal resistance tends to become smaller at small channel height, indicating that the heat transfer performance can be enhanced at small channel height.

Allen (2007) had investigated fluid flow and heat transfer in microchannels experimentally and numerically. Fluid flow and heat transfer experiments were conducted on a copper micro channel heat exchanger with constant surface temperature. The experimentally obtained friction factor were found fairly well agreement with theoretical correlations and moreover the experimental Nusselt number results agreed with theory very well in the transition and turbulent regime, but the results show a higher Nusselt number in the laminar regime than predicted by theoretical correlations. Philips created a CFD model to simulate the fluid in the inlet plenum and the micro-channels. The results from these simulations showed good agreement with the experimental data in the transition/turbulent regime as well as with theoretical correlations for laminar and turbulent flow.

Chein and Chuang (2007) studied the performance microchannel heat sinks using nanofluids as the coolants. Lower wall temperature was obtained by taking the assumption that nanoparticles increases heat transfer. It was clear from the study that the microchannel heat sink with nanofluids can absorb more heat than water based microchannel heat sink.

Sabbah et al. (2008) observed that the prediction of heat transfer in micro-channels becomes difficult with increase in complicacy of the geometry of the micro-channels, requiring three dimensional analysis of heat transfer in both solid and liquid phases. Computational Fluid Dynamics (CFD) models were implemented in order to study and optimize the thermal and hydraulic performance of micro channel heat sinks. Despite the small width of the channels, the conventional Navier Stokes and energy conservation equations still apply to the flow due to the continuum of the working fluid where the channel width is many times larger than the mean free path of liquid molecules (water). The micro-channel is characterized by the laminar flow in it, due to the small hydraulic diameter of the channel which results in low Reynolds numbers.

Myung Ki Sung (2008) introduced a hybrid cooling scheme for the management of high flux electronic devices. The scheme benefits from both micro jet-impingement and flow in microchannel. Cooling performance was assessed using HFE 7100 as working fluid. Good results were obtained using k–ε model. It was shown to have complex interaction of jets with microchannel flow to obtain the desired cooling

effect. An increase in jet velocities proved to be an effective way of deeper penetration into the microchannel thereby reducing wall temperature greatly. Even though the thermo physical properties of the selected fluid were poor, the scheme facilitated the dissipation of 304.9 W/cm$^{2.}$

Pradeep Dixit (2008) devised a novel scheme of silicon micro pillars based on multilayered water cooled heat sink to enhance the thermal performance of micro electronics. Heat dissipation rate was significantly improved by selecting smaller diameter (0.5–2 μm) and larger height (~100 μm) of the micro pillars. Due to the selected geometry of the micro pillars convective heat transfer was enhanced hence improving the overall thermal performance. Thermal performance was compared between simple model without pillars and with silicon pillars. The analytical results showed that heat dissipation characteristics of silicon pillars were better than the model without pillars by an average of about 16%.

A. Armellini (2009) performed a study on separated flow structures around a cylindrical obstacle. The cylindrical obstacles were of low aspect ratio. The cylinders were confined at both ends with water as the working fluid. The flow was tested for Reynolds number (*Re* = 800, 1800, 2800). The distinctive features of the flow were very high core turbulence and undeveloped boundary layers around the obstacle.

M.Meis (2010) described the effects of heat transfer and pressure losses by vortex promoters in a 2-D laminar flow in a microchannel. The working fluid was taken as water with temperature dependant viscosity and thermal conductivity. Three cross sections were mainly studied at different aspect ratios which were circular, rectangular, and triangular. . The effect of, the Reynolds number, and the relative position and orientation of the obstacle were also taken into account.

Rebrov et al. (2011) has reviewed the experimental and numerical results on fluid flow distribution, heat transfer and combination thereof, available in the open literature. They have found that the experiments with single channels are in good agreement with predictions using the published correlations. The review consists of two parts. In the first, the main methods to control flow distribution were reviewed. Several different designs of inlet/outlet chambers were presented together with corresponding models used for optimization of flow distribution.

M. Yakut Ali (2011) demonstrated the use of nano copper wires in microchannel heat sink to study the thermal characteristics of heat sink. The diameter of nano wires was 200 nm and 50 μm in length. The hydraulic diameter of the channel was taken to be 672 μm. The pressure drop and heat transfer characteristics of copper nano wires enhanced heat sink was studied and compared with bare copper heat sink. The Data were collated for Reynolds number ranging from 106-636 with deionised water as the working fluid. The best results were obtained at Reynolds number of 106 with maximum enhancement of nusselt number of about 24%. The increase in performance was due to increase in net surface area and wet ability characteristics due to the presence of carbon nano wires.

P. Mohajeri Khameneh (2011) demonstrated the three-dimensional simulations of the single-phase laminar flow and forced convective heat transfer of water in microchannels with small rectangular sections having specific hydraulic diameters and distinct geometric configurations numerically. The numerical results indicated that the laminar heat transfer was to be dependent upon the aspect ratio and the ratio of the hydraulic diameter to the centre to centre distance of the microchannels. The geometries and operating conditions of that indicated microchannel were created using a finite volume-based computational fluid dynamics technique. The aim of this paper is to obtain computational Nusselt number in laminar flow using Fluent CFD Solver and to validate it with available experimental studies. Acquired numerical results have an admissible compatibility with available experimental studies. Then, pressure drop values in the present model were explored for each Reynolds number. Finally, the effects of geometric parameters on the average Nusselt number in the laminar flow were illustrated numerically.

Junkyu Jung (2012) studied the flow over low aspect ratio pillars confined in a microchannel. The aspect ratio of the circular pillar was taken to be (L/D = 1.5).The characteristic dimension was taken to be the diameter of the pillar with Reynolds number ranging from 100 -700. Various regimes of flow were studied like steady flow, transition from steady to unsteady flow and unsteady flow. Subsequently the flow was controlled using a jet employed in the downstream direction. This was done to induce the disturbances in the flow to promote turbulence in the flow and better mixing. Together with passive flow control (i.e., a circular pillar), turbulent kinetic energy was significantly increased in a controllable manner throughout the flow field.

Yingying Wang (2013) performed an experimental study to assess the thermal performance of pillars with air as a working fluid. Area averaged temperature was measured by a resistance temperature detector. The values were collated with the Reynolds number ranging from 100-5600.The microchannel with pillar had heat transfer coefficient twice to that of a microchannel without pillars. Among the shapes studied, Triangular pillar performed the best in the range of $17.7 \leqslant (Nu) \leqslant 88.9$.Turbulent kinetic energy provided criteria of how well the flow is mixed. Turbulent Kinetic energy is directly linked to thermal performance.

Jamil A.Khan (2014) devised a two phase microchannel heat sink to meet the ultra heat flux applications especially in defence electronics by implementing active structures (jet in microchannel) and passive structures(nanostructures).This is achieved by taking advantage of high surface area to volume ratio and high latent heat of vaporization. Flow boiling seems to be a very promising concept in high heat dissipation rate but it comes with instability in boiling and pressure fluctuations. Active structures helped in enhancing heat transfer by introducing turbulence in the flow field and changing the bubble dynamics whereas passive structures did the same by altering the surface properties to suit the boiling performance. Passive control techniques are useful to remove large amount of heat from limited space.

Daxiang Deng (2015) developed an unique re-entrant microchannel heat sink consisting of 14 parallel copper microchannels having hydraulic diameter of 781 μm. The flow regime was single phase convective heat transfer and the performances were assessed both experimentally and numerically. De-ionised water was used as the coolant with Reynolds number ranging from 150-1100 with three different values of heat flux and two inlet temperatures of 33 and 60 °C. It was shown that the average thermal resistance got reduced by 22% as compared to simple rectangular microchannel. Also they had comparable pressure losses. The enhancement in heat transfer was due to the acceleration of the fluid and mixing of fluid flow.

Afzal Husain (2016) proposed a novel idea by combining the heat sink based microchannel with jet impingement. A 3-D model was designed to study the thermal performance. The study was done for steady state, incompressible with laminar conditions. On one side of the substrate heat flux was imposed and micro-channels, -pillars and -jet impingements were arranged on the other side of the substrate. The

new design was compared with the conventional models with respect to ratios of standoff (distance of nozzle exit to impingement surface) to jet diameter and jet pitch to jet diameter. The thermal performance was judged by pressure drop, heat transfer coefficient and overall thermal resistance. It was observed that high jet pitch to jet diameter ratios offered low pressure-drops. High heat transfer coefficients were observed with jet impingement model combined with lower thermal resistance.

Nor Haziq Naqiuddin (2017) did the intensive research on microchannel heat sinks as maintaining the optimum temperature in microelectronics mechanical system is important for reliability and safety. It is known to many researchers that increasing the total heat transfer area to volume ratio could enhance overall heat transfer performance. He observed the drawbacks in straight channel design as the flow gets deteriorated along the flow direction. This will result in uneven cooling performance of the device which is detrimental to overall thermal performance. To counter this shortcomings a geometrically graded microchannel heat sink is introduced to improve the thermal performance of the conventional straight channel heat sink. The thermal performance was compared between fin microchannel and straight channel heat sink. The geometrically graded micro-channel heat sink could reduce the average temperature to 69.6 °C under a load of 2000W.

CHAPTER 3

MATHEMATICAL FORMULATION

The steady state continuity and energy equations with associated boundary conditions were solved using finite-volume approach under the following assumptions:

(i) Laminar steady state conditions

(ii) Incompressible fluid flow

(iii) Constant fluid properties along the length

(iv) Negligible effects due to viscous dissipation

(v) Negligible radiative effects.

Since the cross-section of the microchannel was rectangular so the hydraulic diameter was calculated by the formula given below

$$\mathrm{D} = \frac{4a\mathrm{b}}{a+\mathrm{b}} \tag{3.1}$$

Where 'a' and 'b' are the width and thickness of the microchannel respectively.

The governing equations for the conservation of momentum, mass, energy for the conjugate heat transfer and fluid flow which are solved to assess the overall thermal performance are written below:

$$\nabla.\left(\rho_f V\right) = 0 \tag{3.2}$$

$$V.\nabla\left(\rho_f V\right) = -\nabla p + \nabla.\left(\mu_f \nabla V\right) \tag{3.3}$$

$$V.\nabla\left(\rho_f C_f T_f\right) = \nabla.\left(k_f \nabla T_f\right) \tag{3.4}$$

$$\nabla.\left(k_s \nabla T_s\right) = 0 \tag{3.5}$$

The numerical simulation was carried out using CFD solver in ANSYS. The thermo physical properties of the water are assumed to be independent of temperature. The solver settings were initiated with constant properties of water and the solution was

updated till the solution was converged. For the simulation all the lateral walls of the heat sink except bottom surface were taken to be adiabatic. A uniform heat flux was applied at the bottom surface of the heat sink. A no slip was condition was imposed on the surface of the pillars. The outlet of the channel was given a mass flow rate which was calculated numerically depending on the Reynolds number and hydraulic diameter. Relative pressure of zero magnitude was applied at the inlet of the channel.

The Reynolds number based on the hydraulic diameter of the microchannel is given by

$$Re = \frac{\rho_f V D}{\mu} \tag{3.6}$$

The overall thermal resistance is given by:

$$R_{th} = \frac{\Delta T_{max}}{qL} \tag{3.7}$$

Here, L is the length of the heat sink. The temperature rise in the heat sink is given by

$$\Delta T = T_{f,o} - T_{f,i} \tag{3.8}$$

The power of pumping needed to drive the fluid along the heat sink is given as:

$$P = Q_c \times \Delta p_c \tag{3.9}$$

The static pressure drop of the fluid along the channel is given by:

$$\Delta p_{c=} p_{i,c} - p_{o,c} \tag{3.10}$$

And the total pressure is defined as

$$\Delta p_{t=} \Delta(p_{avg} + \frac{1}{2}\rho V_{avg}^2) \tag{3.11}$$

The heat transfer coefficient is given by

$$h = \frac{q}{T_{w,avg} - T_{f,avg}} \tag{3.12}$$

The heat transfer from the heat sink to the micro channel having conjugate heat transfer is given by:

$$Q = \frac{\Delta T}{R_{th}} + hA_c\Delta T \tag{3.13}$$

The heat transfer in a heat sink with pillars was found to be more than the heat sink with pillars as the temperature difference between inlet and outlet of the channel was more in the heat sink with pillars for the same values of the heat flux and mass flow rate of the coolant.

CHAPTER 4

METHODOLOGY

4.1 Simulation of Heat Transfer and Pressure Losses In Single Phase Straight Rectangular Microchannel Heat Sink

This chapter deals with the CFD simulation of single phase straight rectangular micro channel heat sink. The main purpose of the study is to the assess the overall thermal performance of the heat sink in terms of heat transfer and pressure drop characteristics. The experimental configuration shown in figure was developed by Weilin Qu and Issam Muduwar (2002).

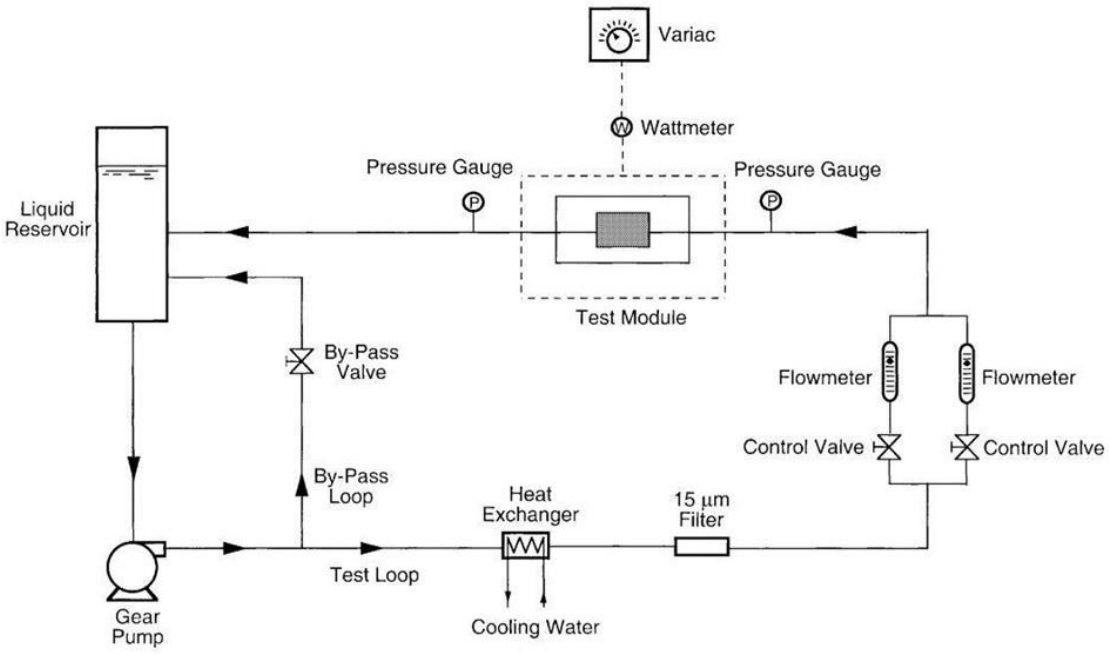

Figure 4.1: Schematic of flow loop [21]

4.2 Problem Description

4.2.1 Flow loop-

The experimental study done by Qu and Mudawar is modelled and simulated in this study. Figure is describing the flow loop designed for experimental study and the deionised water is supplied to the heat sink at desired volumetric flow rate , pressure and temperature. The water which is going to the sink is heated by an heat exchanger to the required inlet temperature. The rotameter was also installed to measure the flow rate of water. The electric power was supplied to the heat sink which was supposed to be removed by the water.

4.2.2Test module

The test module comprised of heat sink, cover plate and 12 cartridge heaters. The heat sink was made of copper. Twenty one small rectangular slots were machined into the top surface of heat sink. These slots were 231 μm wide and 712 μm deep. Below the top surface of heat sink four 0.36mm diameter holes were drilled and K-type thermocouples were installed to analyse the distribution of temperature inside the heat sink. The arrangement was such to ensure the uniform heat flux distribution. Type- K thermocouples were also installed at the inlet and the outlet of the sink housing so as to measure the inlet and outlet temperature of water.

4.3 Heat Sink Geometry

In the present study only one of the 21 microchannel is taken into account for the numerical simulation. The dimensions are given in table for a single unit cell of heat sink

Table 1: Unit cell dimensions used for simulation

W_{wall}(μm)	W_C (μm)	H_{s2}(μm)	H_c (μm)	H_{s1}(μm)	L(mm)
118	226	12700	710	5637	44.7

4.3.1 Construction of geometry

The geometry was constructed using SOLID WORKS as per the dimensions and the file was imported into the CFX module of ANSYS 15.0 for further analysis. The design of geometry consisted of two solid parts namely heat sink and channel. Both are designed as per the dimensions given in Table 1. Both the parts are designed as solid but the heat sink is designated as solid and channel as fluid. Both the parts were assembled as a single entity using mate component in solid work.

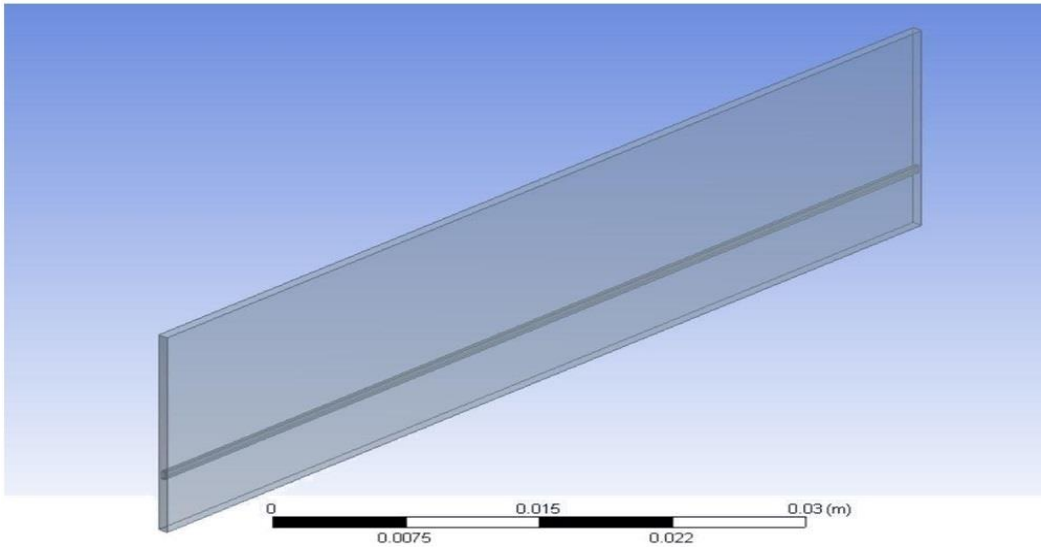

Figure 4.2: Geometry of single phase straight rectangular microchannel heat sink

4.4 Meshing

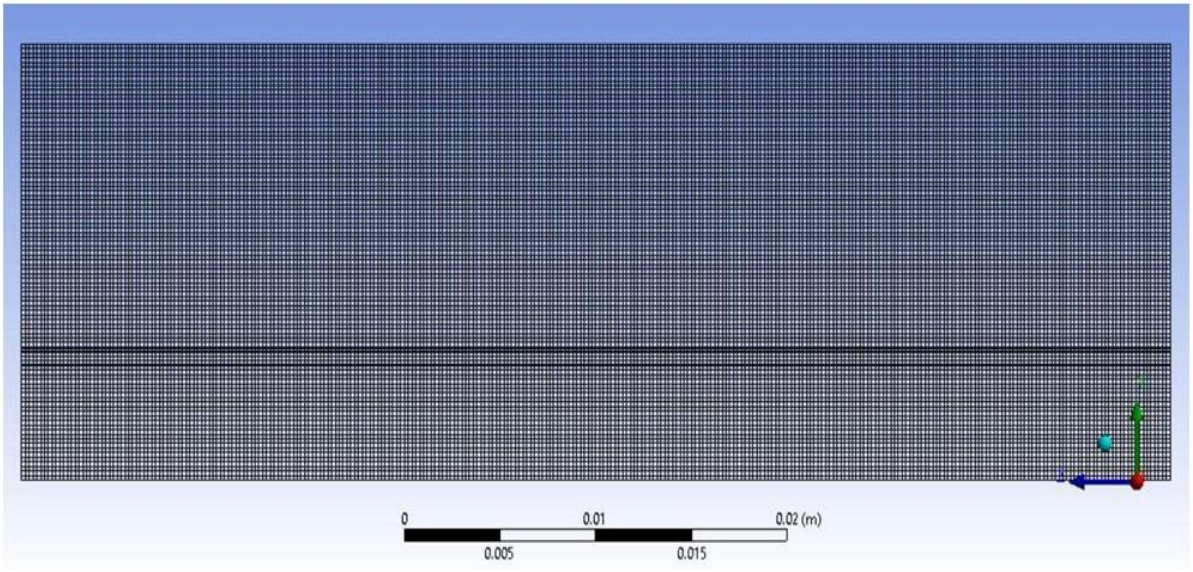

Figure 4.3 Meshing in CFX

Table 2: Details of mesh

Physics preference	CFD
Solver preference	CFX
Smoothing	Medium
Transition	Slow
Transition ratio	0.272
Minimum size	2e-5
Maximum face size	2.5e-4
Maximum size	2e-4
Nodes	118000
Elements	84000

The mesh was made for microchannel heat sink. Initially the mesh was made medium. For good accuracy of results the mesh was made finer. Meshing was followed by named selections which were treated as boundary conditions.

4.5 Set up Details

Two domains were created namely solid and fluid. The heat sink modelled in solid works was designated as solid and the channel was designated as fluid in the set up. After giving the domains, boundaries were given for both the domains

Inlet and outlet boundary conditions were created in the fluid domain. Adiabatic wall and heat flux wall were created as the boundary conditions in solid domain. Bottom surface of the heat sink was treated as heat flux wall and other surfaces as adiabatic.

4.5.1 Boundary conditions-

(i) No slip condition

(ii) Outlet of channel is based on mass flow rate rather than velocity

(iii) Inlet temperature was given as 293 K.

(iv) Relative pressure at inlet and outlet was taken as 0 bar

(v) Heat flux of 100 W/cm^2 and 200 W/cm^2 was applied on the bottom surface of heat sink.

Table 3: Zone specification

Heat sink front wall	Wall
Heat sink top wall	Wall
Heat sink back wall	Wall
Heat sink bottom wall	Heat flux
Heat sink right wall	Wall
Heat sink left wall	Wall
Channel entry	Static pressure
Channel outlet	Mass flow rate
Default Interface	Wall

Table 4: Solver settings

Min. Iterations	1
Max. Iterations	250
Residual type	RMS
Residual target	1E-4
Time scale control	Auto time scale

4.6 Simulation of Heat Transfer and Pressure Losses In Single Phase Microchannel Heat Sink With Pillars

In this chapter 3-D simulation is done for single phase microchannel heat sink with pillars. The pillars act as heat transfer augmenting surfaces. It is analysed to check for the overall thermal performance in terms of heat transfer and pressure losses.

4.6.1 Problem description

Water is flowing through a single phase microchannel heat sink with pillars. For this pillars were installed in the microchannel along the flow. The dimensions of the heat sink and channel are same as that of the model used in the simulation in the chapter 4.The only difference is that the pillars are installed along the length of microchannel.

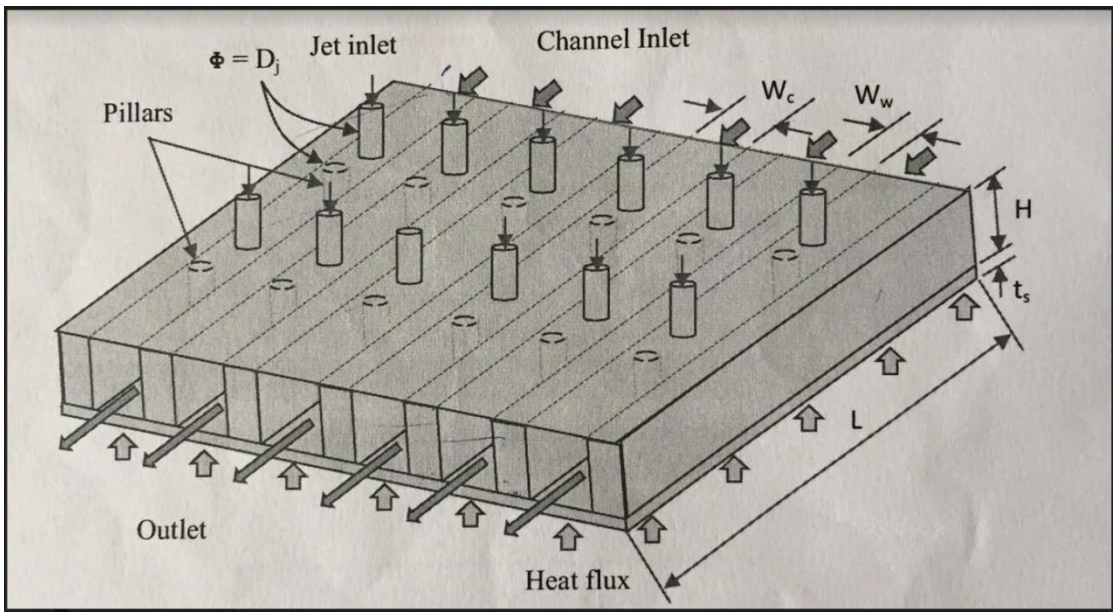

Figure 4.4: Schematic of micro-channel heat sink with pillars [14]

Table- 5: Unit cell dimensions

W_w(µm)	W_c(µm)	H_{wall2}(µm)	H_c(µm)	H_{wall1}(µm)	L(mm)
118	226	12700	710	5637	44.7

The heat transfer characteristics and pressure losses are studied for the microchannel heat sink with pillars.

4.7 Construction of Geometry

The geometry was constructed using SOLID WORKS as per the dimensions and the file was imported into the CFX module of ANSYS 15.0 for further analysis.

The heat sink was modelled as per the dimensions given in table 5. The number of pillars to be installed was given according to the length of the channel which is 44.7 mm.

A total of 19 pillars were installed along the channel length with diameter of 0.02602 mm and length of 0.60mm. The pillars were arranged in zigzag pattern. To achieve the design two linear patterns were created. First linear pattern consists of 10 instances with spacing 4.80 mm and the second linear pattern consists of 9 instances with spacing of 4.80 mm. The pillars were created on a base with the same width and length except the thickness. The heat sink was modelled as a different solid part. The base with pillars and heat sink was assembled in solid works using mate component.

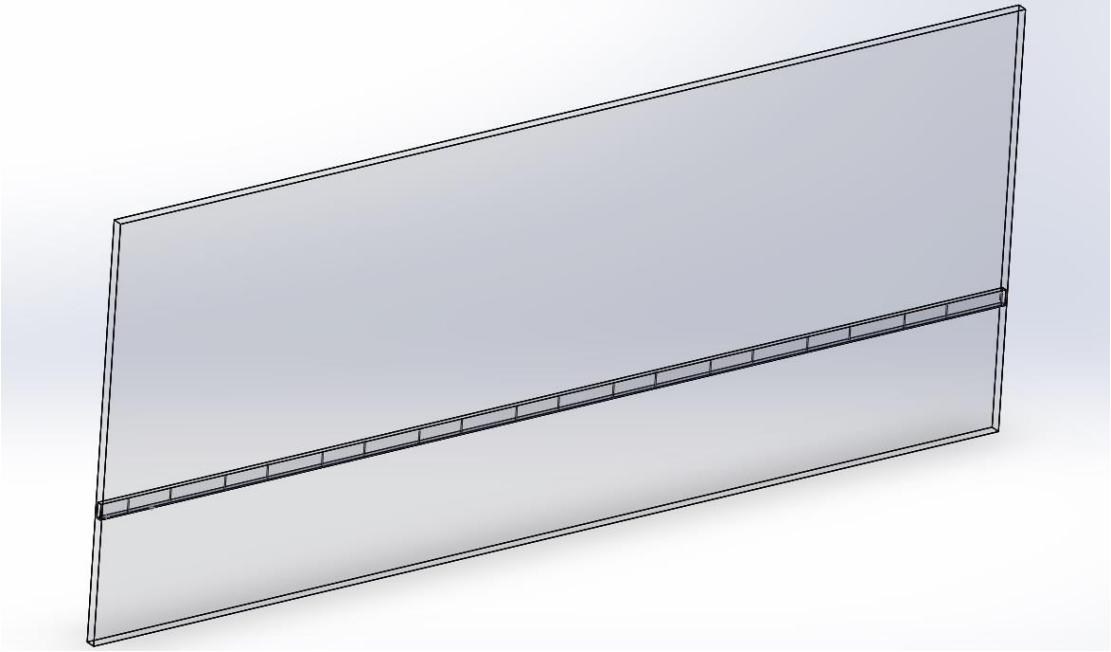

Figure 4.5: Geometry of micro-channel heat sink with pillars

4.8 Meshing

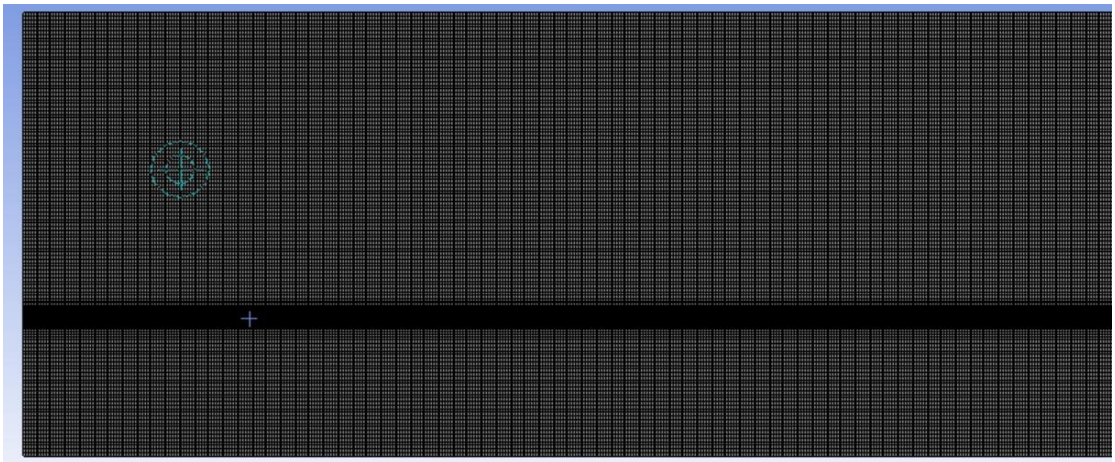

Figure 4.6: Meshing in ANSYS CFX

Table 6: Details of mesh

Physics preference	CFD
Solver preference	CFX
Smoothing	Medium
Transition	Slow
Transition ratio	0.272
Minimum size	2e-5
Maximum face size	2.5e-4
Maximum size	2e-4
Nodes	655839
Elements	1871432

The mesh was made for microchannel heat sink with pillars. Initially the mesh was made medium. For good accuracy of results the mesh was made finer. Meshing was followed by named selections which were treated as boundary conditions.

4.9 Set up Details

Two domains were created namely solid and fin boundary and fluid. The heat sink was designated as solid domain. The surface of the fin was designated as fin

boundary. To define the fluid domain subtract (Boolean operation) command was used in the CFX as there were obstructions in the form of pillars along the channel. To create the fluid domain an outer solid part was created in the solid works around the base containing the pillars. The base with pillars was subtracted from the solid part to create the fluid path. The pillars as well as the heat sink were assigned the copper material.

After defining the domains, the boundary conditions were defined. Inlet and outlet boundary conditions were created in the fluid domain. Adiabatic wall and heat flux wall were created as the boundary conditions in solid domain. Bottom surface of the heat sink was treated as heat flux wall and other surfaces as adiabatic.

4.9.1 Boundary conditions

(i) No slip condition

(ii) Outlet of channel is based on mass flow rate rather than velocity

(iii) Inlet temperature was given as 293 K.

(iv) Relative pressure at inlet and outlet was taken as 0 bar

(v) Heat flux of 100 W/cm^2, 125 W/cm^2, 200 W/cm^2 and 225 W/cm^2 was applied on the bottom surface of heat sink.

Table 7: Zone specification

Heat sink front wall	Wall
Heat sink top wall	Wall
Heat sink back wall	Wall
Heat sink bottom wall	Heat flux
Heat sink right wall	Wall
Heat sink left wall	Wall
Channel entry	Static pressure
Channel outlet	Mass flow rate
Default Interface	Wall

Table 8: Solver settings

Min. Iterations	1
Max. Iterations	250
Residual type	RMS
Residual target	1E-4
Time scale control	Auto time scale

CHAPTER 5

VALIDATION

5.1 Straight Rectangular Microchannel

In this validation is done using CFD as a tool for a single phase and straight rectangular microchannel heat sink. The data for pressure losses and temperature difference between inlet and outlet were collated and graphical validation is done by plotting graphs between temperature difference and pressure drop against Reynolds number. The heat flux taken for the validation was 100W/cm^2 and 200W/cm^2. The Reynolds number taken for the flow was 390, 590, 790, 990, 1190 ensuring that flow regime is laminar.

5.1.1 Results for 100 W/cm^2 at the bottom wall with different sets of Reynolds number

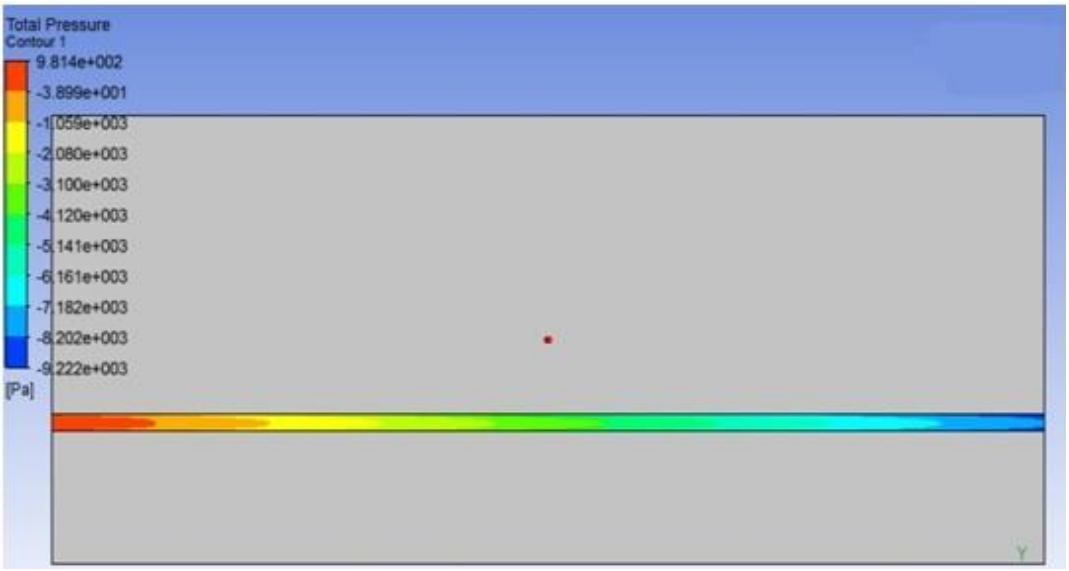

Figure 5.1: Contours of pressure at Re=390

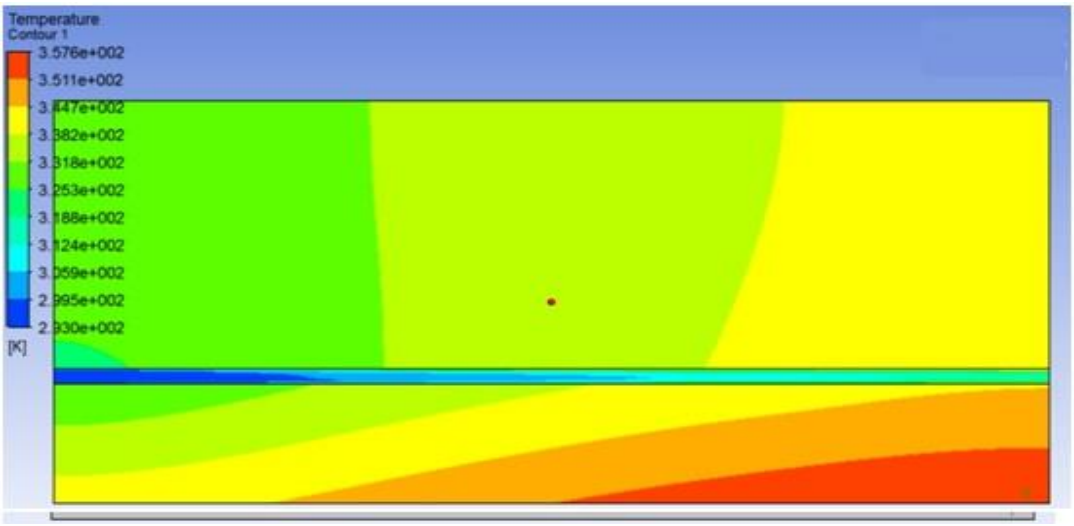

Figure 5.2: Contours of temperature at Re=390

(i) In the Figures 5.1 and 5.2 , contours of temperature and pressure are shown for a single phase microchannel heat sink at Reynolds number 390

(ii) In Figure 5.1, pressure penalty along the channel is 0.1 bars.

(iii) In Figure 5.2 , outlet temperature of channel is 318.8 K

(iv) In Figure 5.2, the maximum temperature is at the base of the wall which is 357.6 K and the wall temperature seems to be increasing along the flow direction.

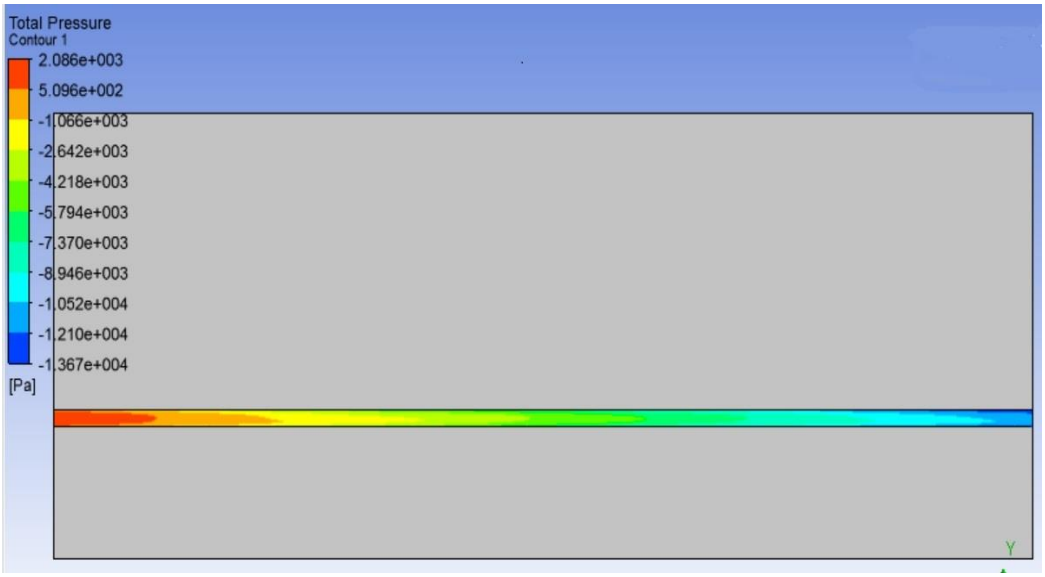

Figure 5.3: Contours of pressure at Re=590

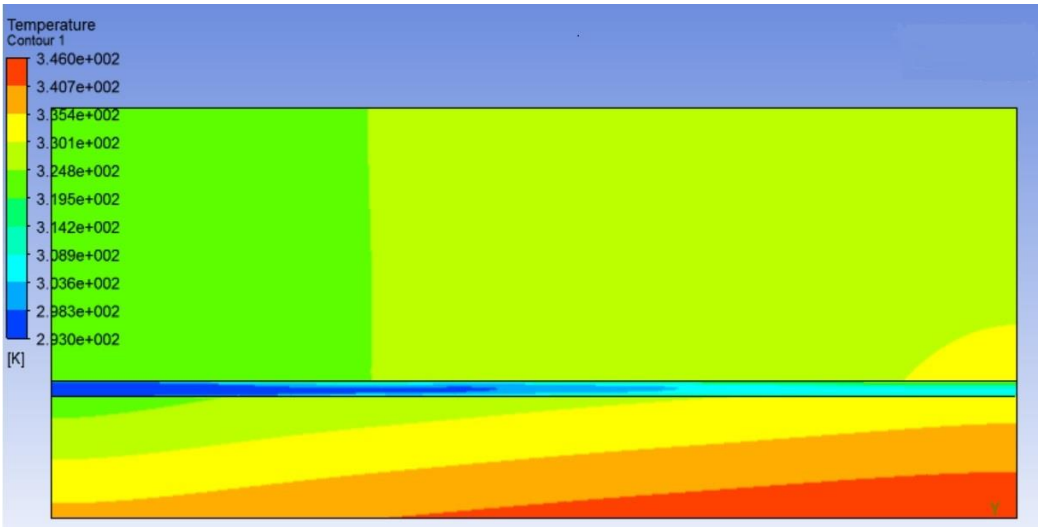

Figure 5.4: Contours of temperature of heat sink and water at Re=590

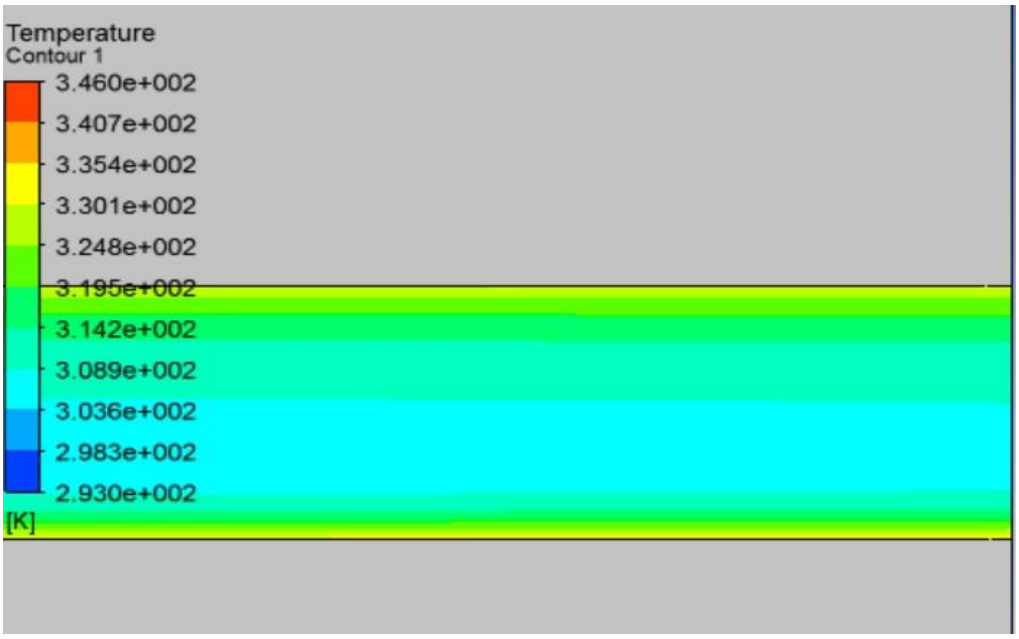

Figure 5.5: Contours of temperature at outlet at Re=590

(i) In the Figures 5.3 to 5.5, contours of temperature and pressure are shown for a single phase microchannel heat sink at Reynolds number 590

(ii) In Figure 5.3, pressure penalty along the channel is 0.16 bar.

(iii) In Figure 5.5, outlet temperature of channel is 308.9.8 K

(iv) In Figure 5.4, the maximum temperature is at the base of the wall which is 346.0 K and the wall temperature seems to be increasing along the flow direction.

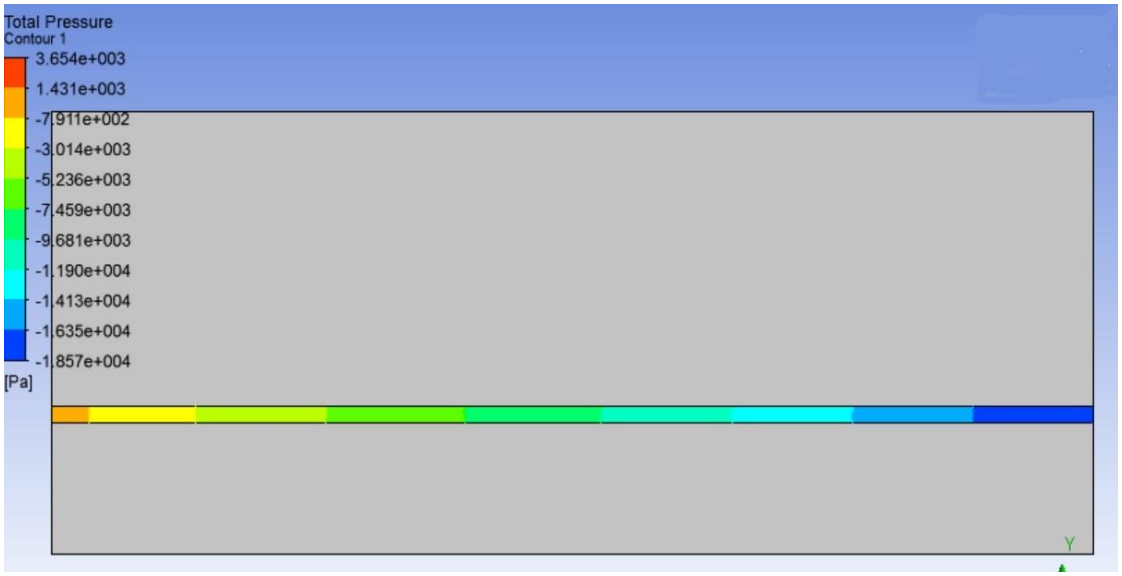

Figure 5.6: Contours of pressure at Re=790

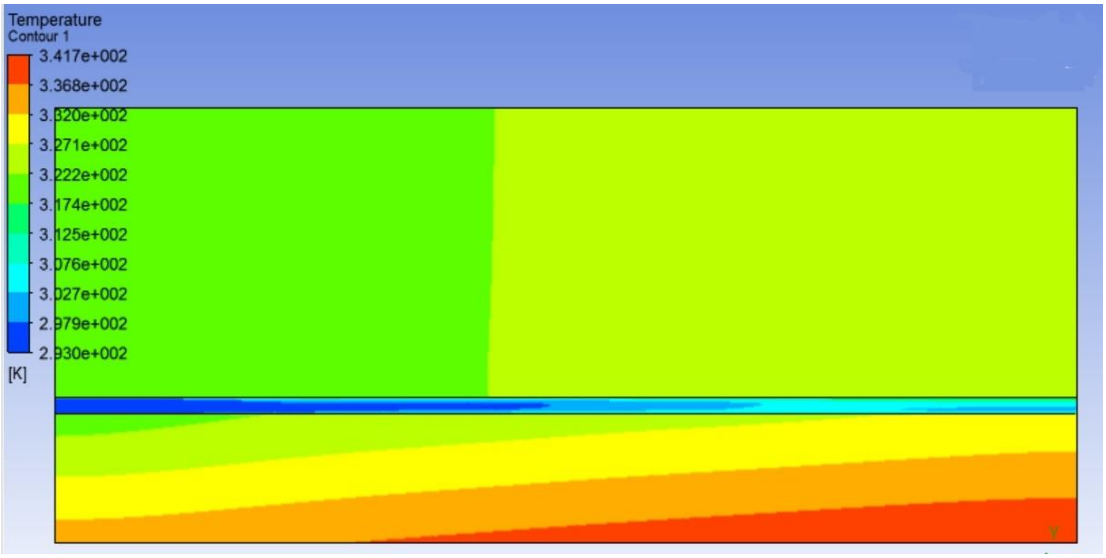

Figure 5.7: Contours of temperature of heat sink and water at Re=790

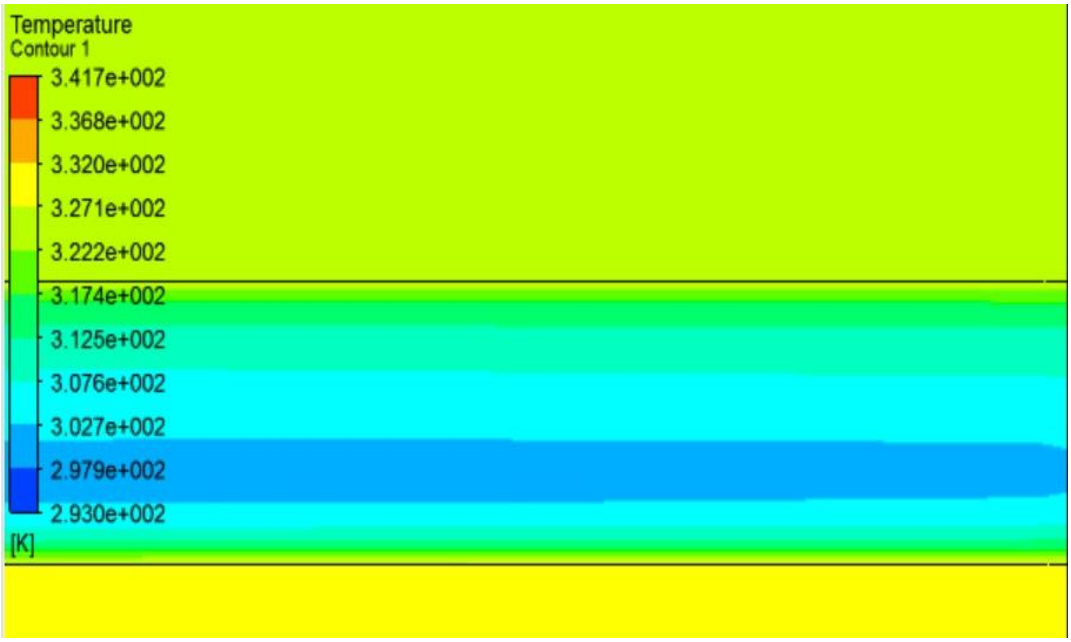

Figure 5.8: Contours of temperature at outlet at Re=790

(i) In the Figures 5.6 to 5.8, contours of temperature and pressure are shown for a single phase microchannel heat sink at Reynolds number 790

(ii) In Figure 5.6, pressure penalty along the channel is 0.22 bar.

(iii) In Figure 5.8, outlet temperature of channel is 303.0 K

(iv) In Figure 5.7, the maximum temperature is at the base of the wall which is 341.7 K and the wall temperature seems to be increasing along the flow direction.

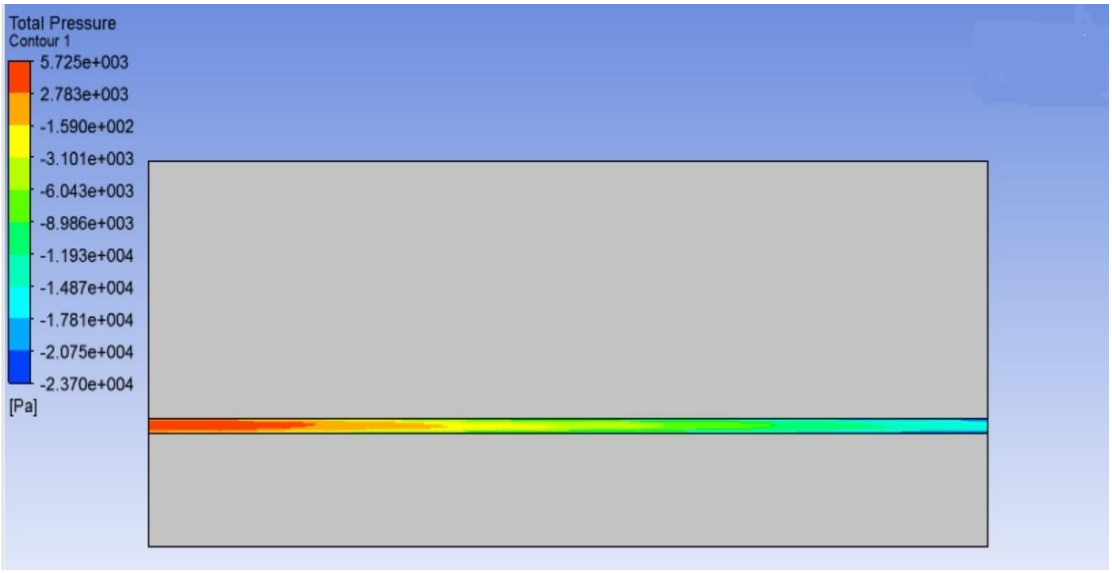

Figure 5.9: Contours of pressure at Re=990

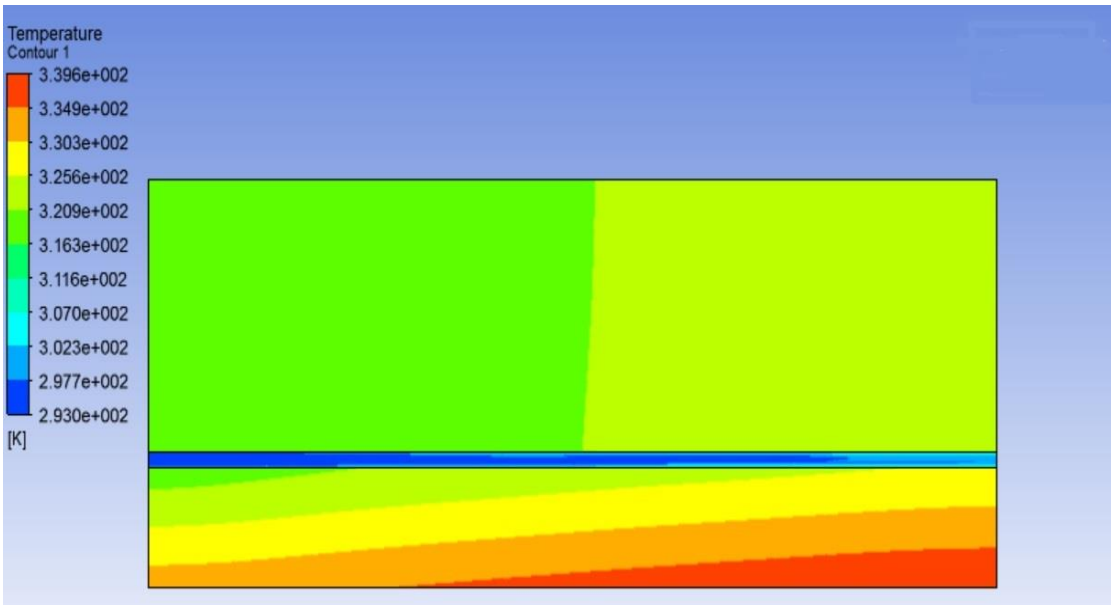

Figure 5.10: Contours of temperature of heat sink and water at Re=990

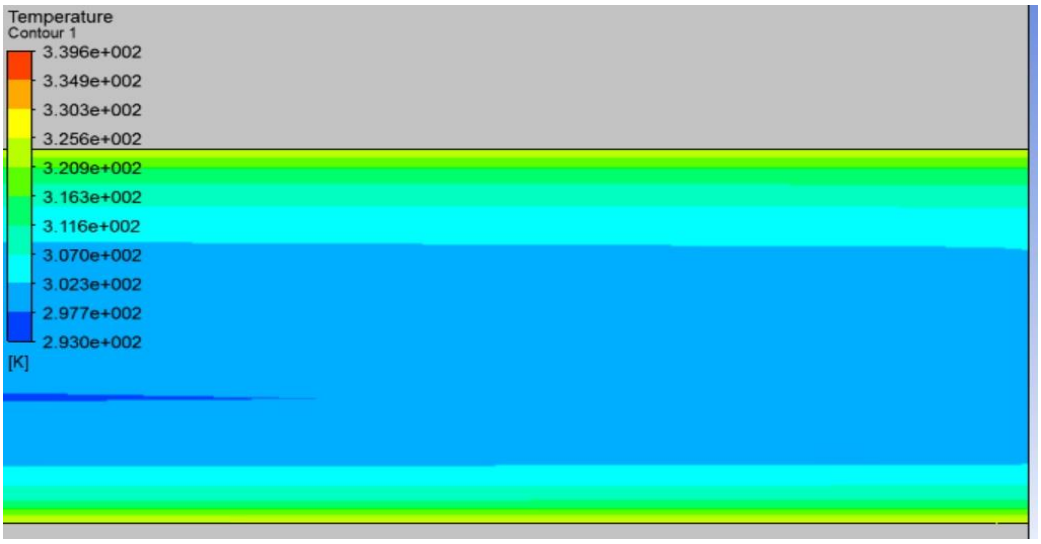

Figure 5.11: Contours of temperature at outlet at Re=990

(i) In the Figures 5.9 to 5.11, contours of temperature and pressure are shown for a single phase microchannel heat sink at Reynolds number 990

(ii) In Figure 5.9, pressure penalty along the channel is 0.29 bar.

(iii) In Figure 5.11, outlet temperature of channel is 300.0 K

(iv) In Figure 5.10, the maximum temperature is at the base of the wall which is 339.6 K and the wall temperature seems to be increasing along the flow direction.

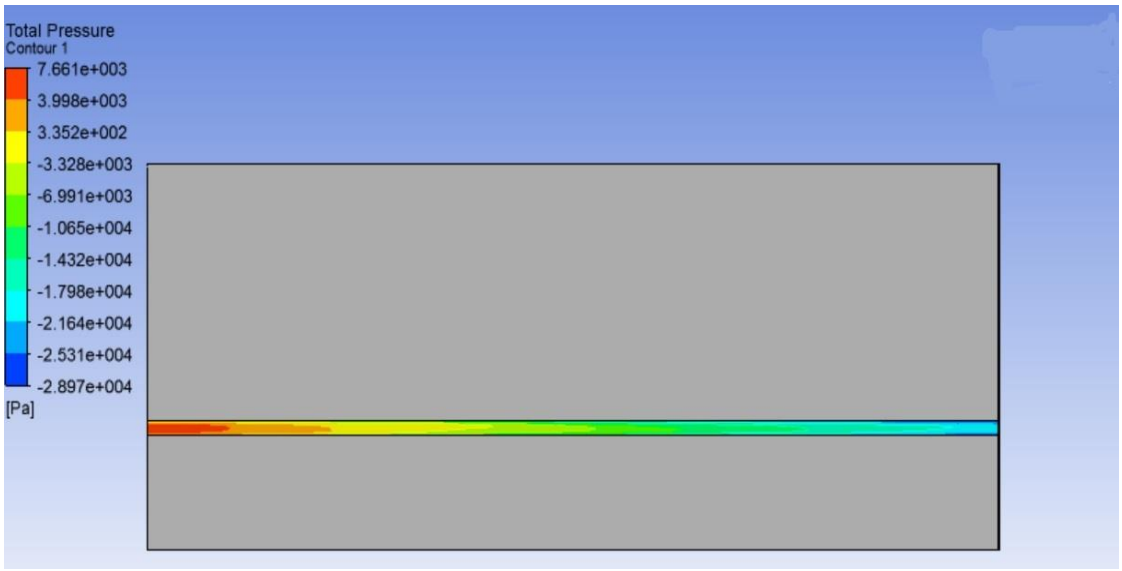

Figure 5.12: Contours of pressure at Re=1190

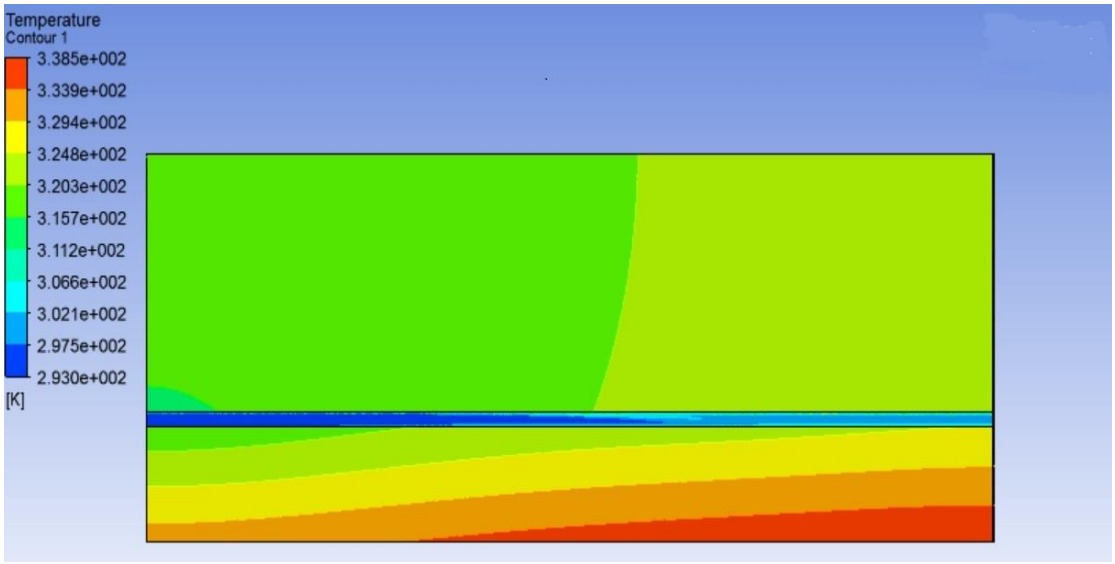

Figure 5.13: Contours of temperature of heat sink and water at Re=1190

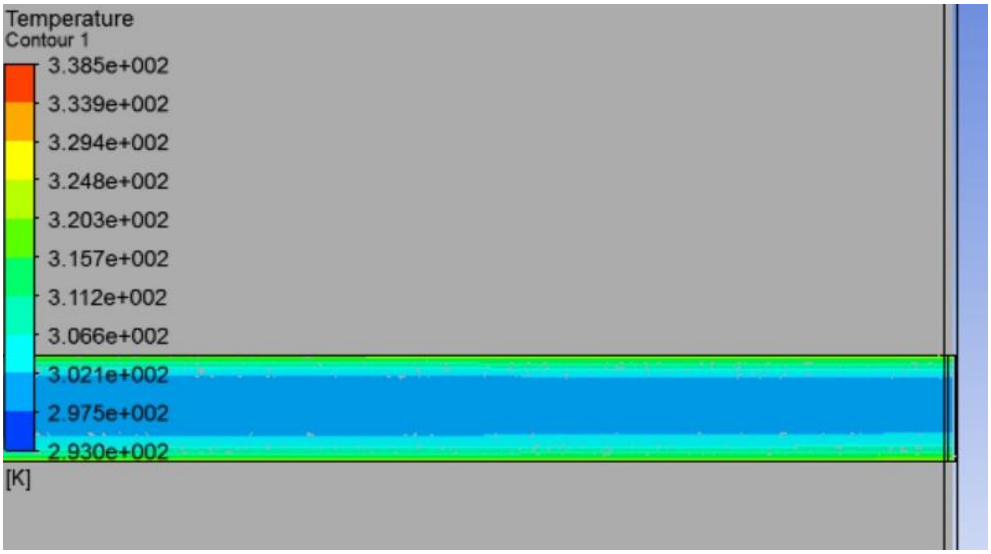

Figure 5.14: Contours of temperature at outlet at Re=1190

(i) In the Figures 5.12 to 5.14, contours of temperature and pressure are shown for a single phase microchannel heat sink at Reynolds number 1190

(ii) In Figure 5.12, pressure penalty along the channel is 0.366 bar.

(iii) In Figure 5.14, outlet temperature of channel is 298.0 K

(iv) In Figure 5.13, the maximum temperature is at the base of the wall which is 338.5 K and the wall temperature seems to be increasing along the flow direction.

5.1.2 Results for 200 W/cm^2 at the bottom wall with different sets of Reynolds number

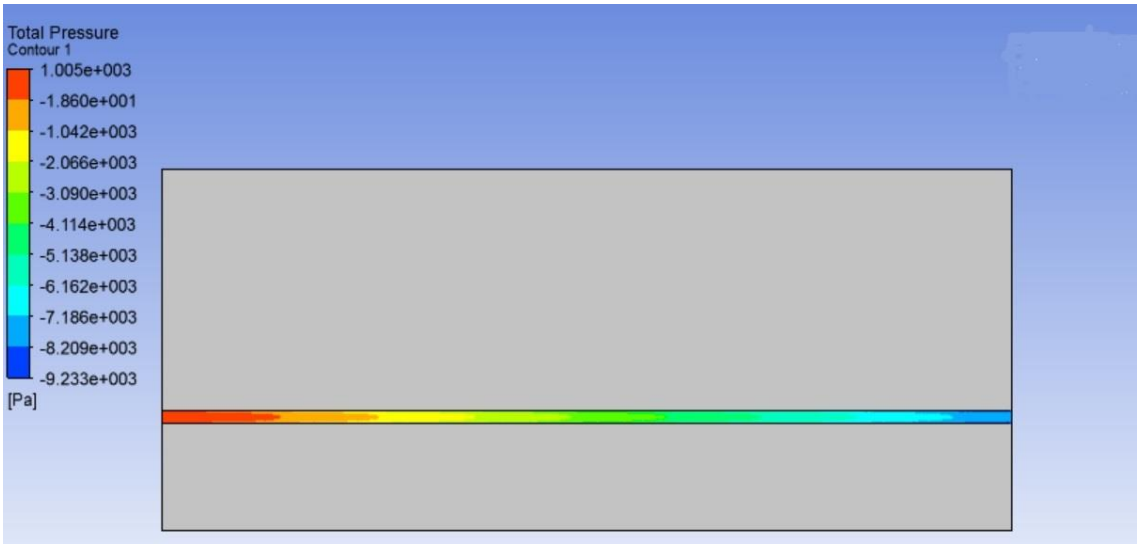

Figure 5.15: Contours of pressure at Re=390

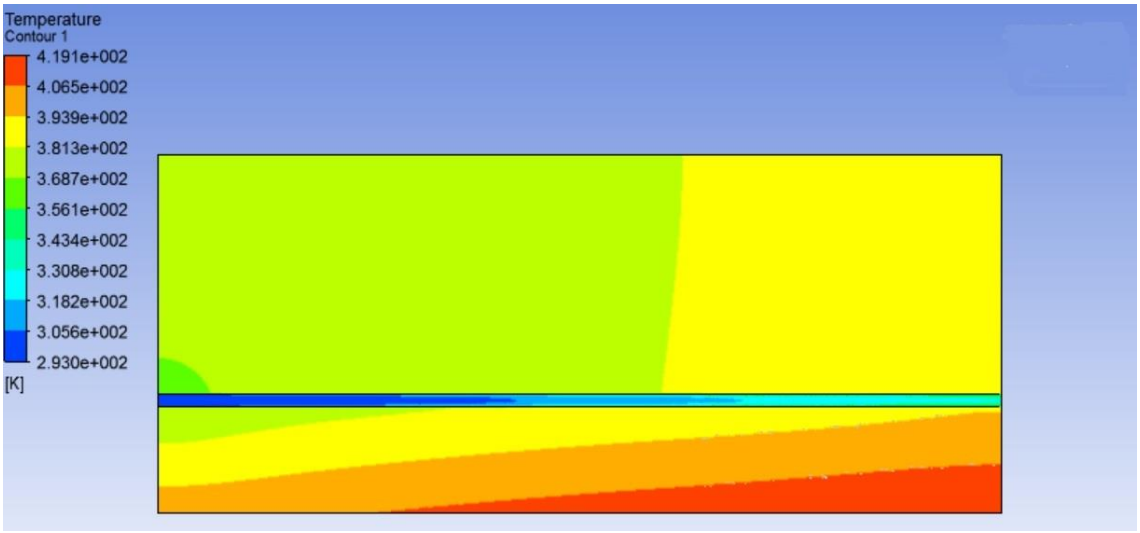

Figure 5.16: Contours of temperature of heat sink and water at Re=390

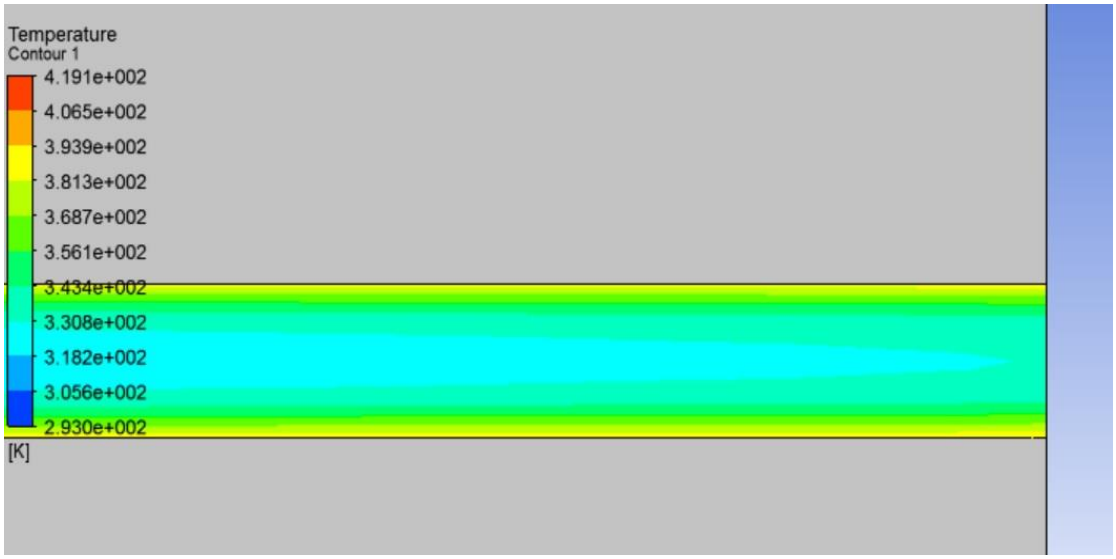

Figure 5.17: Contours of temperature at outlet at Re=390

(i) In the Figures 5.15 to 5.17, contours of temperature and pressure are shown for a single phase microchannel heat sink at Reynolds number 390.

(ii) In Figure 5.15, pressure penalty along the channel is 0.1bar.

(iii) In Figure 5.17, outlet temperature of channel is 332.0 K

(iv) In Figure 5.16, the maximum temperature is at the base of the wall which is 419.1 K and the wall temperature seems to be increasing along the flow direction

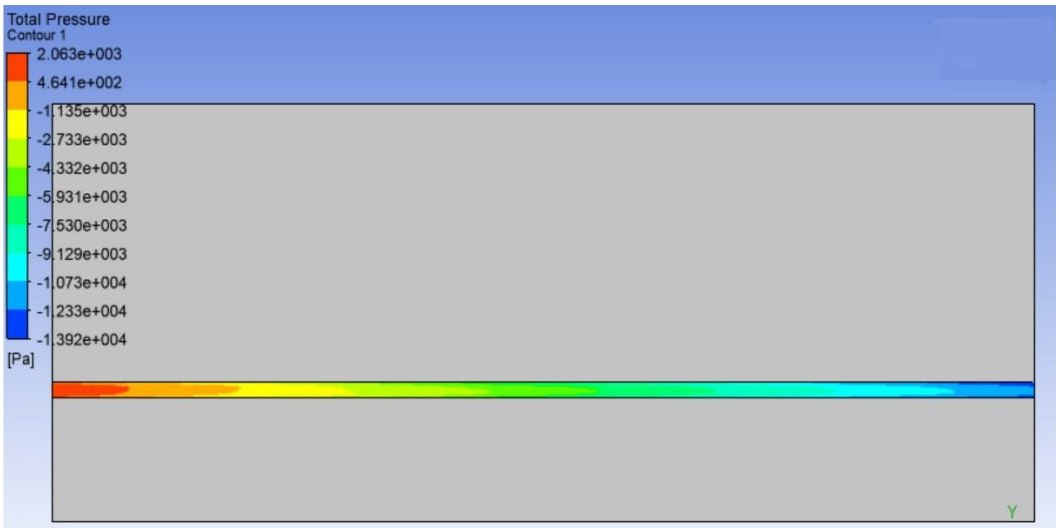

Figure 5.18: Contours of pressure at Re=590

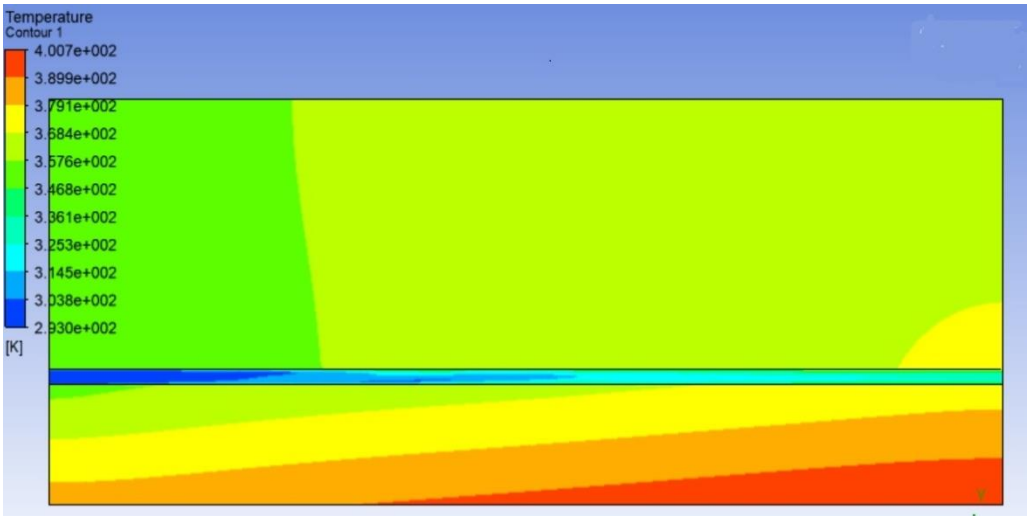

Figure 5.19: Contours of temperature of heat sink and water at Re=590

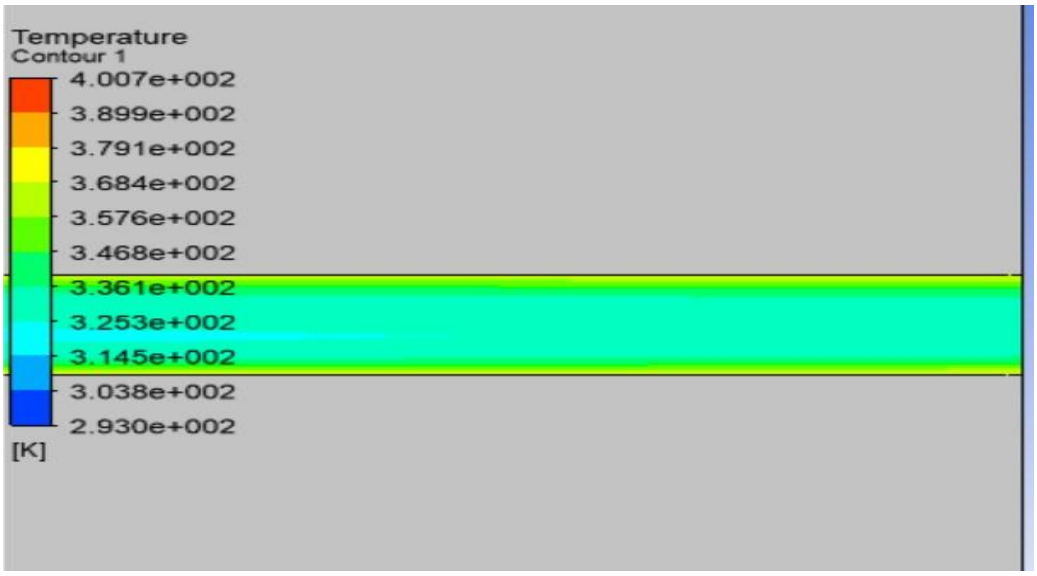

Figure 5.20: Contours of temperature at outlet at Re=590

(i) In the Figures 5.18 to 5.20, contours of temperature and pressure are shown for a single phase microchannel heat sink at Reynolds number 590.

(ii) In Figure 5.18, pressure penalty along the channel is 0.16 bar.

(iii) In Figure 5.20, outlet temperature of channel is 325.3 K

(iv) In Figure 5.19, the maximum temperature is at the base of the wall which is 400.7 K and the wall temperature seems to be increasing along the flow direction

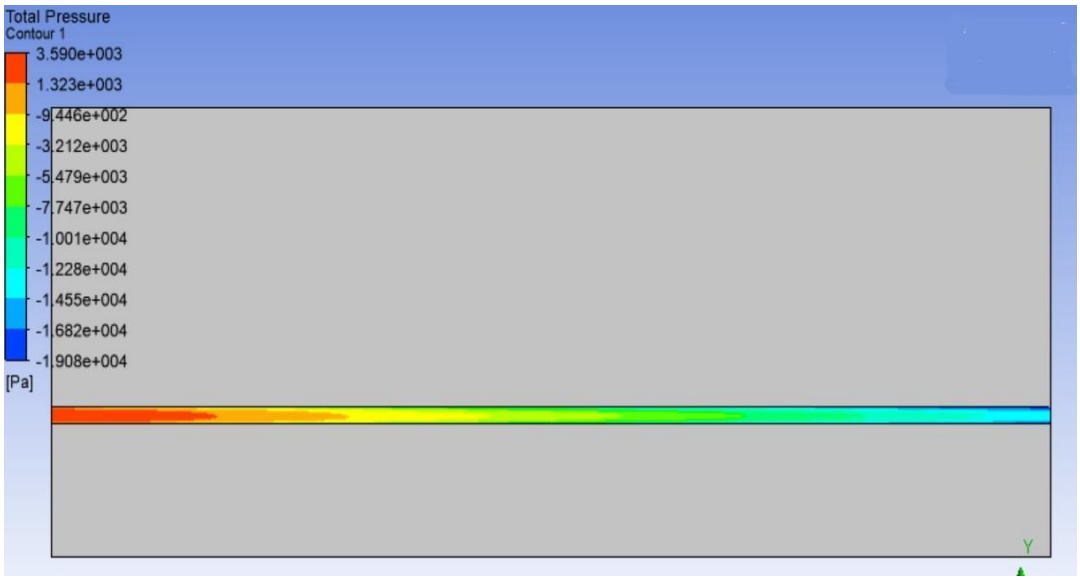

Figure 5.21: Contours of pressure at Re=790

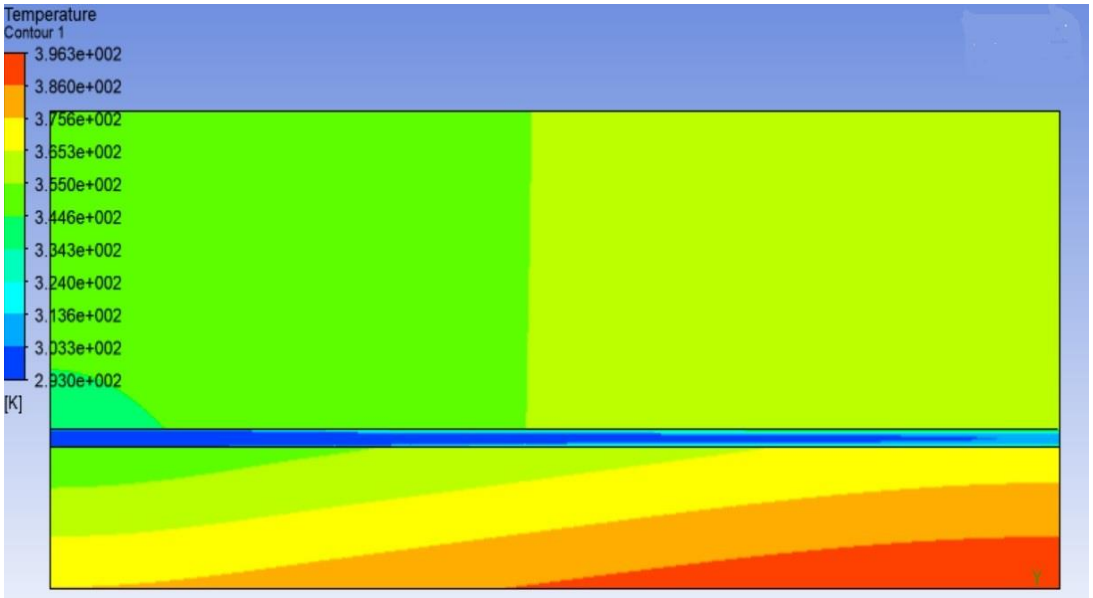

Figure 5.22: Contours of temperature of heat sink and water at Re=790

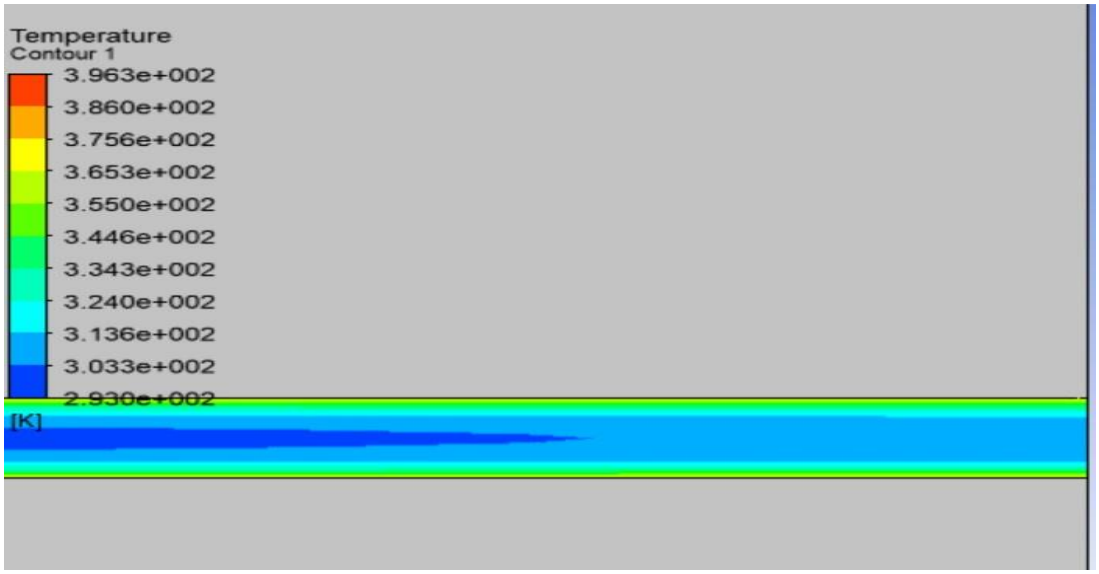

Figure 5.23: Contours of temperature at outlet at Re=790

(i) In the Figures 5.21 to 5.23, contours of temperature and pressure are shown for a single phase microchannel heat sink at Reynolds number 790

(ii) In Figure 5.21, pressure penalty along the channel is 0.22 bar.

(iii) In Figure 5.23, outlet temperature of channel is 316.0 K

(iv) In Figure 5.22, the maximum temperature is at the base of the wall which is 396.3 K and the wall temperature seems to be increasing along the flow direction

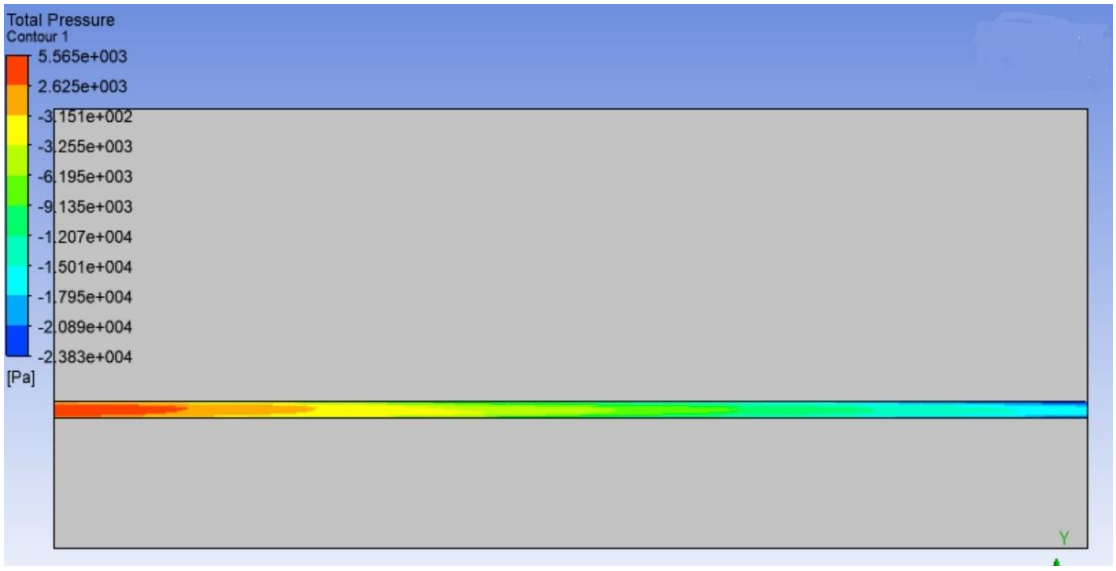

Figure 5.24: Contours of pressure at Re=990

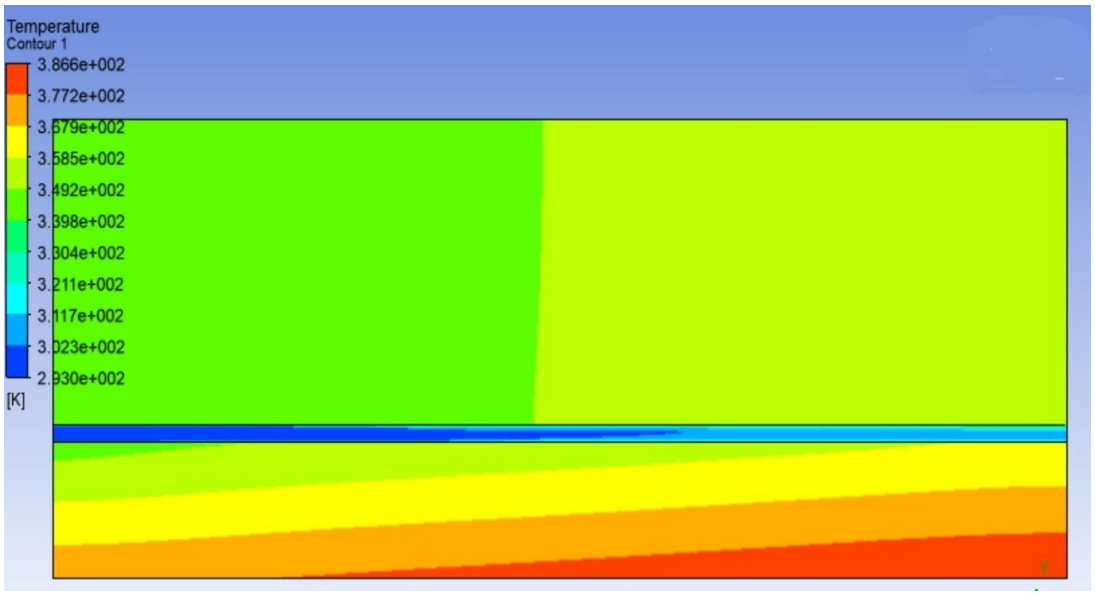

Figure 5.25: Contours of temperature of heat sink and water at Re=990

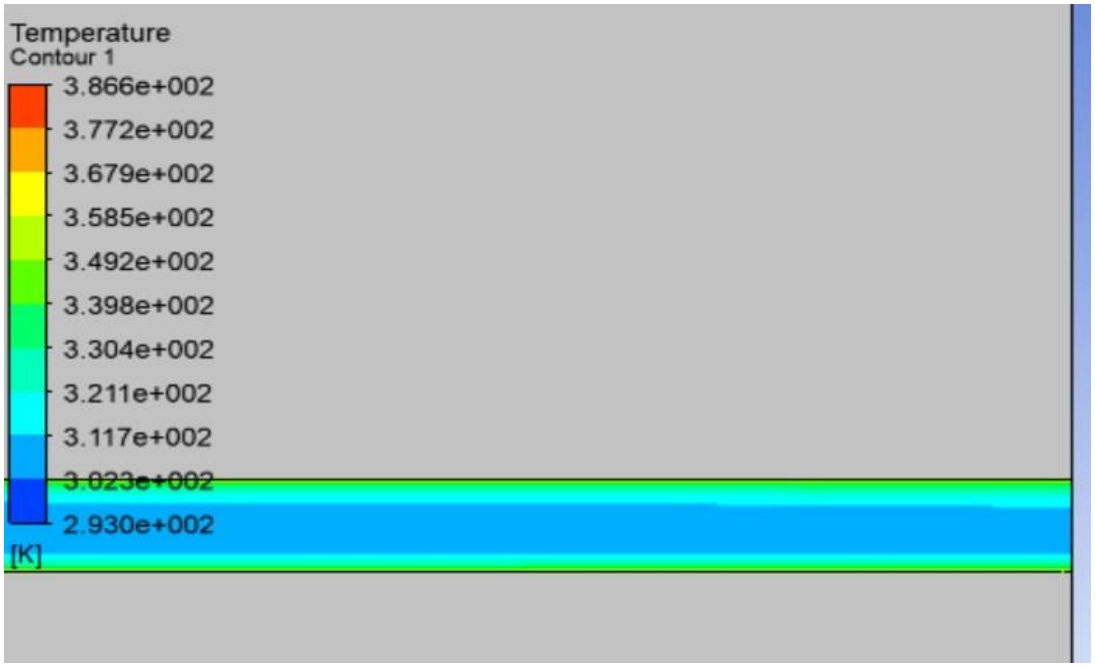

Figure 5.26: Contours of temperature at outlet at Re=990

(i) In the Figures 5.24 to 5.26, contours of temperature and pressure are shown for a single phase microchannel heat sink at Reynolds number 990

(ii) In Figure 5.24, pressure penalty along the channel is 0.27 bar.

(iii) In Figure 5.26, outlet temperature of channel is 311.7 K

(iv) In Figure 5.25, the maximum temperature is at the base of the wall which is 386.6 K and the wall temperature seems to be increasing along the flow direction

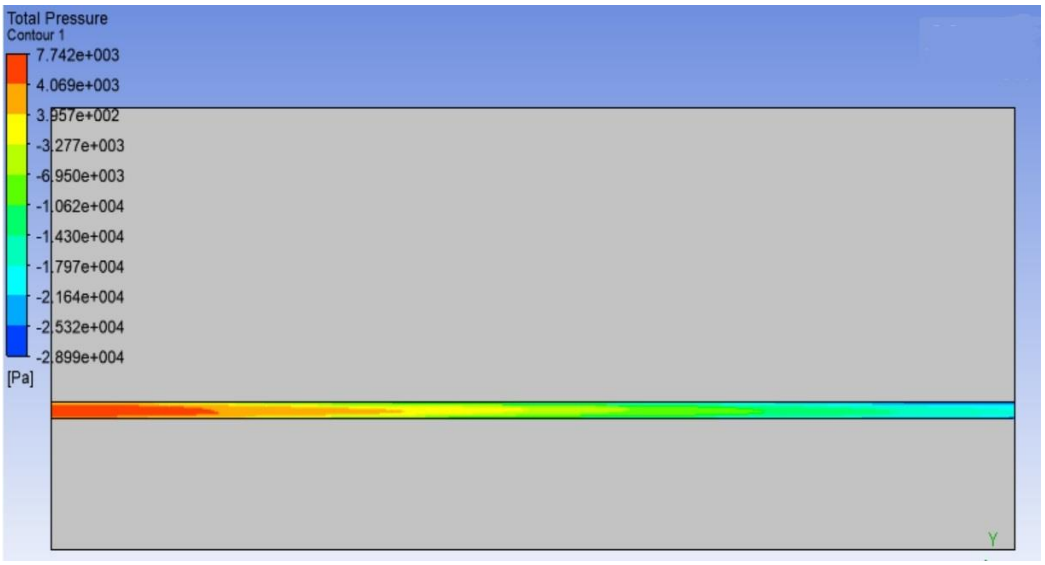

Figure 5.27: Contours of pressure at Re=1190

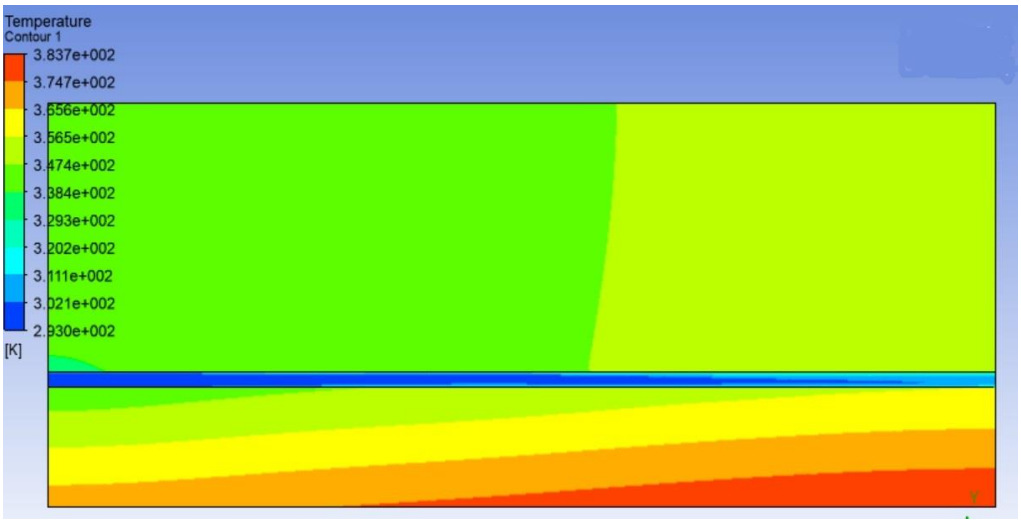

Figure 5.28: Contours of temperature of heat sink and water at Re=1190

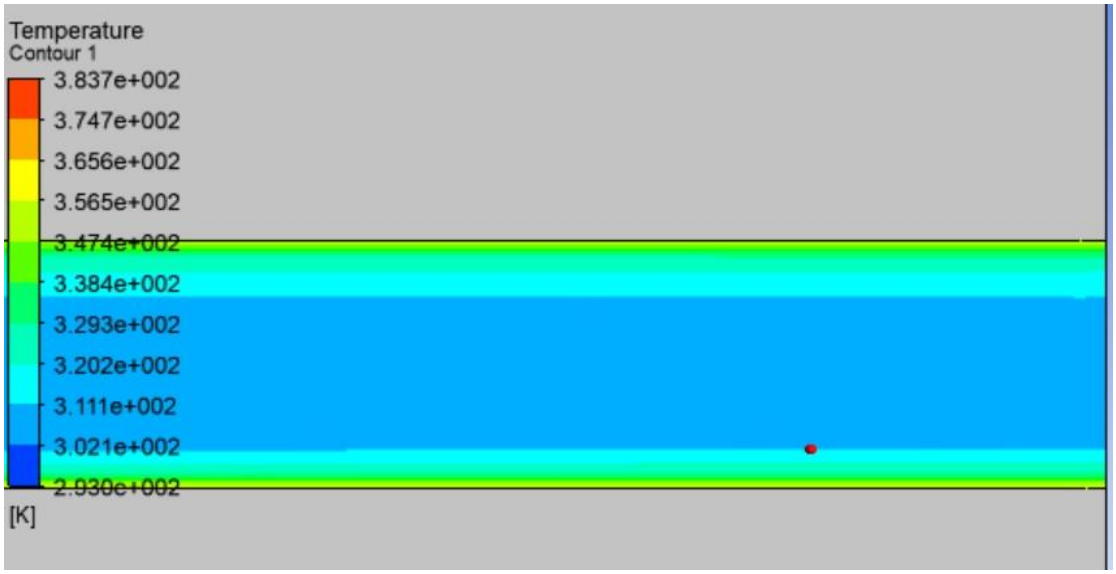

Figure 5.29: Contours of temperature at outlet at Re=1190

(i) In the Figures 5.27 to 5.29, contours of temperature and pressure are shown for a single phase microchannel heat sink at Reynolds number 1190.

(ii) In Figure 5.27, pressure penalty along the channel is 0.36 bar.

(iii) In Figure 5.29, outlet temperature of channel is 311.0 K

(iv) In Figure 5.28, the maximum temperature is at the base of the wall which is 383.7 K and the wall temperature seems to be increasing along the flow direction.

5.2 Problem Validation

Case 1:

For the validation of the problem, the experimental pressure drop along the flow was compared with the results found from CFD. The data for pressure penalties at various Reynolds number against heat flux of 100W/cm^2 and 200 W/cm^2 were collated from the figures 5.1, 5.3, 5.6, 5.9, 5.12 and figures 5.15, 5.18, 5.21, 5.24, 5.27 respectively.

Table 9: Heat flux value at bottom wall =100W/cm$^{2`}$

Reynolds number	Experimental pressure drop (bar)	Computational pressure drop (bar)
390	0.1	0.1
590	0.17	0.16
790	0.23	0.22
990	0.32	0.29
1190	0.41	0.366

Table 10 - : Bottom wall heat flux value=200W/cm^2

Reynolds number	Experimental pressure drop (bar)	Computational pressure drop (bar)
390	0.08	0.10
590	0.15	0.16
790	0.21	0.22
990	0.30	0.27
1190	0.40	0.36

It is clear from Table 9 and Table 10 that the computational values for pressure penalties for heat flux values of 100 W/cm^2 and 200 W/cm^2 for different values of Reynolds number were found to be in close agreement with experimental pressure penalty along the flow. Hence the model is successfully validated on the basis of pressure losses along the flow.

Case 2: The model is further validated on the basis of temperature difference. The values for temperature difference were collated and compared between the results obtained from the designed geometry and experimental geometry for the same values

of heat flux 100W/cm^2 and 200 W/cm^2 from figures 5.2, 5.5, 5.8, 5.11 &5.14 and figures 5.17, 5.20, 5.23, 5.26, 5.29 respectively.

Table 11: Heat flux value at bottom wall =100W/cm^2

Reynolds number	Experimental temperature rise (K)	Computational temperature rise (K)
390	28	25.8
590	18	15.9
790	12	10
990	10	7
1190	9	5

Table 12 - : Bottom wall heat flux value=200W/cm^2

Reynolds number	Experimental temperature rise (K)	Computational temperature rise (K)
390	48	42
590	32	31
790	24	23
990	20	18.7
1190	16	15

It is clear from Table 11 and Table 12 that the computational values for rise in temperature for heat flux values of 100 W/cm^2 and 200 W/cm^2 for different values of Reynolds number were found to be in close agreement with experimental temperature rise. Hence the model is successfully validated on the basis of temperature rise along the flow.

5.3 Graphical Validation

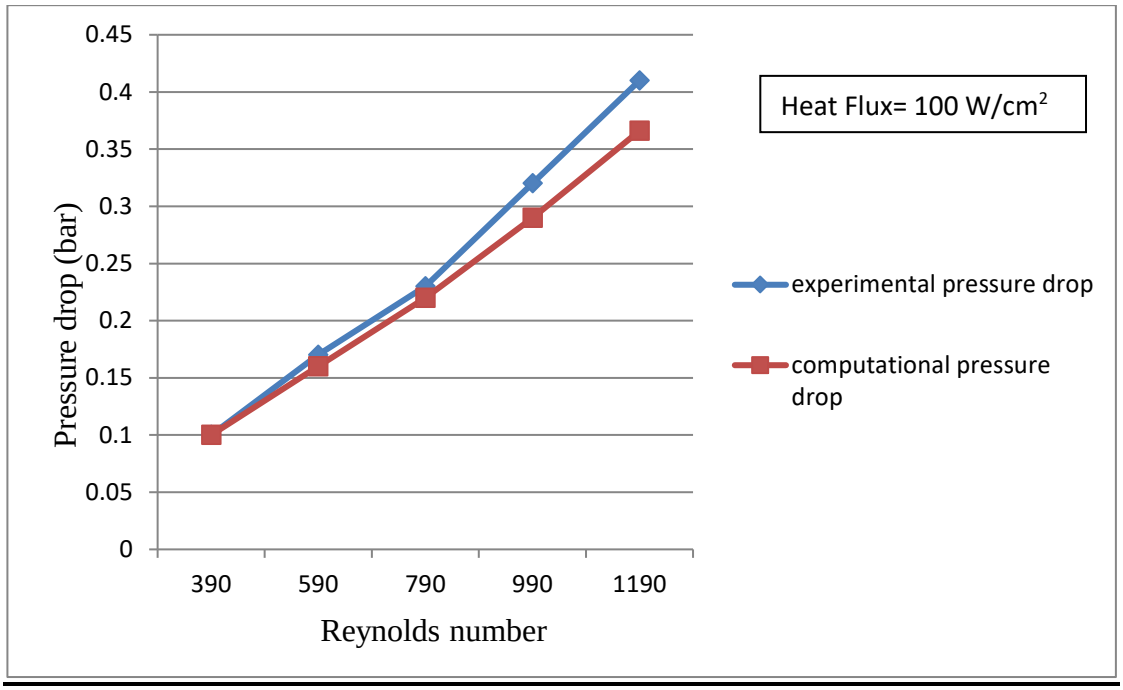

Fig 5.30: Pressure loss vs Reynolds number

Fig 5.30 is showing the results and comparison between computational and experimental pressure drop at a heat flux of 100 W/cm^2

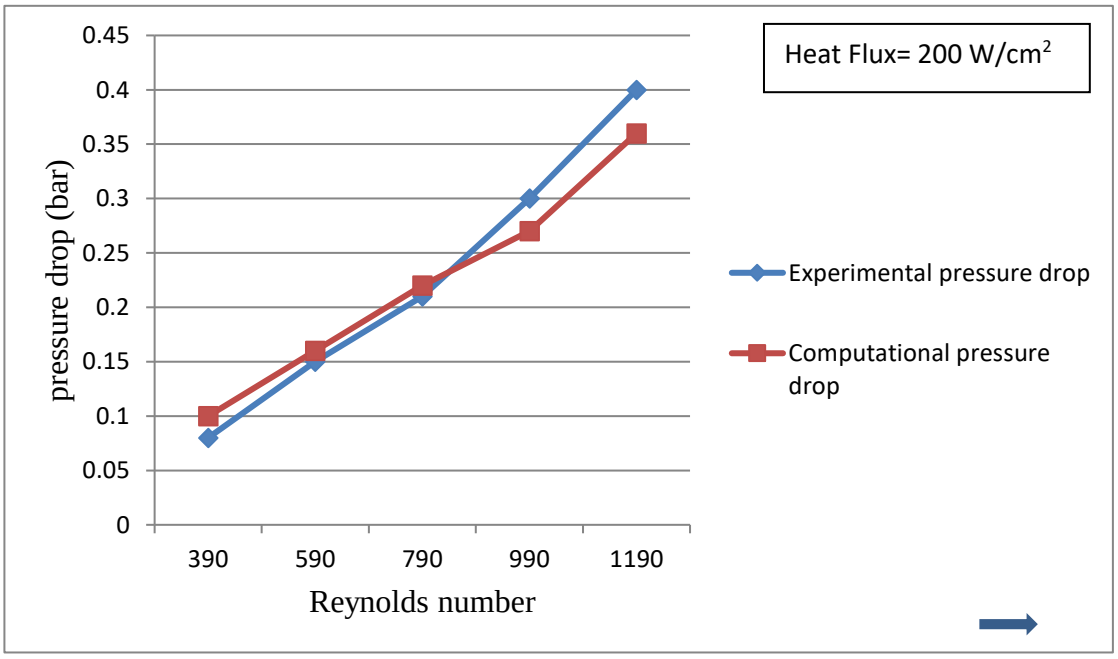

Fig 5.31: Pressure loss vs Reynolds number

Fig 5.31 is showing the results and comparison between computational and experimental pressure drop at a heat flux of 200 W/cm^2

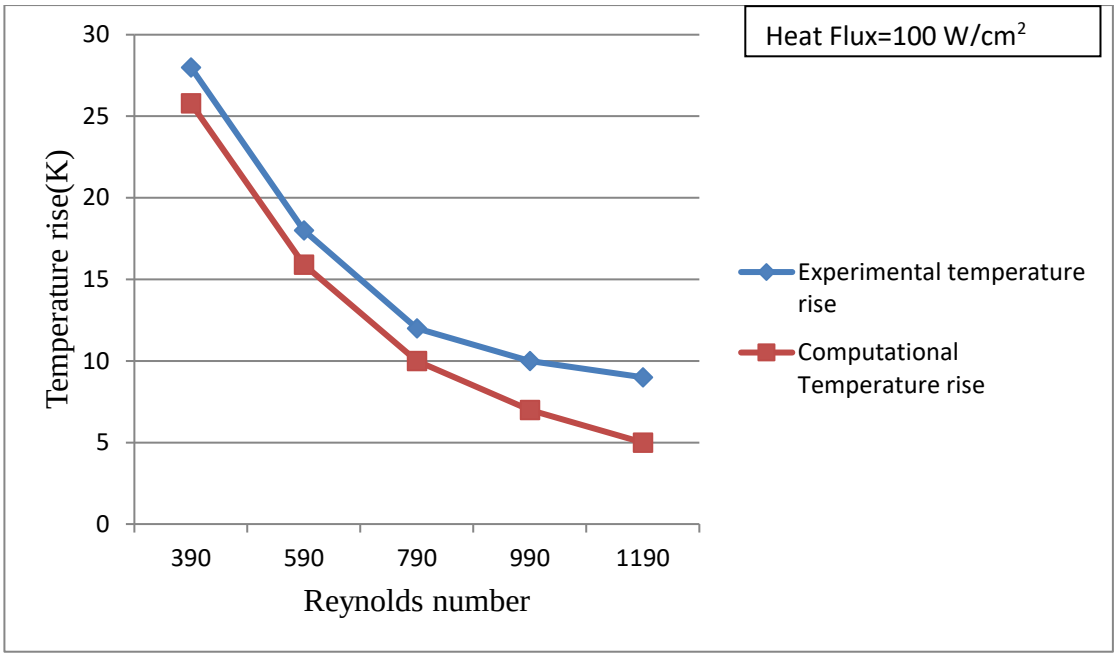

Fig 5.32: Rise in temperature vs Reynolds number

Fig 5.32 is showing the results and comparison between computational and experimental rise in temperature at a heat flux of 100 W/cm^2.

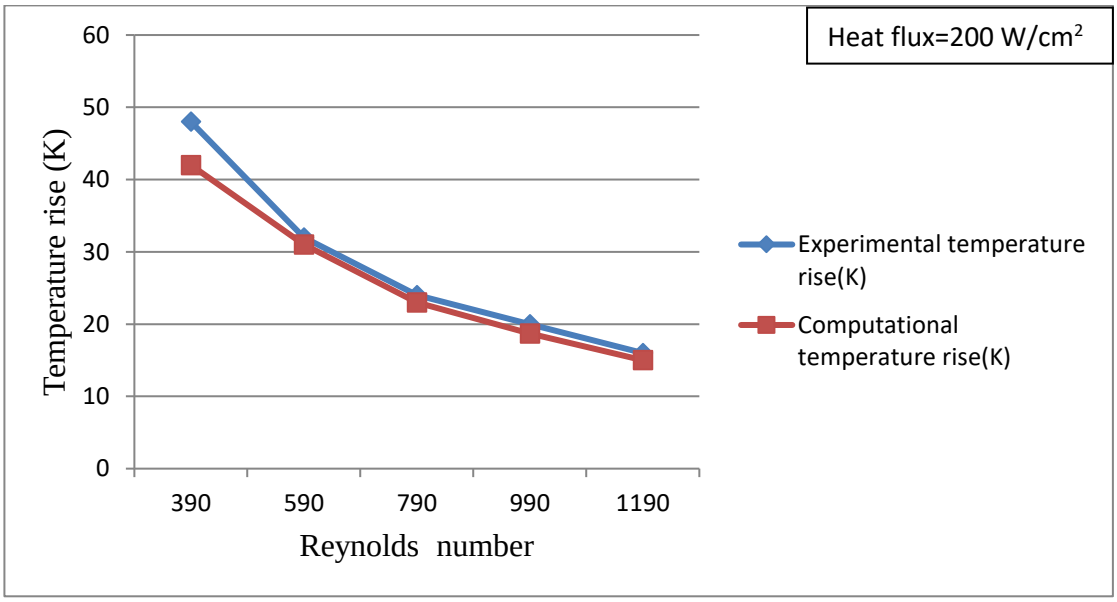

Fig 5.33: Rise in temperature vs Reynolds number

Fig 5.33 is showing the results and comparison between computational and experimental rise in temperature at a heat flux of 200 W/cm^2.

CHAPTER 6

SIMULATION RESULTS

6.1 Simulation Results for Microchannel Heat Sink With Pillars

The CFD study is done for a new designed geometry of a microchannel heat sink with pillars. The thermal performance is judged by the pressure drop and temperature rise along the flow. The study is done for two values of heat flux 100 W/cm^2 and 200 W/cm^2 which is applied at the bottom wall. The Reynolds numbers taken for the study were 390, 590, 790, 990, and 1190.

6.1.1 Heat Flux of 100 W/cm^2 applied at the bottom wall for different Reynolds number

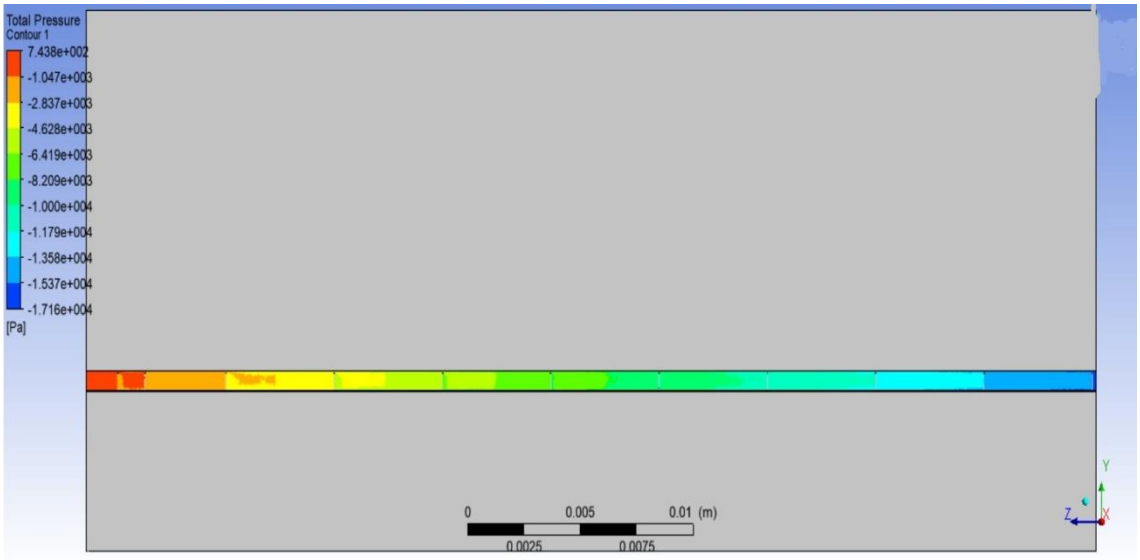

Fig 6.1: Contours of pressure at Re=390

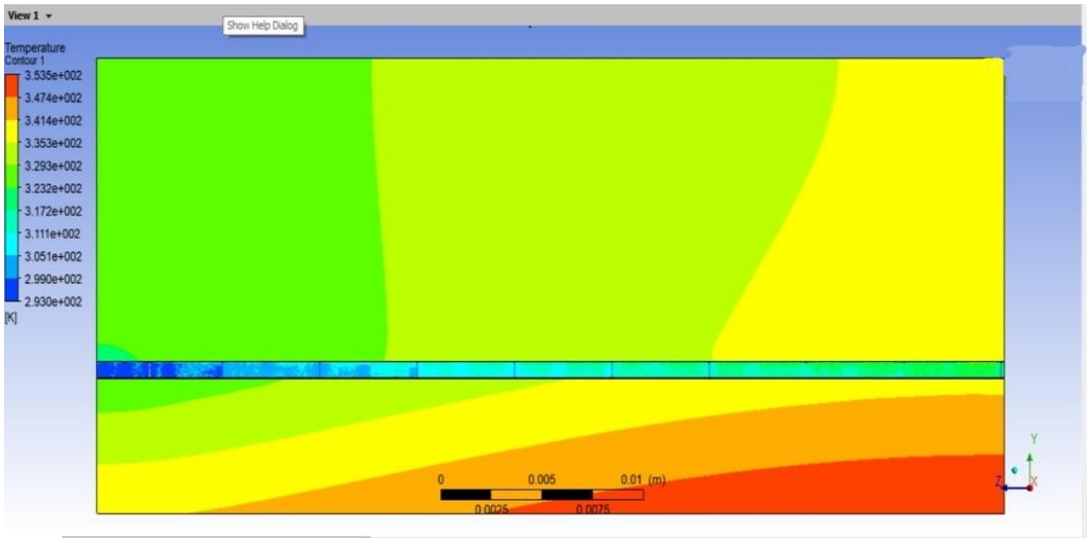

Fig 6.2: Contours of temperature of heat sink and water at Re=390

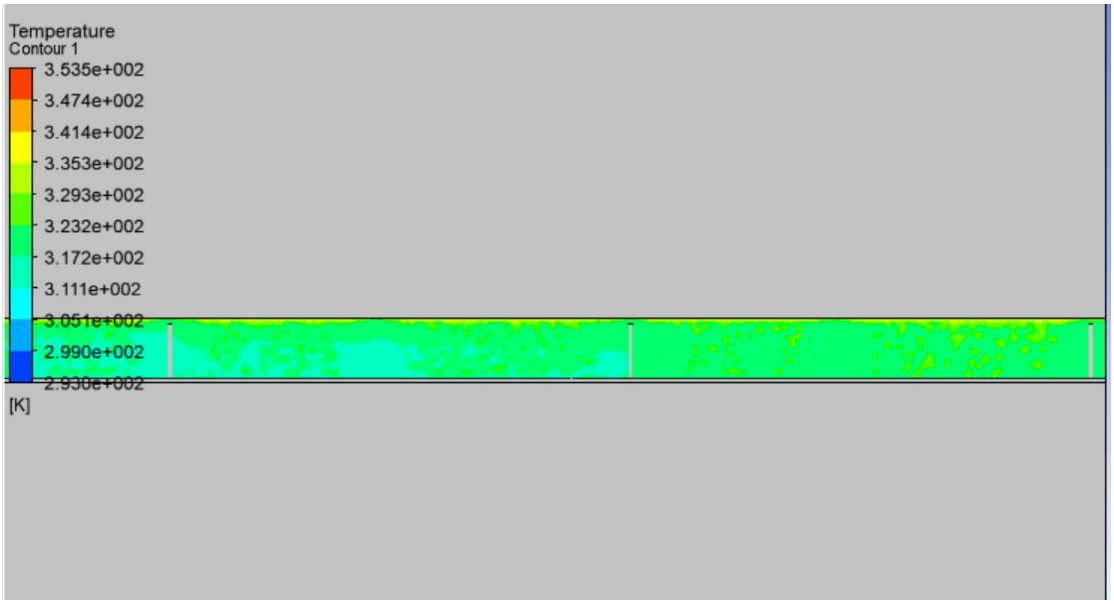

Figure 6.3: Contours of temperature at outlet at Re=390

(i) In the Figures 6.1 to 6.3, contours of temperature and pressure are shown for a single phase microchannel heat sink with pillars at Reynolds number 390.

(ii) In Figure 6.1, pressure penalty along the channel is 0.18 bar.

(iii) In Figure 6.3, outlet temperature of channel is 323.2 K

(iv) In Figure 6.2, the maximum temperature is at the base of the wall which is 353.5 K and the wall temperature seems to be increasing along the flow direction.

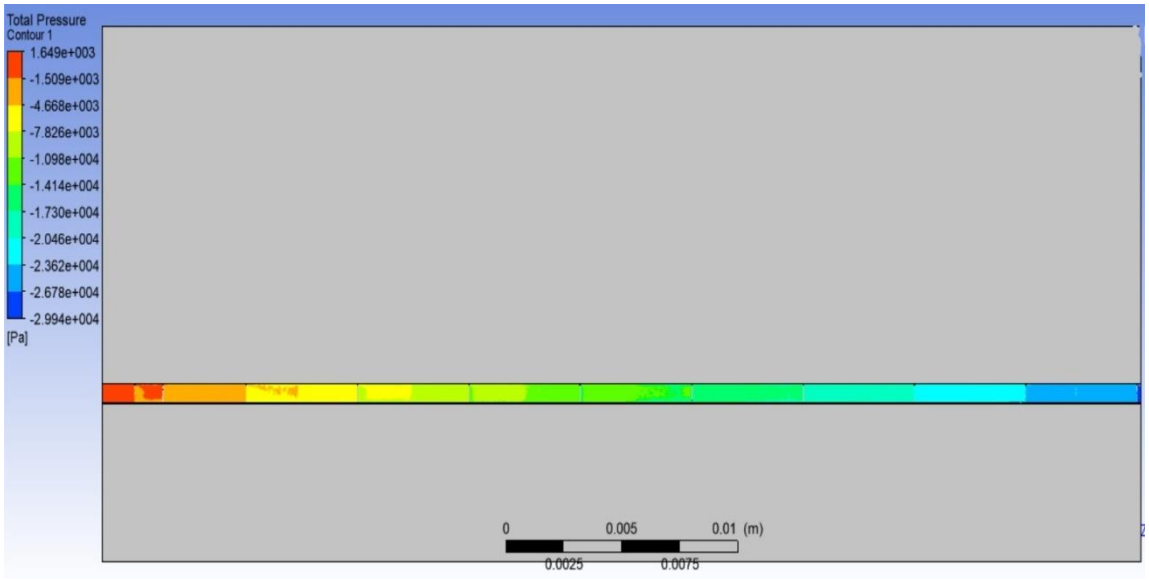

Fig 6.4: Contours of pressure at Re=590

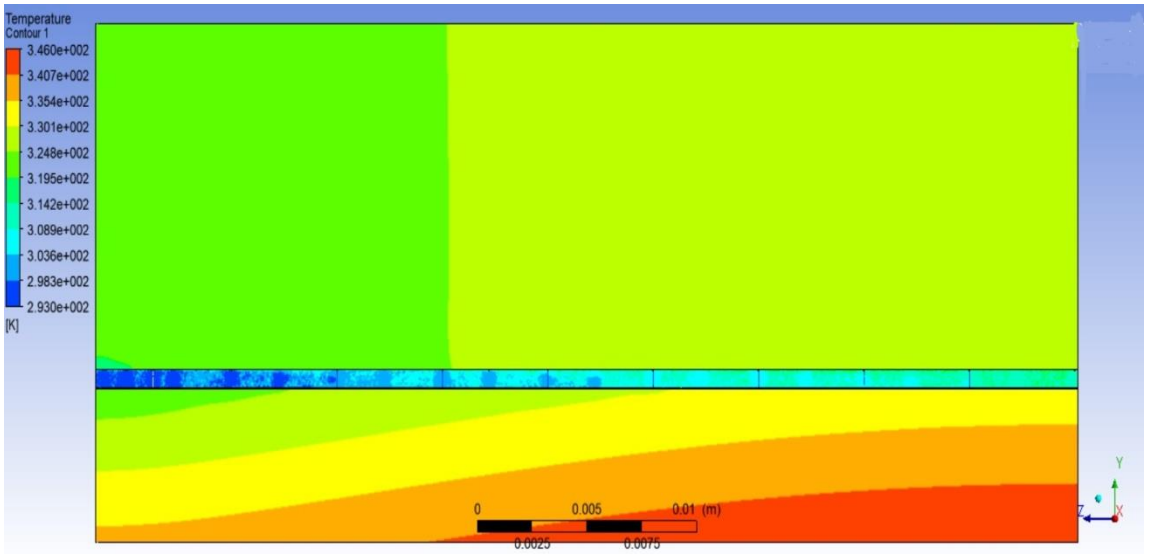

Fig 6.5: Contours of temperature of heat sink and water at Re=590

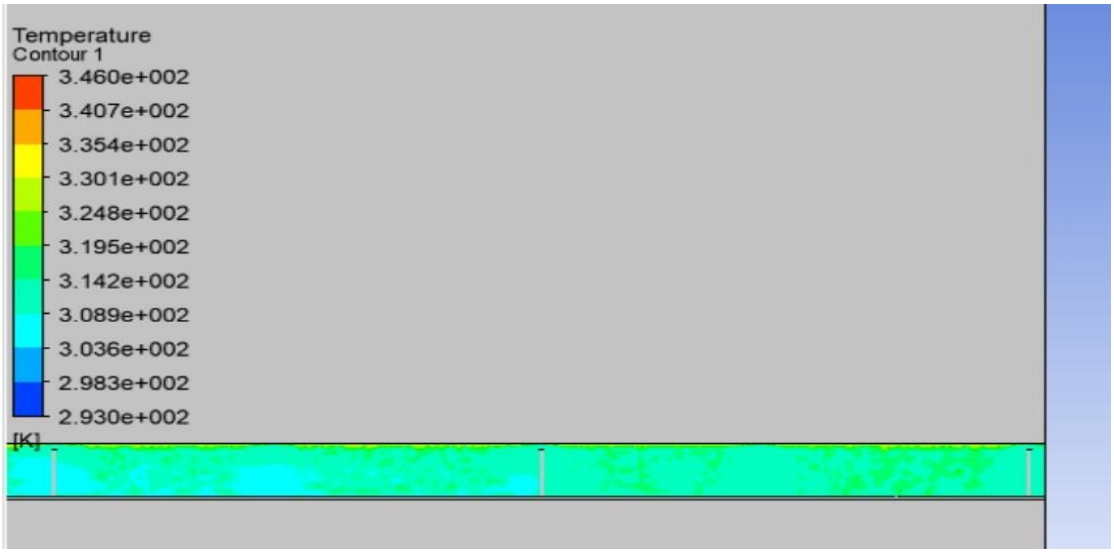

Figure 6.6: Contours of temperature at outlet at Re=590

(i) In the Figures 6.4 to 6.6, contours of temperature and pressure are shown for a single phase microchannel heat sink with pillars at Reynolds number 590.

(ii) In Figure 6.4, pressure penalty along the channel is 0.316 bar.

(iii) In Figure 6.6, outlet temperature of channel is 314.2 K

(iv) In Figure 6.5, the maximum temperature is at the base of the wall which is 346.0 K and the wall temperature seems to be increasing along the flow direction.

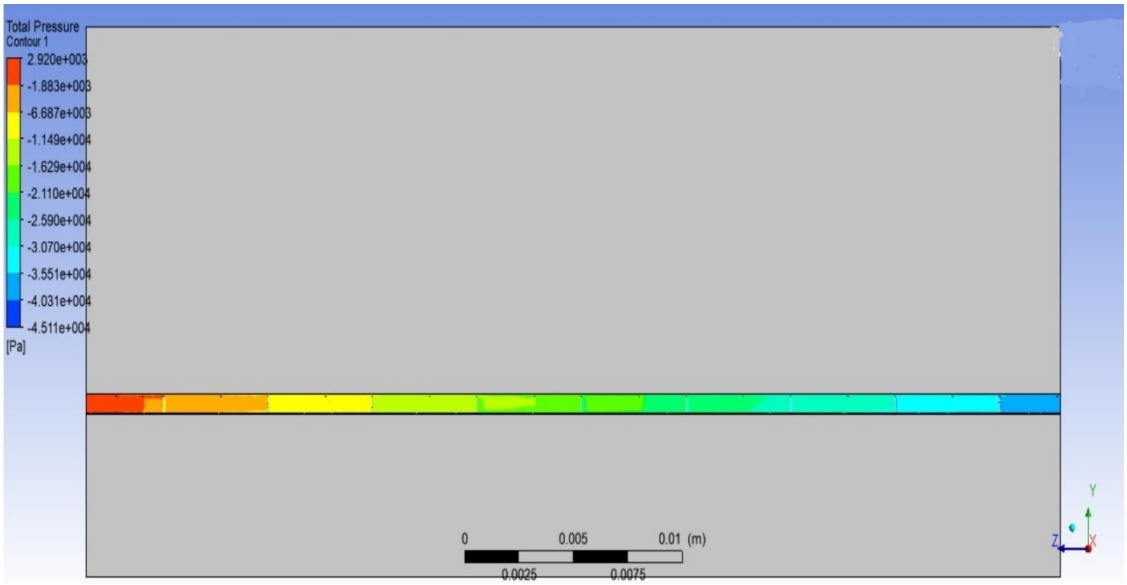

Fig 6.7: Contours of pressure at Re=790

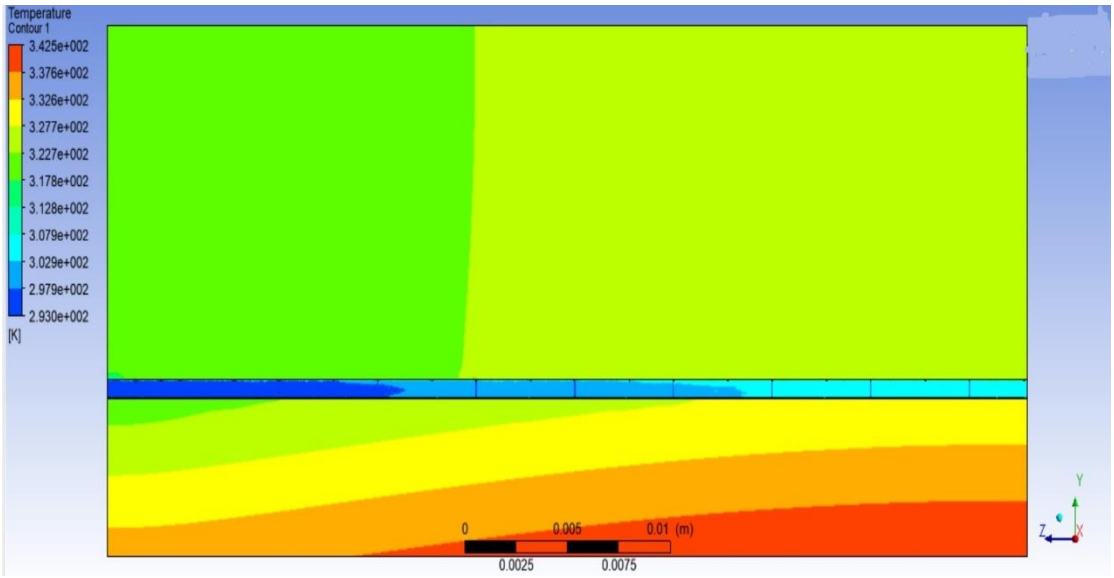

Fig 6.8: Contours of temperature of heat sink and water at Re=790

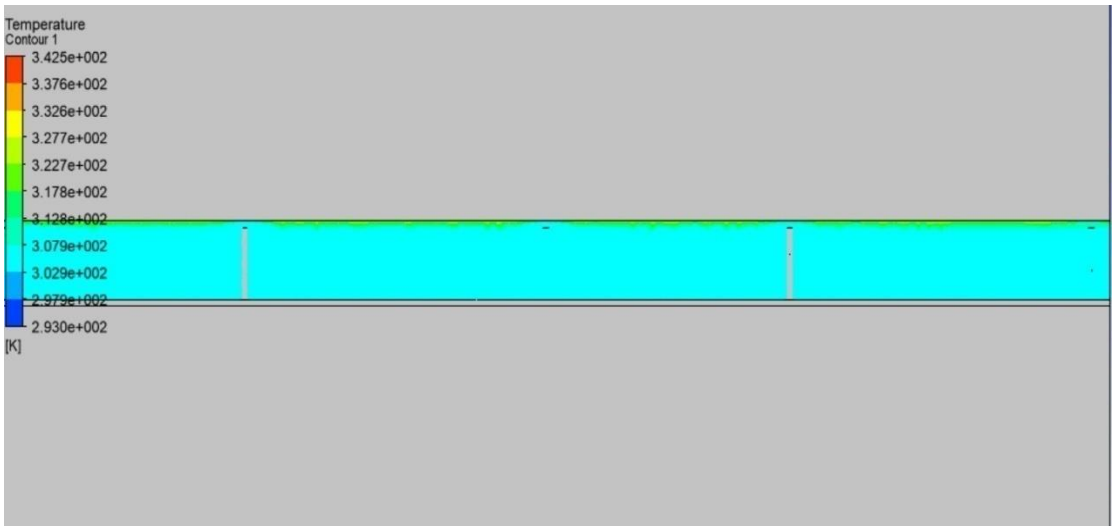

Figure 6.9: Contours of temperature at outlet at Re=790

(i) In the Figures 6.7 to 6.9, contours of temperature and pressure are shown for a single phase microchannel heat sink with pillars at Reynolds number 790.

(ii) In Figure 6.7, pressure penalty along the channel is 0.480 bar.

(iii) In Figure 6.9, outlet temperature of channel is 308.0 K

(iv) In Figure 6.8, the maximum temperature is at the base of the wall which is 342.5 K and the wall temperature seems to be increasing along the flow direction.

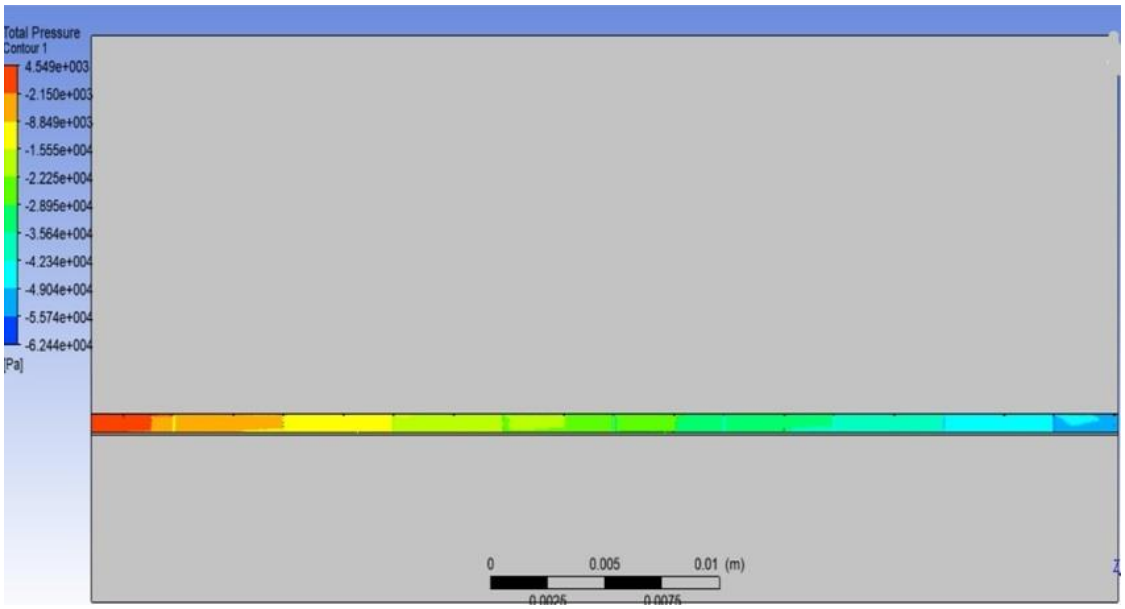

Fig 6.10: Contours of pressure at Re=990

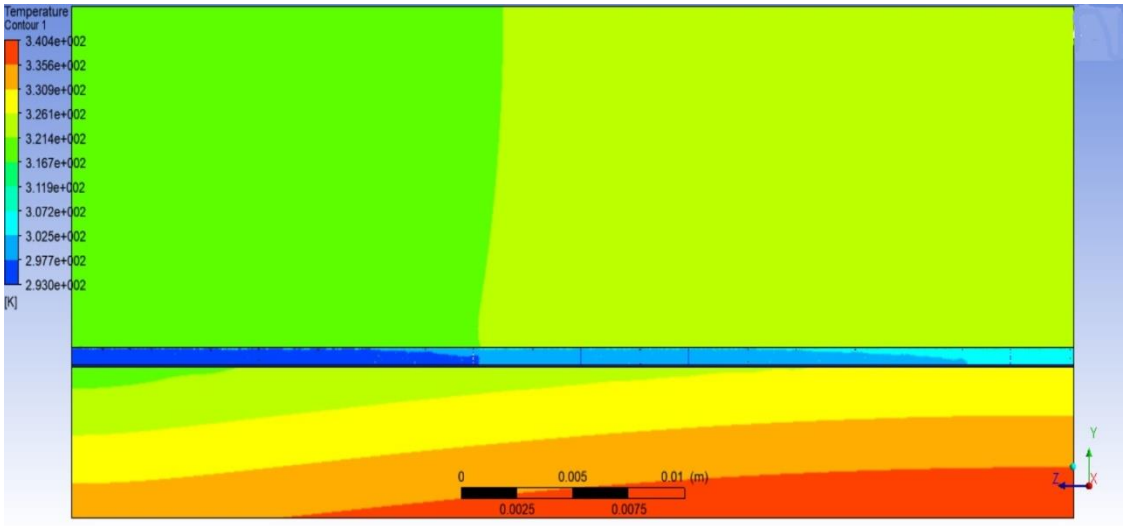

Fig 6.11: Contours of temperature of heat sink and water at Re=990

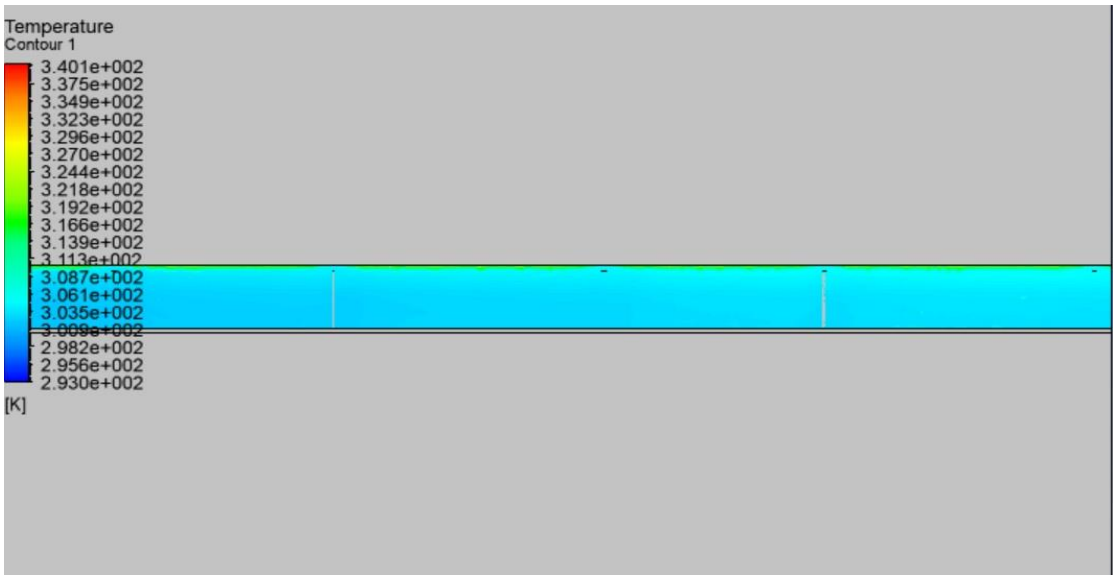

Figure 6.12: Contours of temperature at outlet at Re=990

(i) In the Figures 6.10 to 6.12, contours of temperature and pressure are shown for a single phase microchannel heat sink with pillars at Reynolds number 990.

(ii) In Figure 6.10, pressure penalty along the channel is 0.670 bar.

(iii) In Figure 6.12, outlet temperature of channel is 307.2 K

(iv) In Figure 6.11, the maximum temperature is at the base of the wall which is 340.4 K and the wall temperature seems to be increasing along the flow direction.

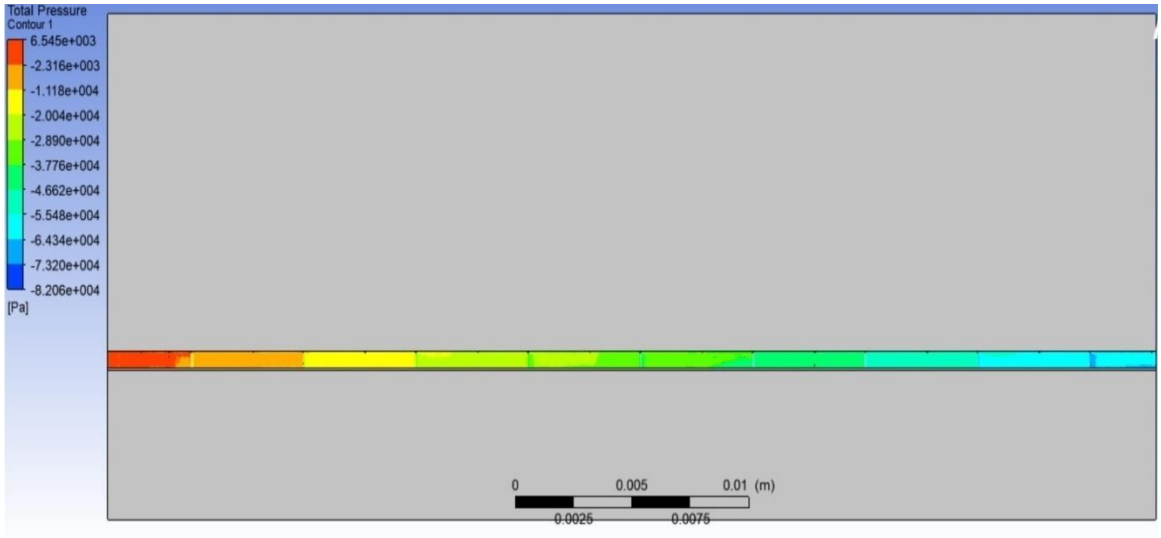

Fig 6.13: Contours of pressure at Re=1190

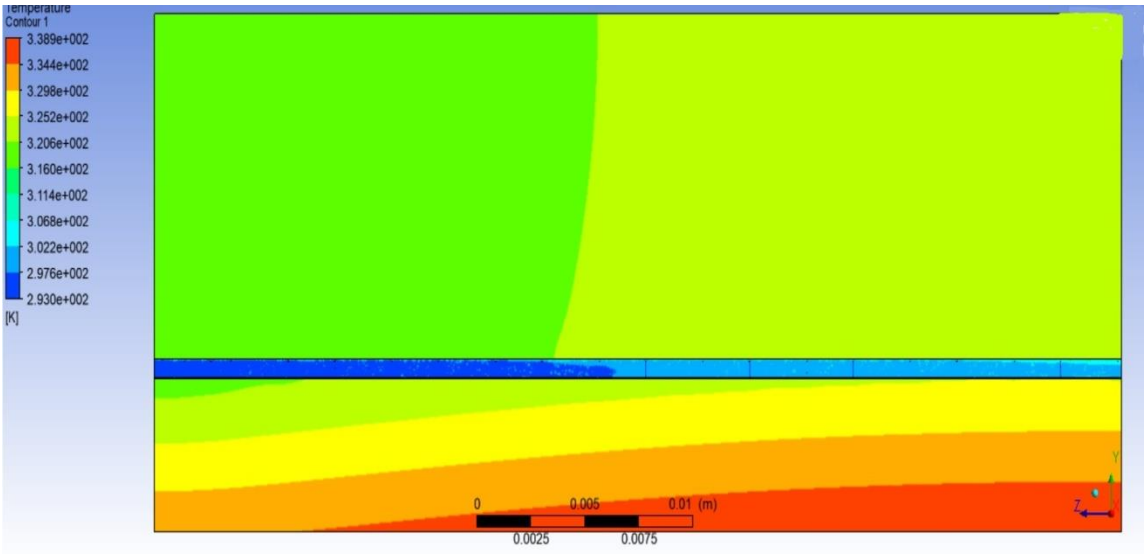

Fig 6.14: Contours of temperature of heat sink and water at Re=1190

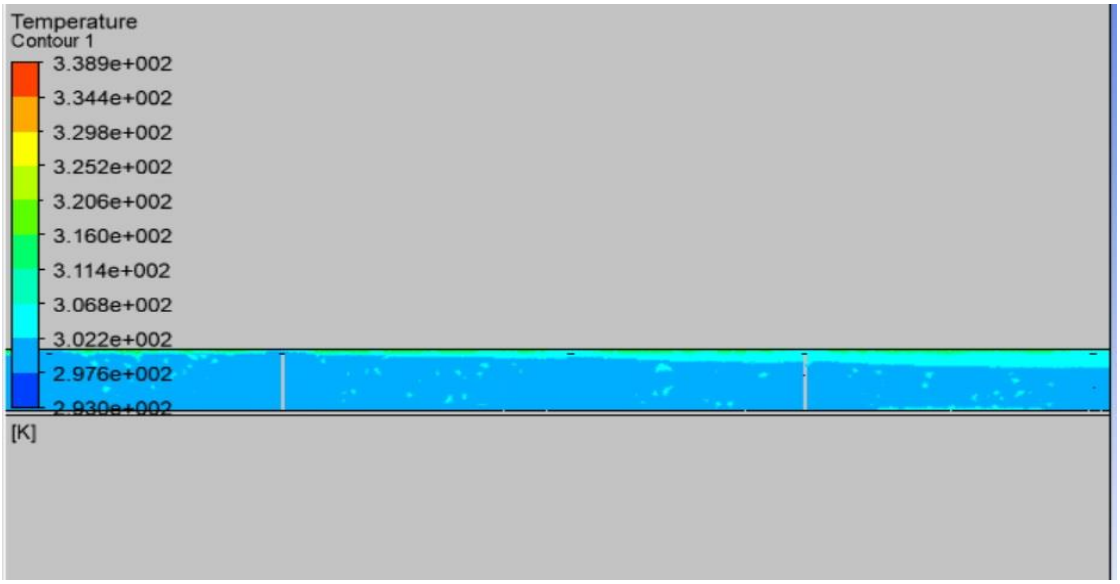

Figure 6.15: Contours of temperature at outlet at Re=1190

(i) In the Figures 6.13 to 6.15, contours of temperature and pressure are shown for a single phase microchannel heat sink with pillars at Reynolds number 1190.

(ii) In Figure 6.13, pressure penalty along the channel is 0.890 bar.

(iii) In Figure 6.15, outlet temperature of channel is 302.2 K

(iv) In Figure 6.14, the maximum temperature is at the base of the wall which is 338.9 K and the wall temperature seems to be increasing along the flow direction.

6.1.2 Heat Flux of 200 W/cm^2 applied at the bottom wall for different Reynolds number

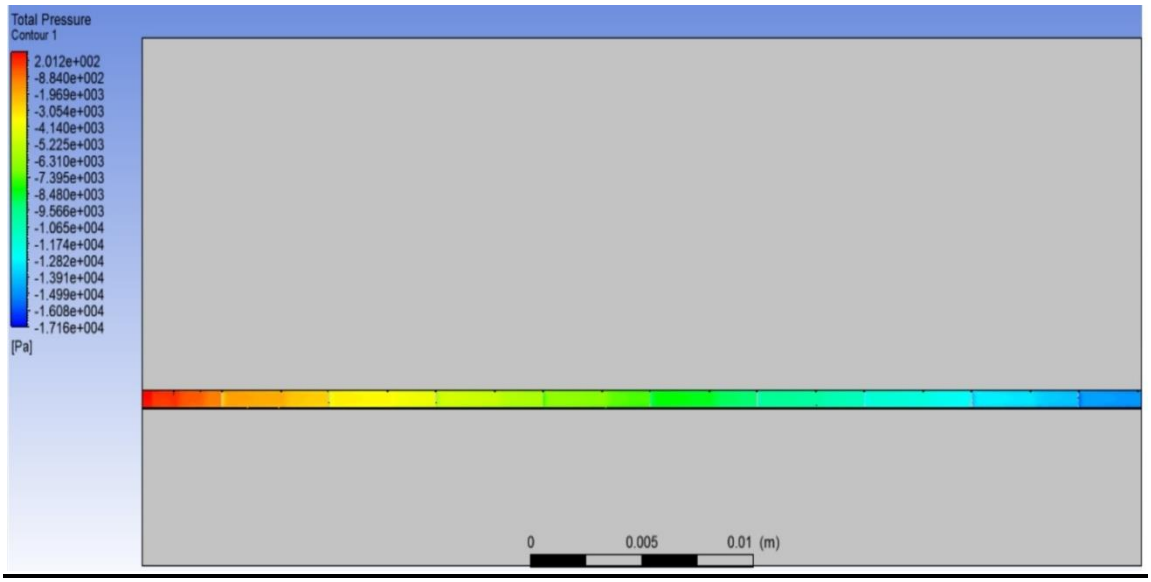

Fig 6.16: Contours of pressure at Re=390

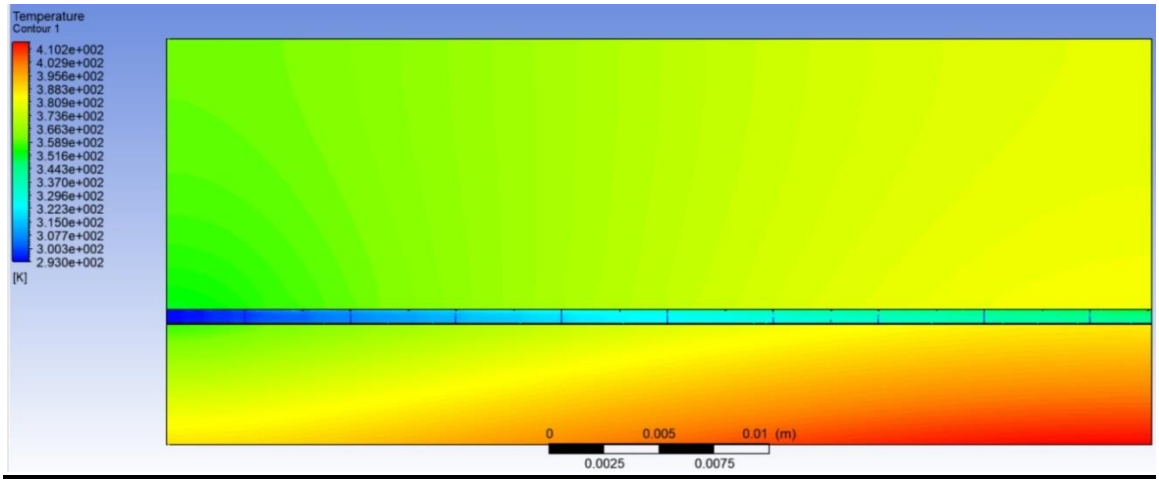

Fig 6.17: Contours of temperature of heat sink and water at Re=390

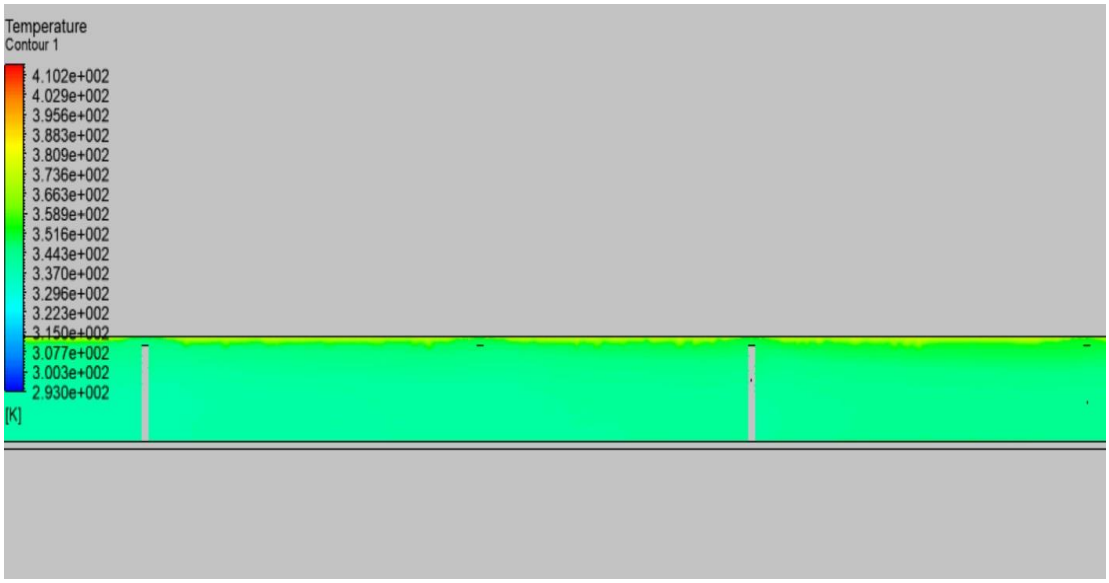

Figure 6.18: Contours of temperature at outlet at Re=390

(i) In the Figures 6.16 to 6.18, contours of temperature and pressure are shown for a single phase microchannel heat sink with pillars at Reynolds number 390.

(ii) In Figure 6.16, pressure penalty along the channel is 0.170 bar.

(iii) In Figure 6.18, outlet temperature of channel is 343.0 K

(iv) In Figure 6.17, the maximum temperature is at the base of the wall which is 410.2 K and the wall temperature seems to be increasing along the flow direction.

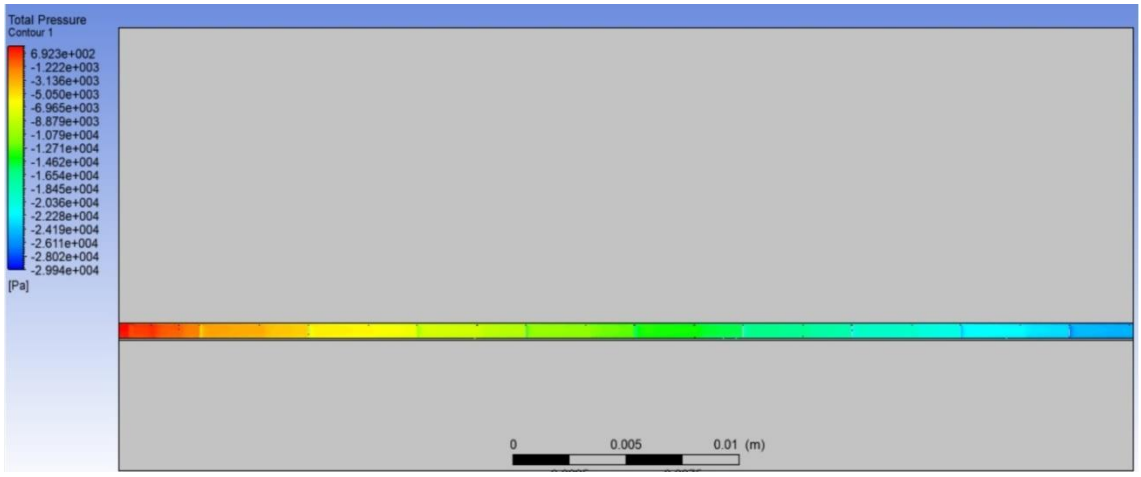

Fig 6.19: Contours of pressure at Re=590

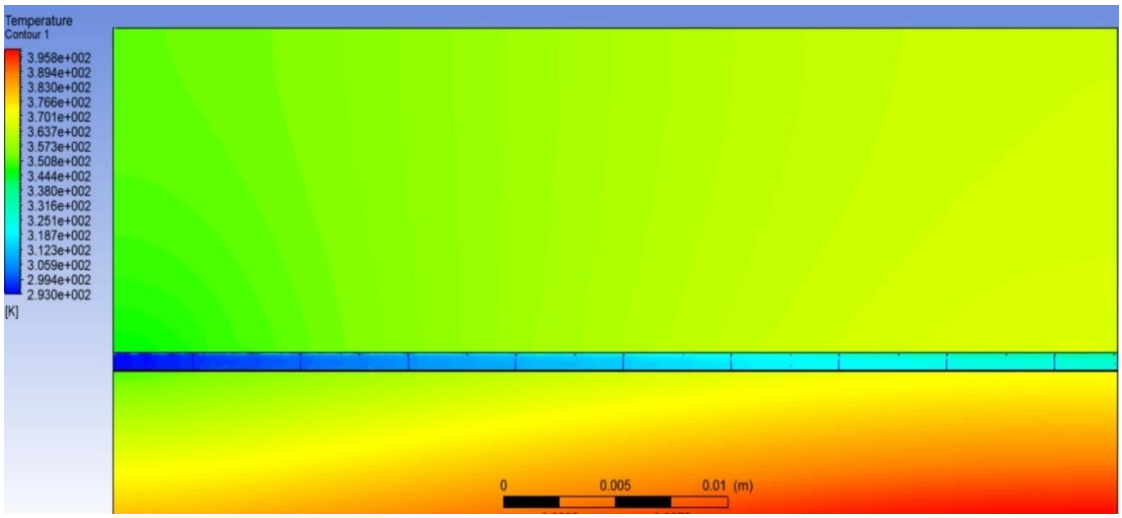

Fig 6.20: Contours of temperature of heat sink and water at Re=590

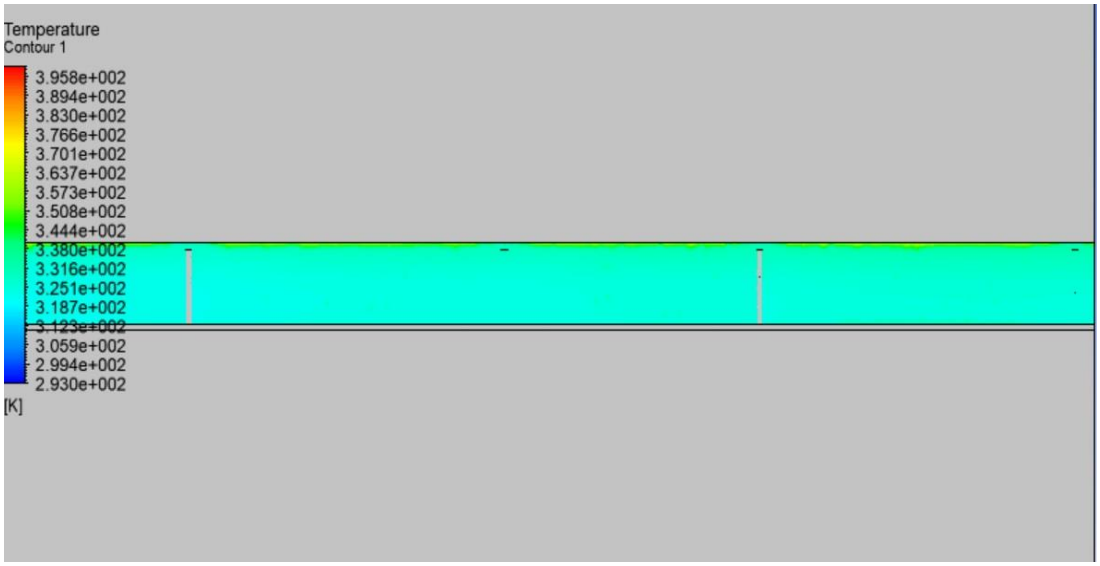

Figure 6.21: Contours of temperature at outlet at Re=590

(i) In the Figures 6.19 to 6.21, contours of temperature and pressure are shown for a single phase microchannel heat sink with pillars at Reynolds number 590.

(ii) In Figure 6.19, pressure penalty along the channel is 0.306 bar.

(iii) In Figure 6.21, outlet temperature of channel is 332.0 K

(iv) In Figure 6.20, the maximum temperature is at the base of the wall which is 395.8 K and the wall temperature seems to be increasing along the flow direction.

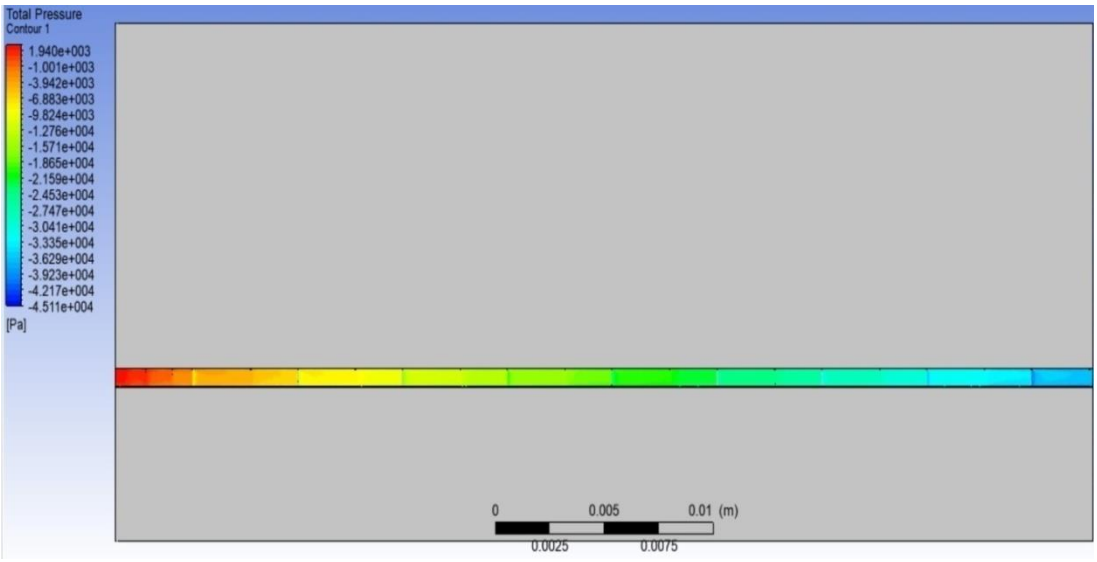

Fig 6.22: Contours of pressure at Re=790

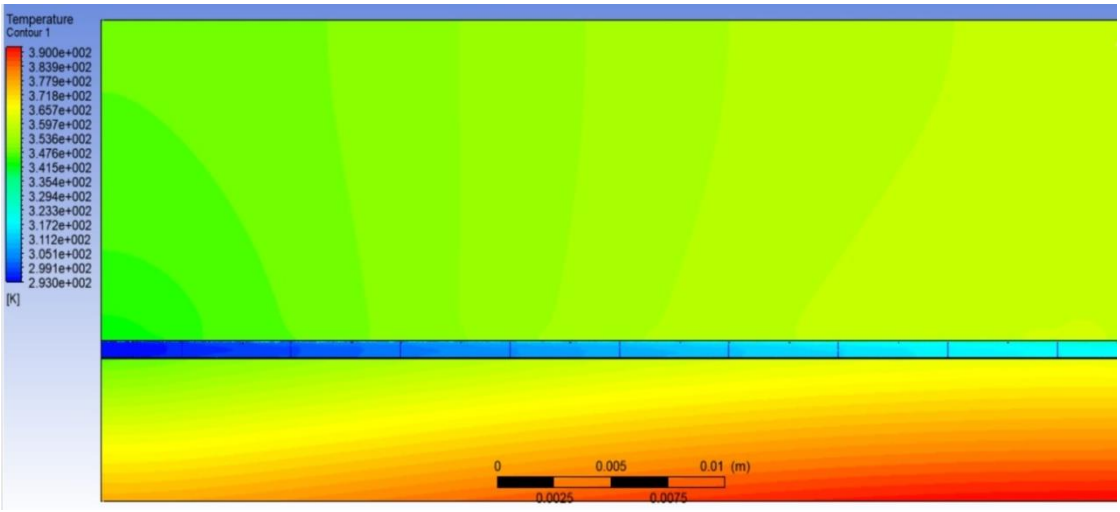

Fig 6.23: Contours of temperature of heat sink and water at Re=790

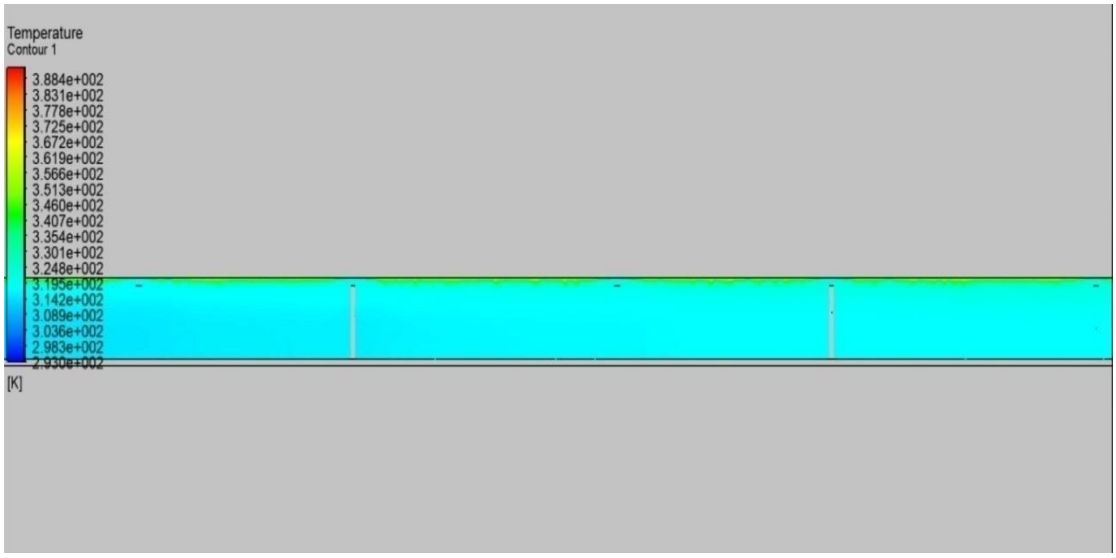

Figure 6.24: Contours of temperature at outlet at Re=790

(i) In the Figures 6.22 to 6.24, contours of temperature and pressure are shown for a single phase microchannel heat sink with pillars at Reynolds number 790.

(ii) In Figure 6.22, pressure penalty along the channel is 0.450 bar.

(iii) In Figure 6.24, outlet temperature of channel is 320.0 K

(iv) In Figure 6.23, the maximum temperature is at the base of the wall which is 395.8 K and the wall temperature seems to be increasing along the flow direction.

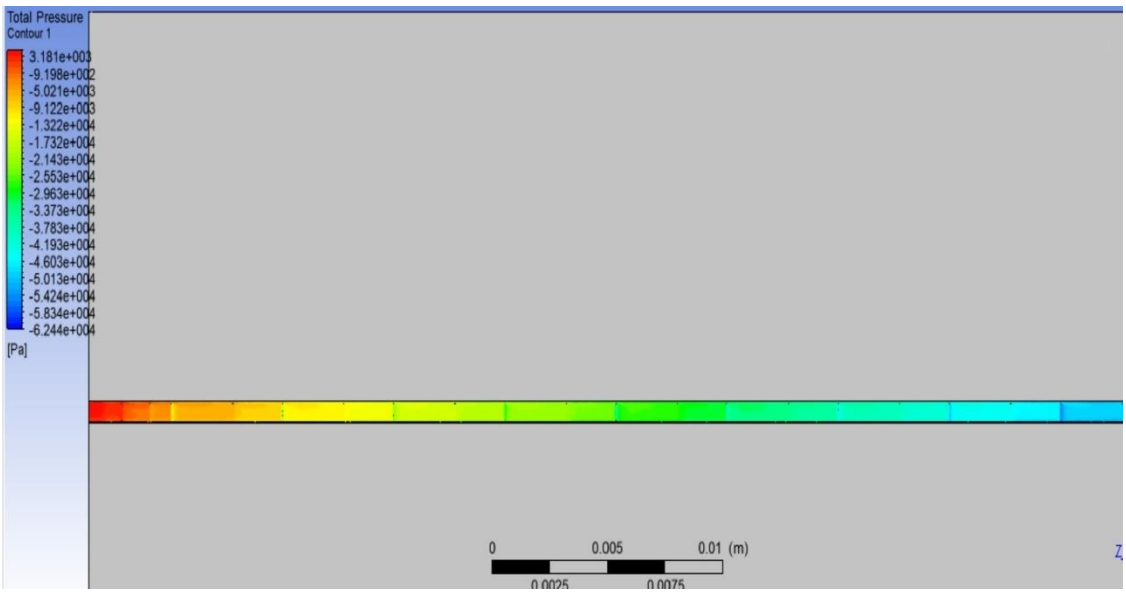

Fig 6.25: Contours of pressure at Re=990

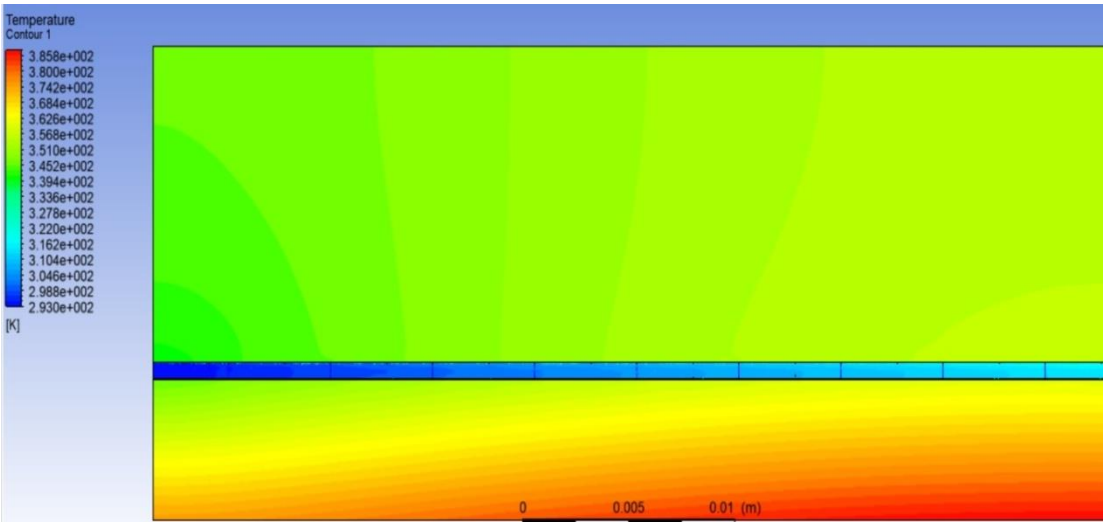

Fig 6.26: Contours of temperature of heat sink and water at Re=990

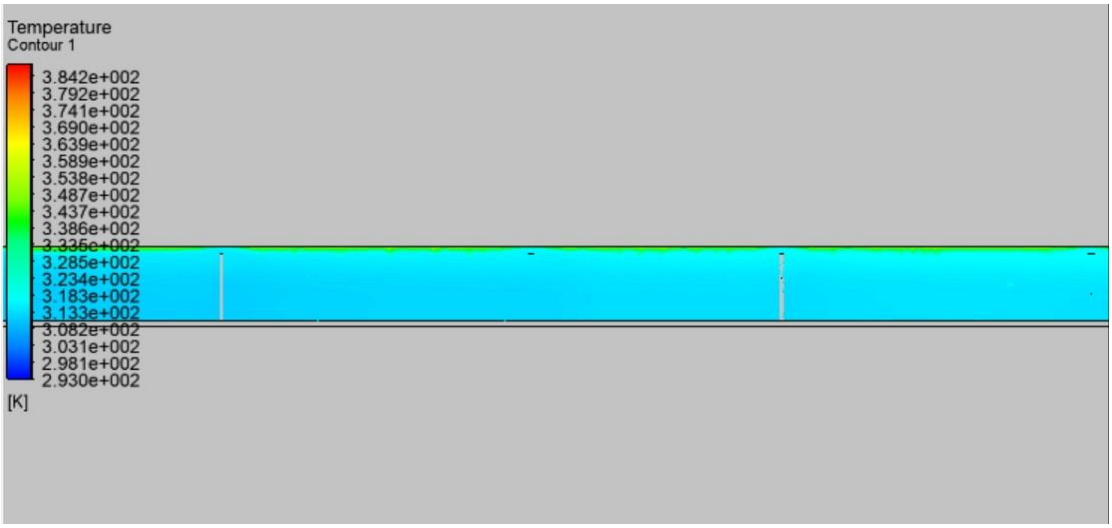

Figure 6.27: Contours of temperature at outlet at Re=990

(i) In the Figures 6.25 to 6.27, contours of temperature and pressure are shown for a single phase microchannel heat sink with pillars at Reynolds number 990.

(ii) In Figure 6.25, pressure penalty along the channel is 0.650 bar.

(iii) In Figure 6.27, outlet temperature of channel is 318.3 K

(iv) In Figure 6.26, the maximum temperature is at the base of the wall which is 385.8 K and the wall temperature seems to be increasing along the flow direction.

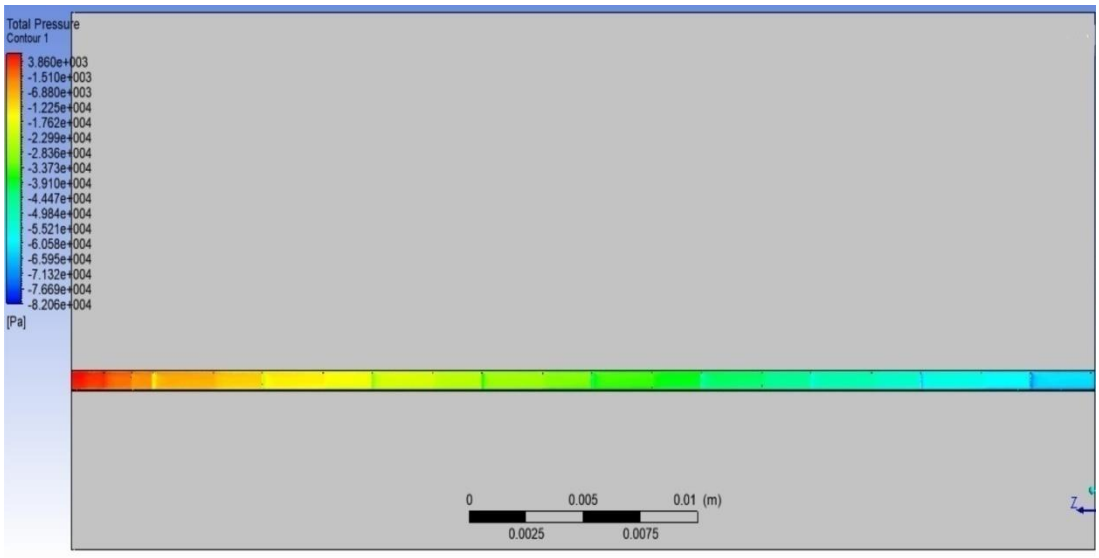

Fig 6.28: Contours of pressure at Re=1190

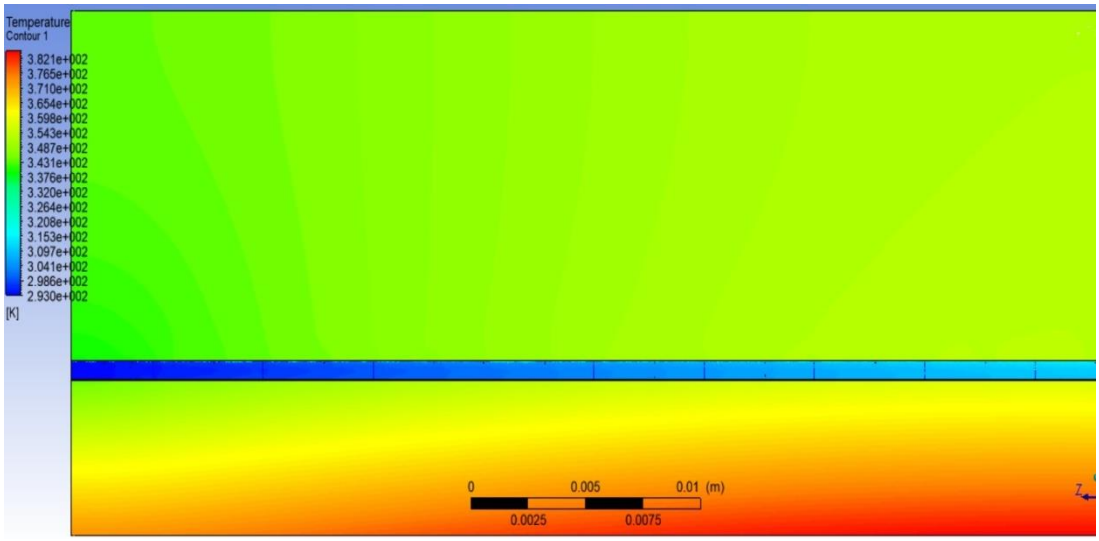

Fig 6.29: Contours of temperature of heat sink and water at Re=1190

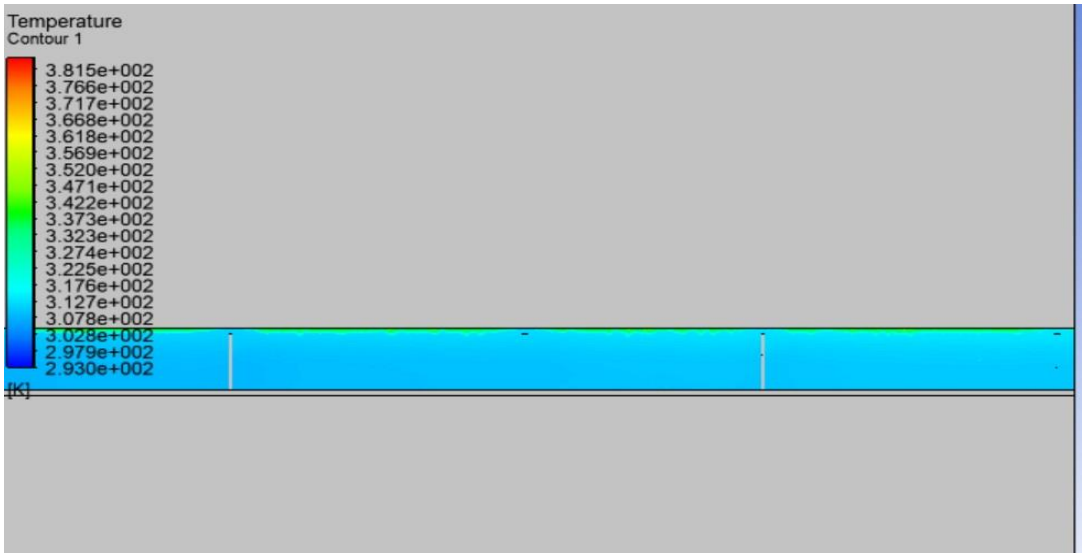

Figure 6.30: Contours of temperature at outlet at Re=1190

(i) In the Figures 6.28 to 6.30, contours of temperature and pressure are shown for a single phase microchannel heat sink with pillars at Reynolds number 1190.

(ii) In Figure 6.28, pressure penalty along the channel is 0.860 bar.

(iii) In Figure 6.30, outlet temperature of channel is 317.0 K

(iv) In Figure 6.29, the maximum temperature is at the base of the wall which is 382.1 K and the wall temperature seems to be increasing along the flow direction.

6.1.3 New Heat Flux of 125 W/cm^2 applied at the bottom wall for different Reynolds number

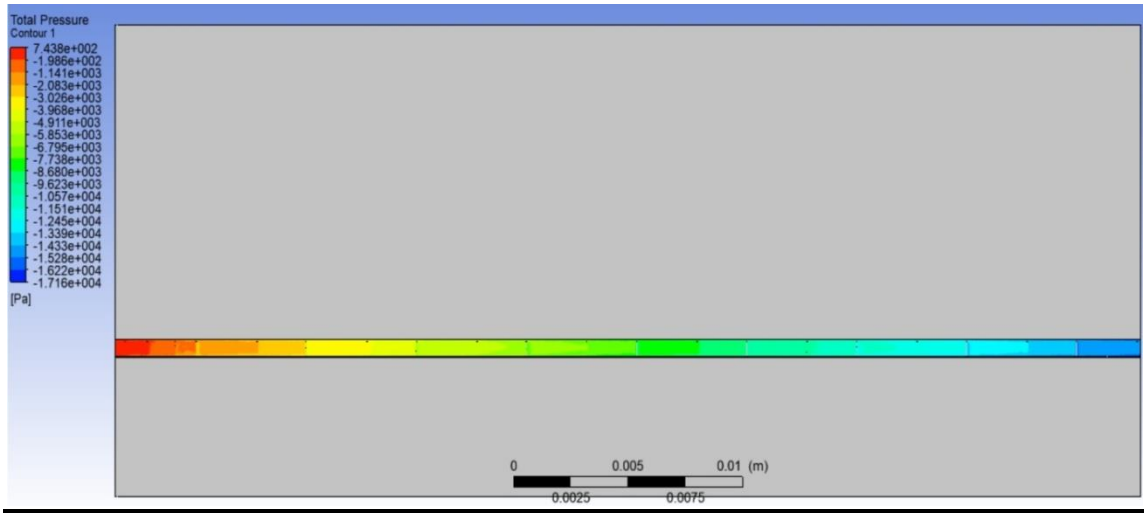

Fig 6.31: Contours of pressure at Re=390

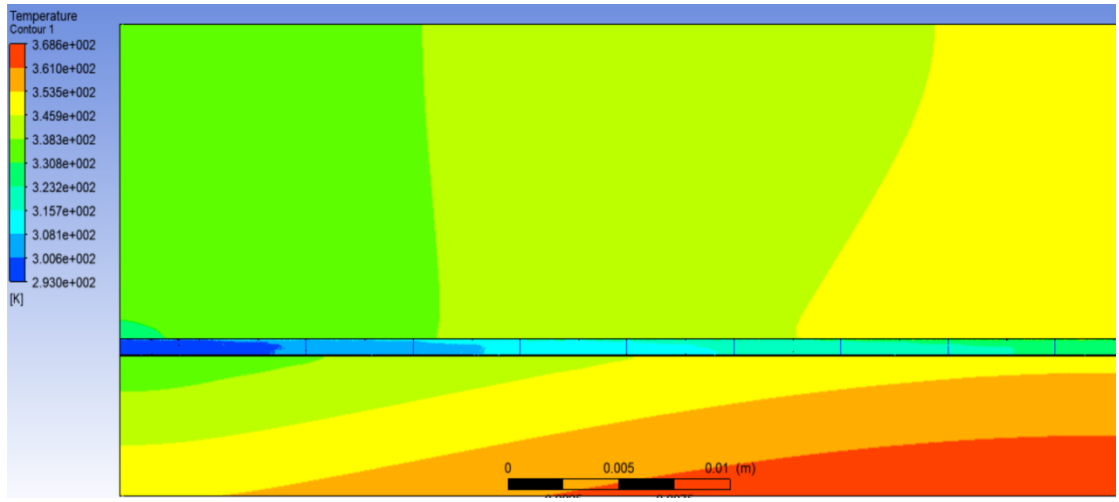

Fig 6.32: Contours of temperature of heat sink and water at Re=390

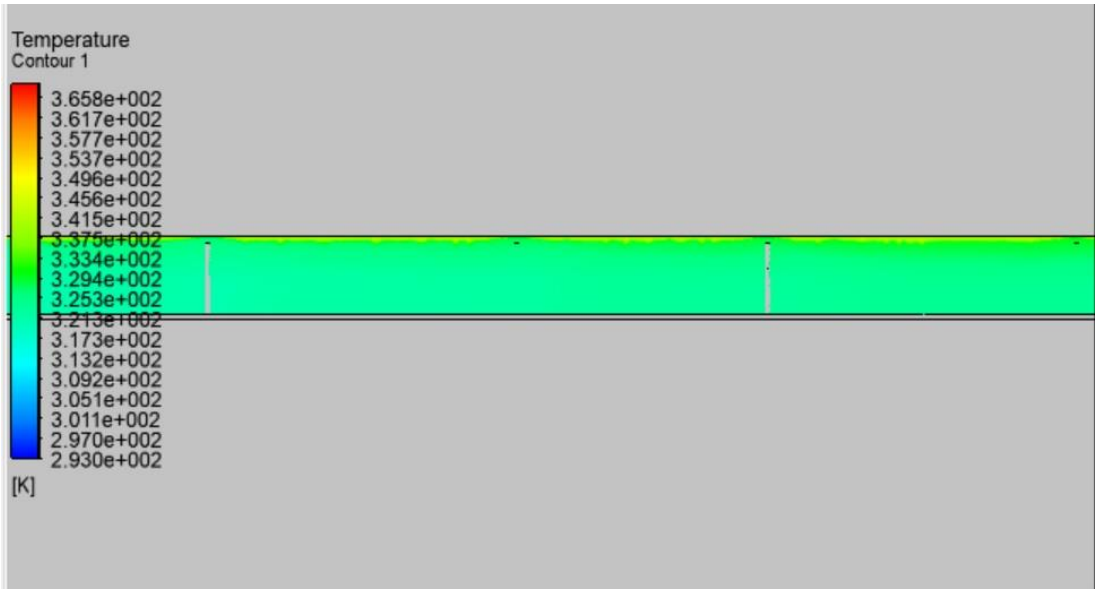

Figure 6.33: Contours of temperature at outlet at Re=390

(i) In the Figures 6.31 to 6.33, contours of temperature and pressure are shown for a single phase microchannel heat sink with pillars at Reynolds number 390.

(ii) In Figure 6.31, pressure penalty along the channel is 0.18 bar.

(iii) In Figure 6.33, outlet temperature of channel is 326.0 K

(iv) In Figure 6.32, the maximum temperature is at the base of the wall which is 368.6 K and the wall temperature seems to be increasing along the flow direction.

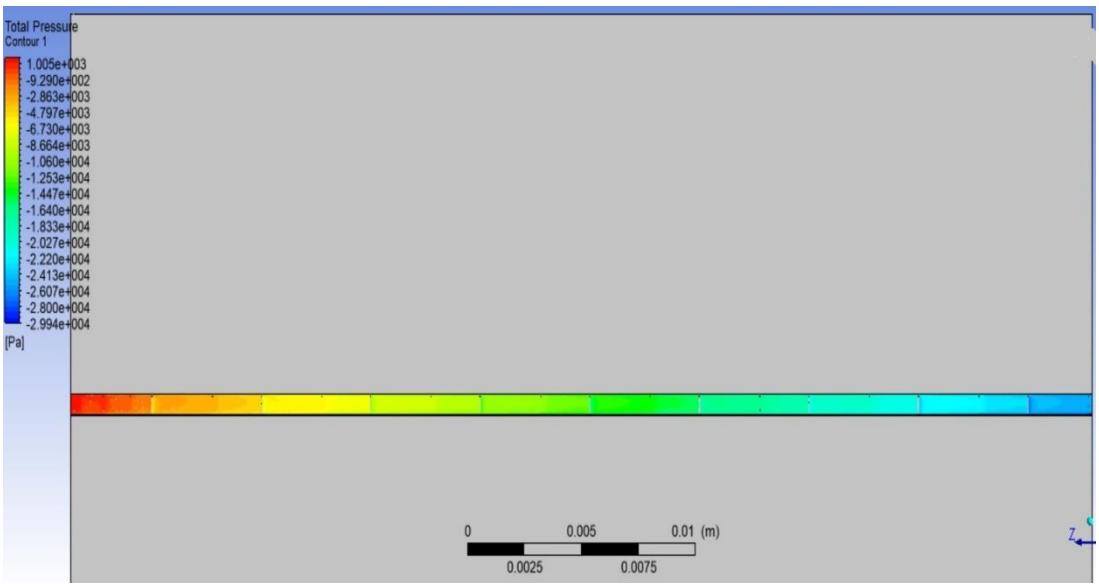

Fig 6.34: Contours of pressure at Re=590

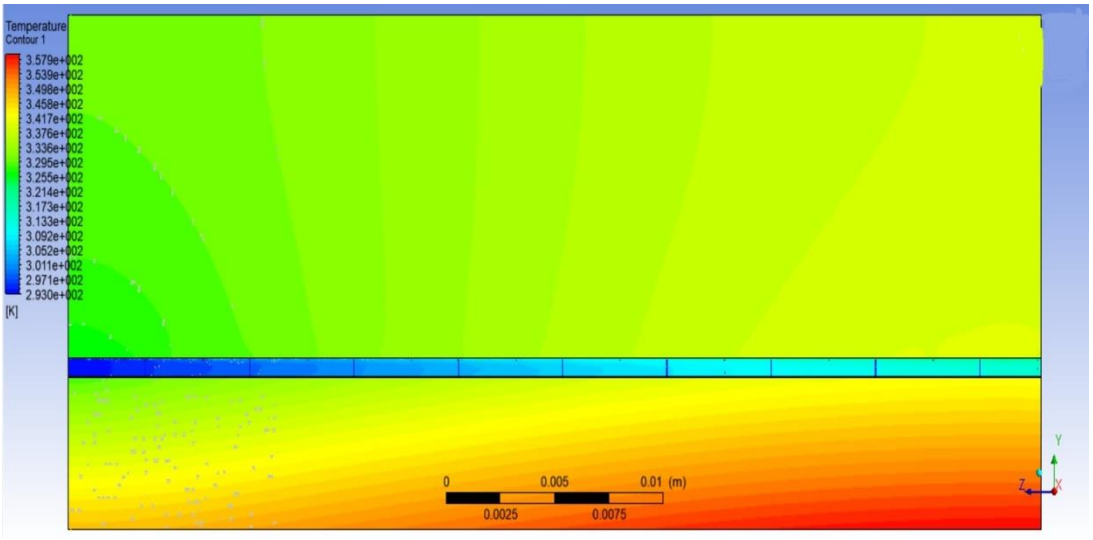

Fig 6.35: Contours of temperature of heat sink and water at Re=590

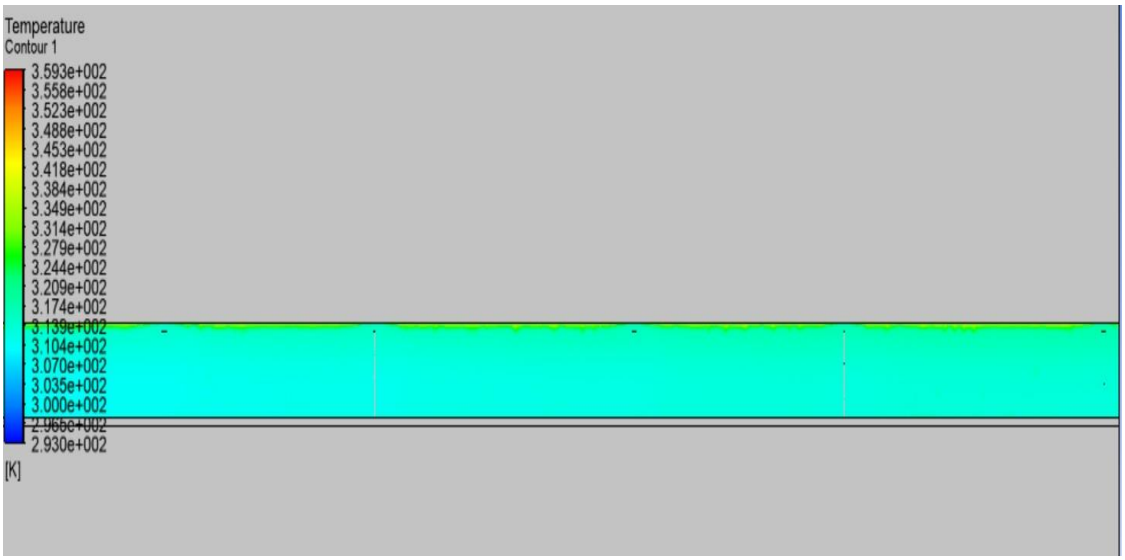

Figure 6.36: Contours of temperature at outlet at Re=590

(i) In the Figures 6.34 to 6.36, contours of temperature and pressure are shown for a single phase microchannel heat sink with pillars at Reynolds number 590.

(ii) In Figure 6.34, pressure penalty along the channel is 0.300 bar.

(iii) In Figure 6.36, outlet temperature of channel is 318.0 K

(iv) In Figure 6.35, the maximum temperature is at the base of the wall which is 358.0 K and the wall temperature seems to be increasing along the flow direction.

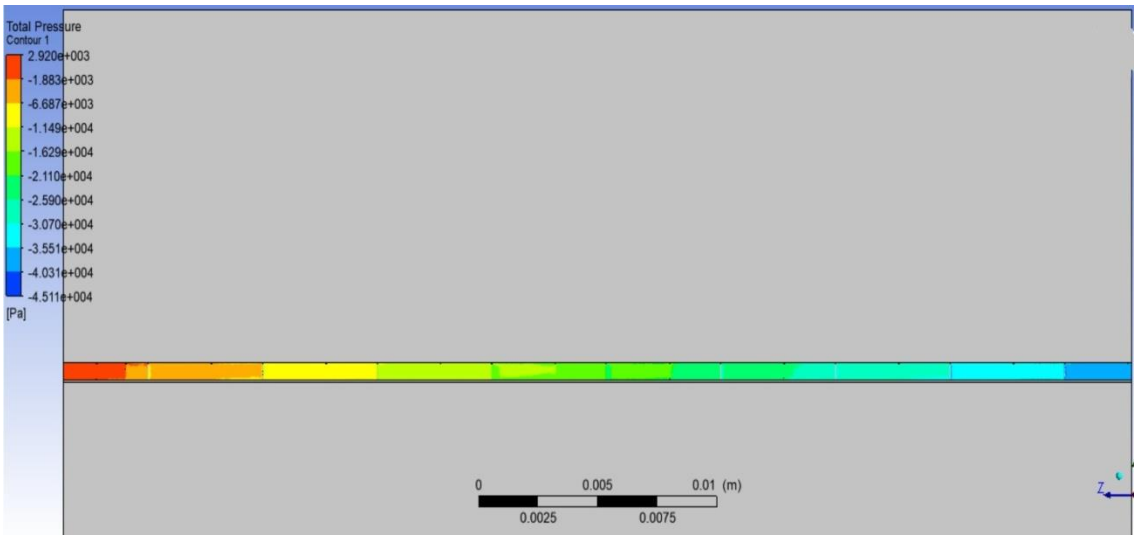

Fig 6.37: Contours of pressure at Re=790

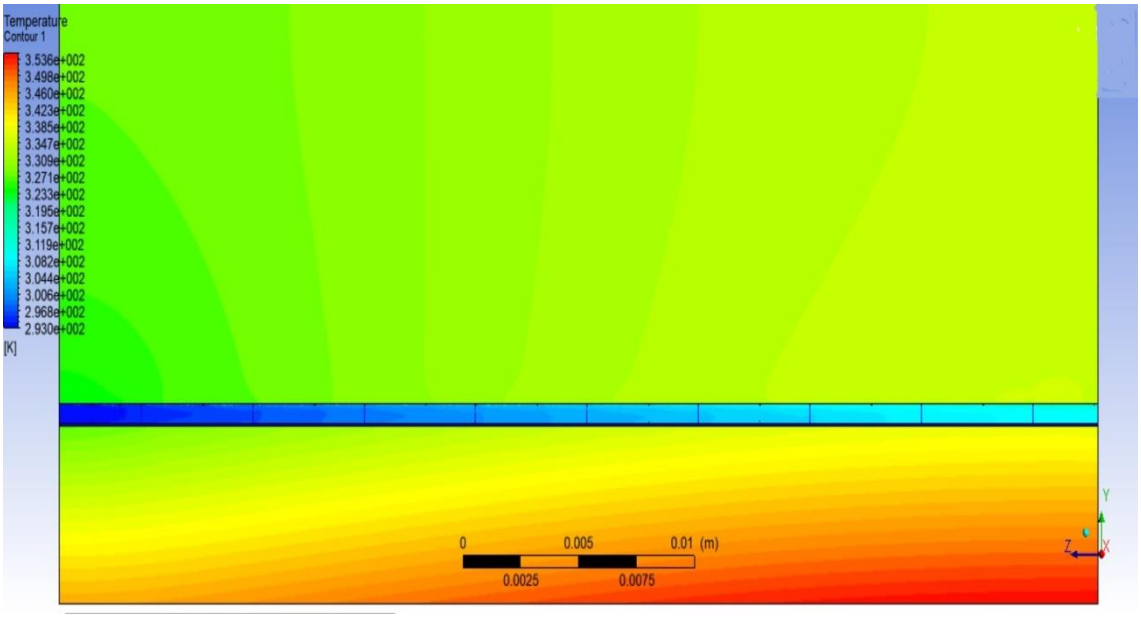

Fig 6.38: Contours of temperature of heat sink and water at Re=790

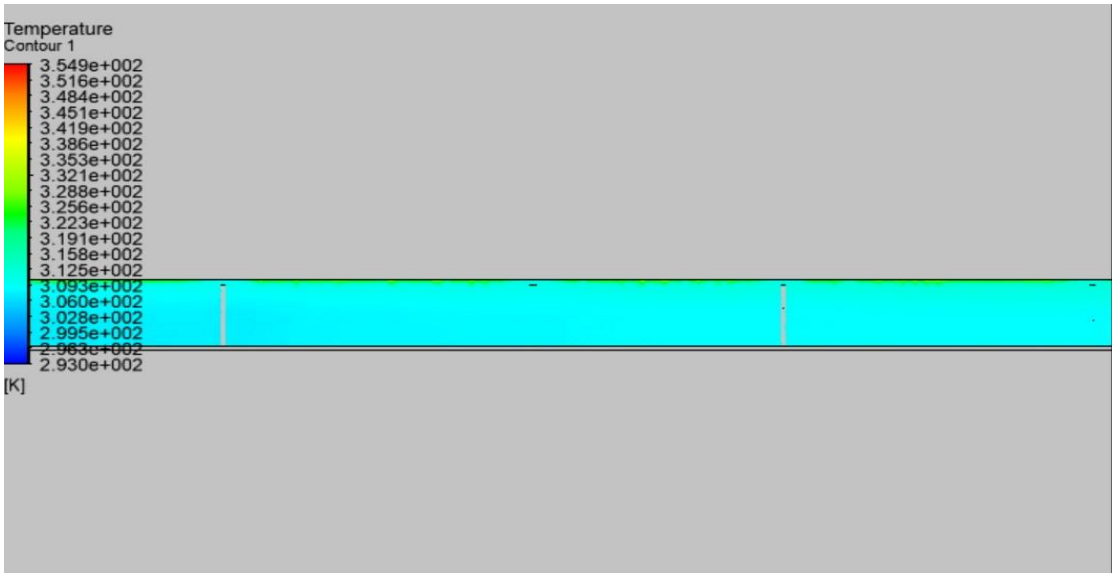

Figure 6.39: Contours of temperature at outlet at Re=790

(i) In the Figures 6.37 to 6.39, contours of temperature and pressure are shown for a single phase microchannel heat sink with pillars at Reynolds number 790.

(ii) In Figure 6.37, pressure penalty along the channel is 0.480 bar.

(iii) In Figure 6.39, outlet temperature of channel is 313.0 K

(iv) In Figure 6.38, the maximum temperature is at the base of the wall which is 354.0 K and the wall temperature seems to be increasing along the flow direction.

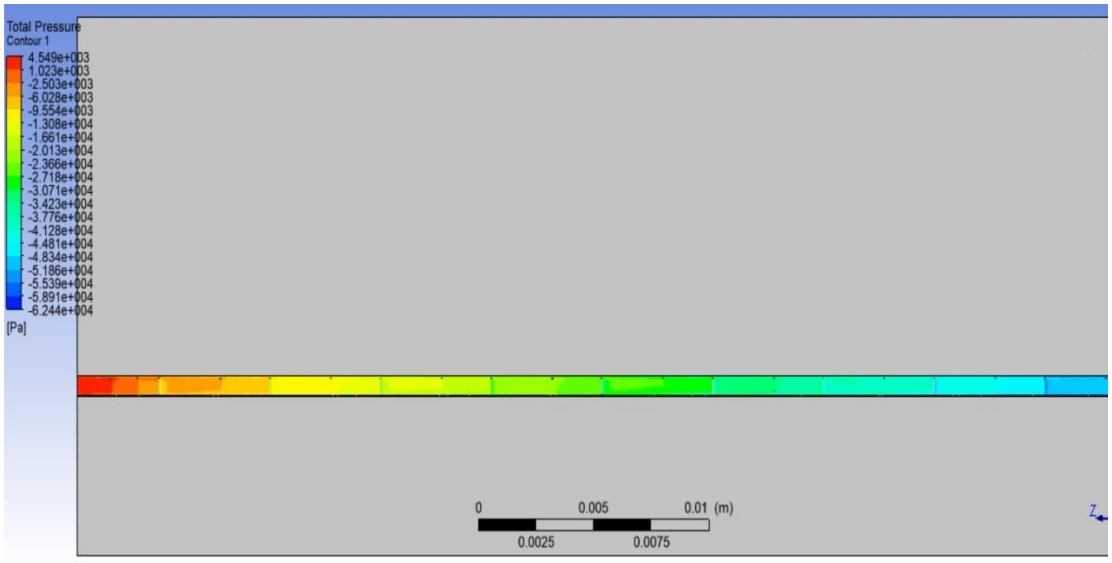

Fig 6.40: Contours of pressure at Re=990

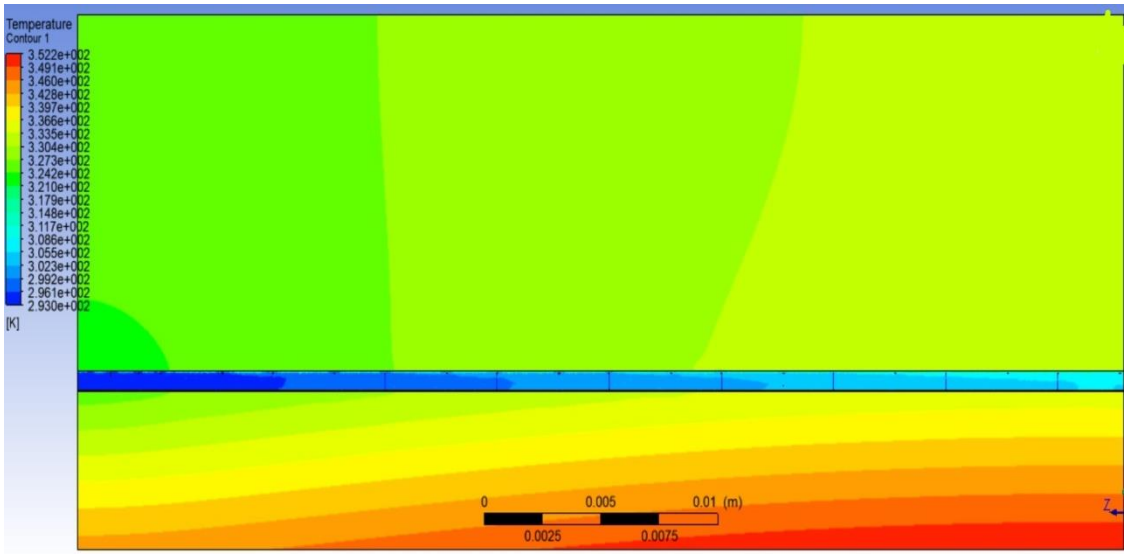

Fig 6.41: Contours of temperature of heat sink and water at Re=990

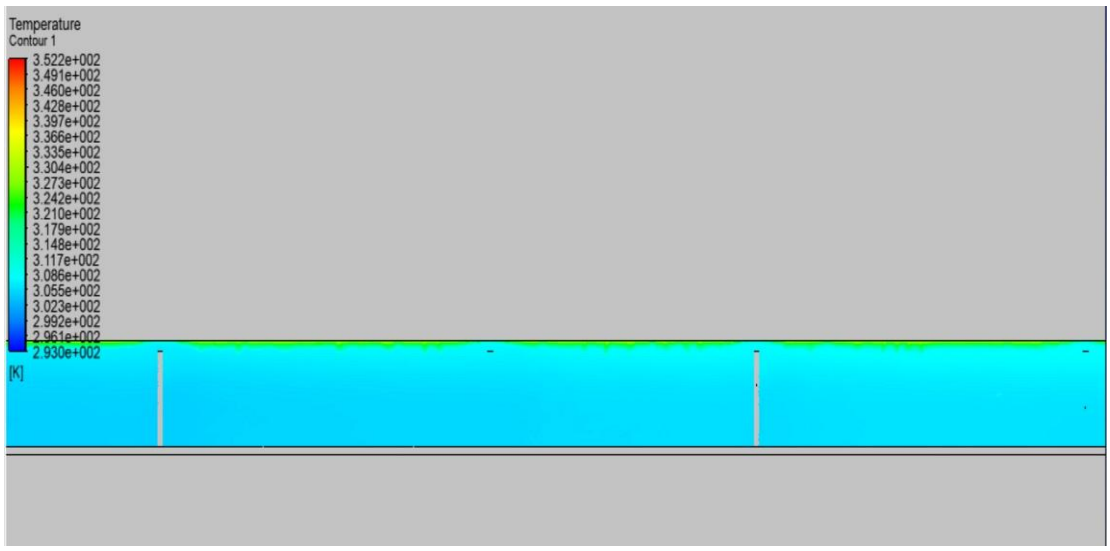

Figure 6.42: Contours of temperature at outlet at Re=990

(i) In the Figures 6.40 to 6.42, contours of temperature and pressure are shown for a single phase microchannel heat sink with pillars at Reynolds number 990.

(ii) In Figure 6.40, pressure penalty along the channel is 0.670 bar.

(iii) In Figure 6.42, outlet temperature of channel is 309.0 K

(iv) In Figure 6.41, the maximum temperature is at the base of the wall which is 352.2 K and the wall temperature seems to be increasing along the flow direction.

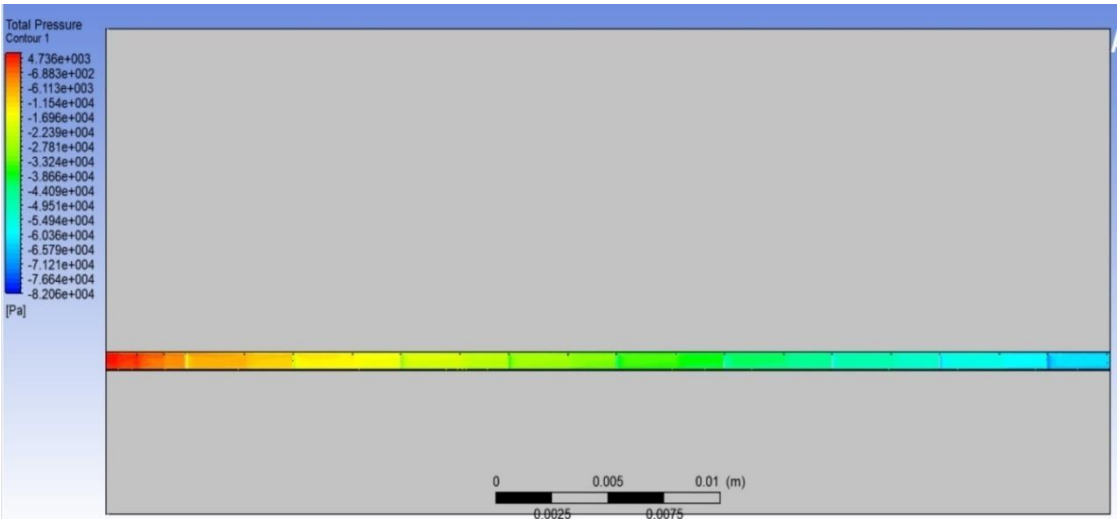

Fig 6.43: Contours of pressure at Re=1190

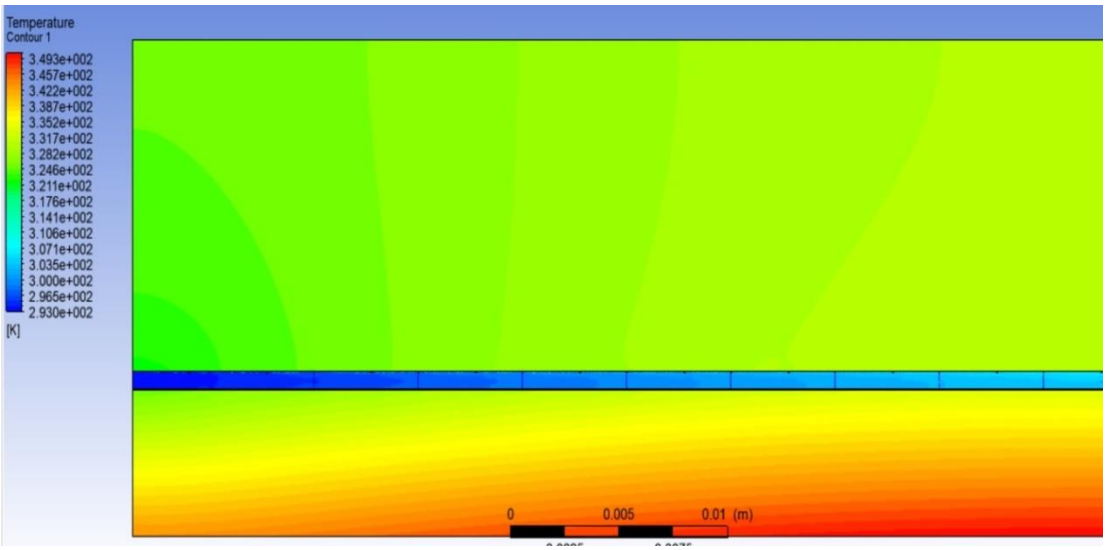

Fig 6.44: Contours of temperature of heat sink and water at Re=1190

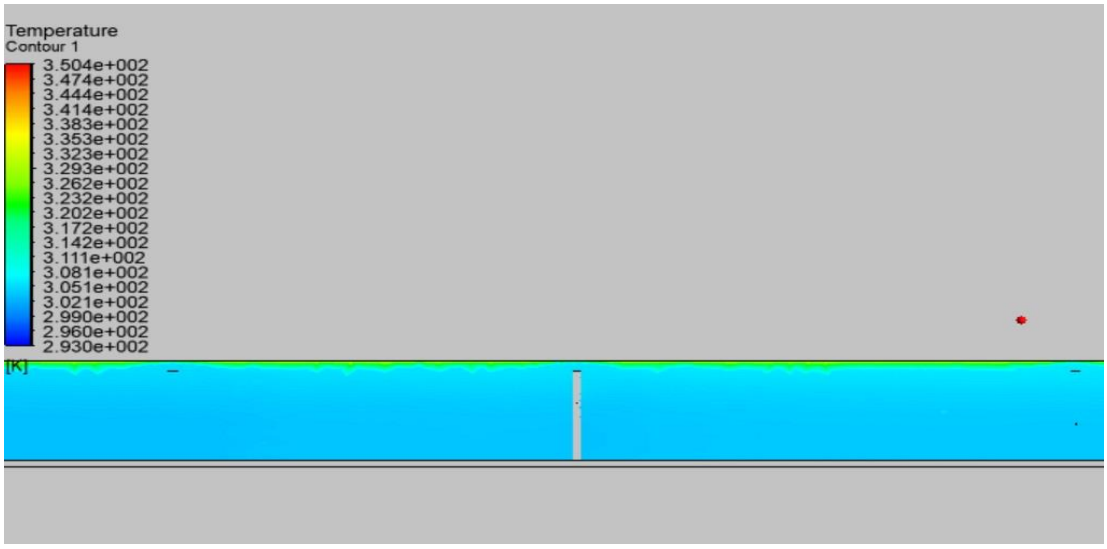

Figure 6.45: Contours of temperature at outlet at Re=1190

(i) In the Figures 6.43 to 6.45, contours of temperature and pressure are shown for a single phase microchannel heat sink with pillars at Reynolds number 1190.

(ii) In Figure 6.43, pressure penalty along the channel is 0.870 bar.

(iii) In Figure 6.45, outlet temperature of channel is 308.0 K

(iv) In Figure 6.44, the maximum temperature is at the base of the wall which is 350.0 K and the wall temperature seems to be increasing along the flow direction.

6.1.4 New Heat Flux of 225 W/cm^2 applied at the bottom wall for different Reynolds number

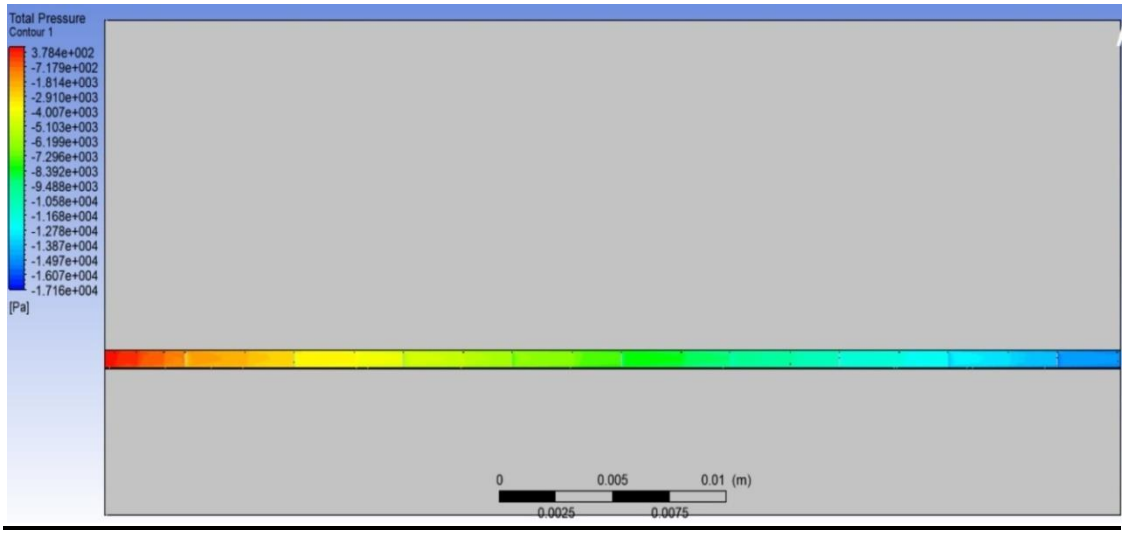

Fig 6.46: Contours of pressure at Re=390

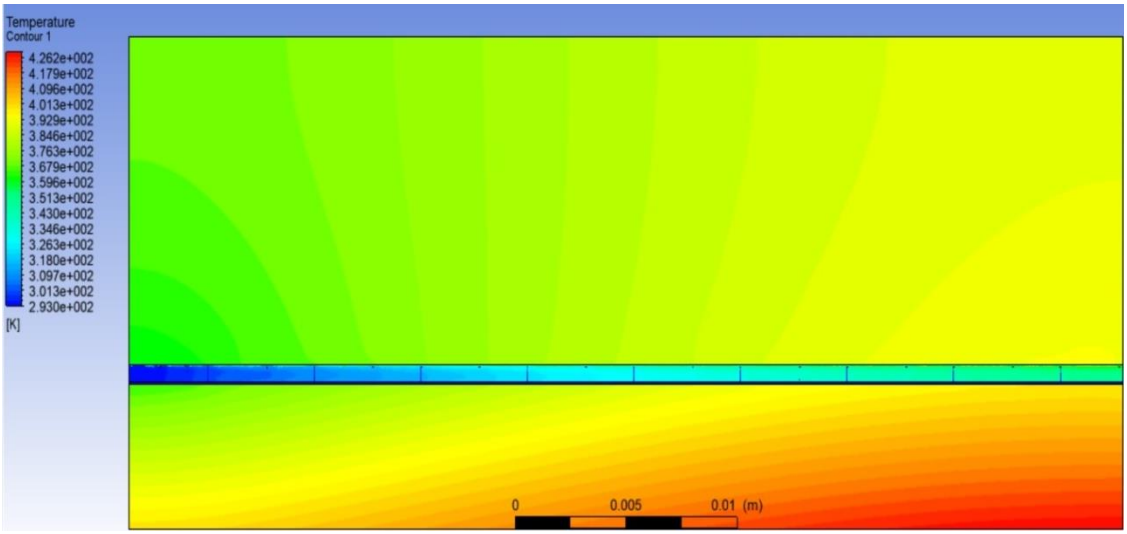

Fig 6.47: Contours of temperature of heat sink and water at Re=390

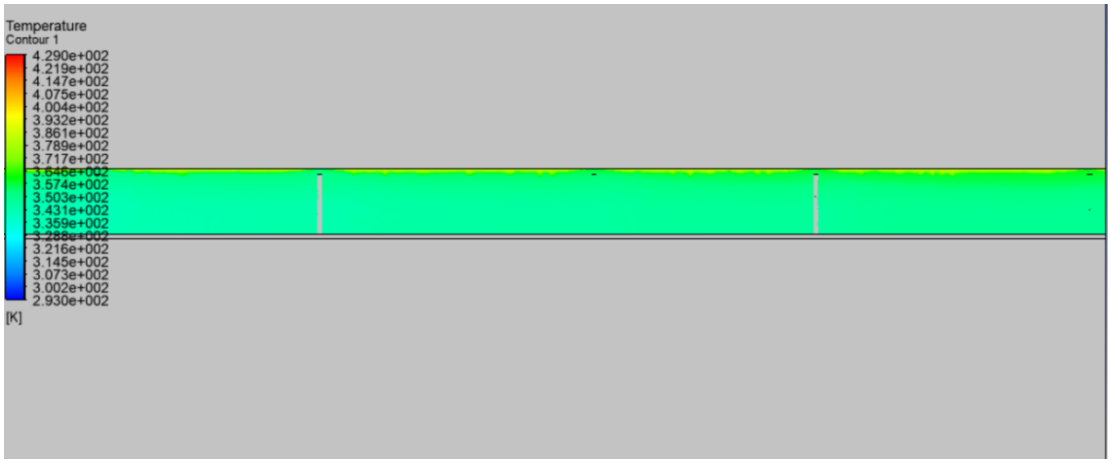

Figure 6.48: Contours of temperature at outlet at Re=390

(i) In the Figures 6.46 to 6.48, contours of temperature and pressure are shown for a single phase microchannel heat sink with pillars at Reynolds number 390.

(ii) In Figure 6.46, pressure penalty along the channel is 0.180 bar.

(iii) In Figure 6.48, outlet temperature of channel is 350.3 K

(iv) In Figure 6.47, the maximum temperature is at the base of the wall which is 426.2 K and the wall temperature seems to be increasing along the flow direction.

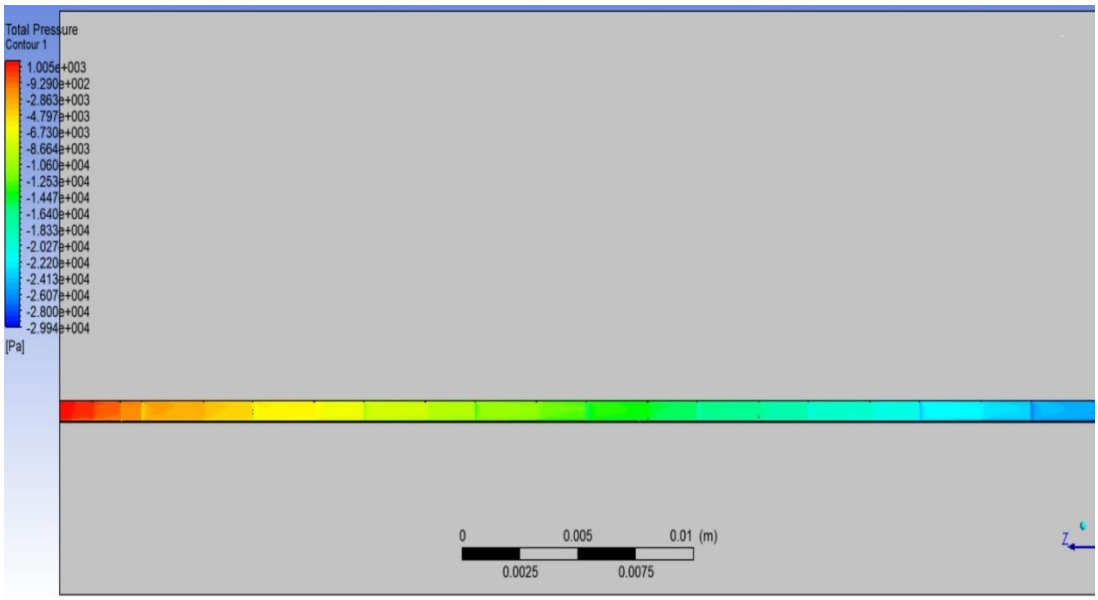

Fig 6.49: Contours of pressure at Re=590

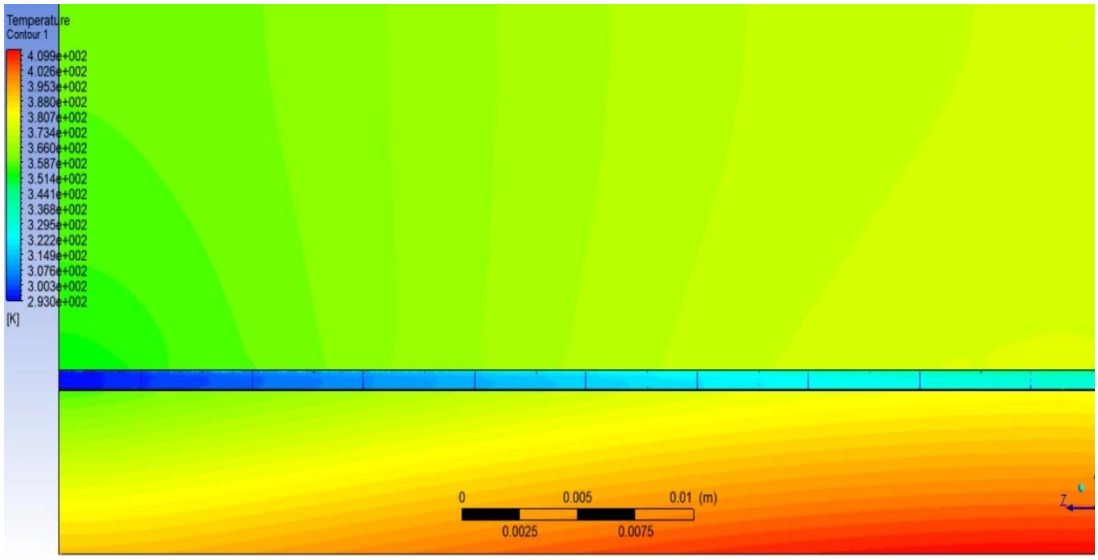

Fig 6.50: Contours of temperature of heat sink and water at Re=590

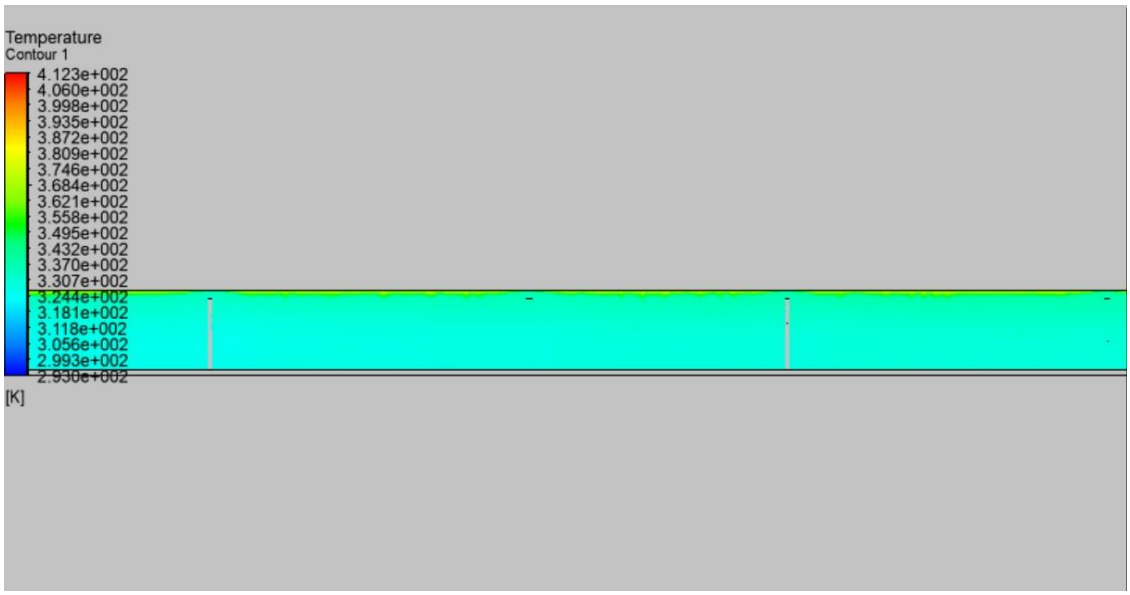

Figure 6.51: Contours of temperature at outlet at Re=590

(i) In the Figures 6.49 to 6.51, contours of temperature and pressure are shown for a single phase microchannel heat sink with pillars at Reynolds number 590.

(ii) In Figure 6.49, pressure penalty along the channel is 0.309 bar.

(iii) In Figure 6.51, outlet temperature of channel is 338.0 K

(iv) In Figure 6.50, the maximum temperature is at the base of the wall which is 412.0 K and the wall temperature seems to be increasing along the flow direction.

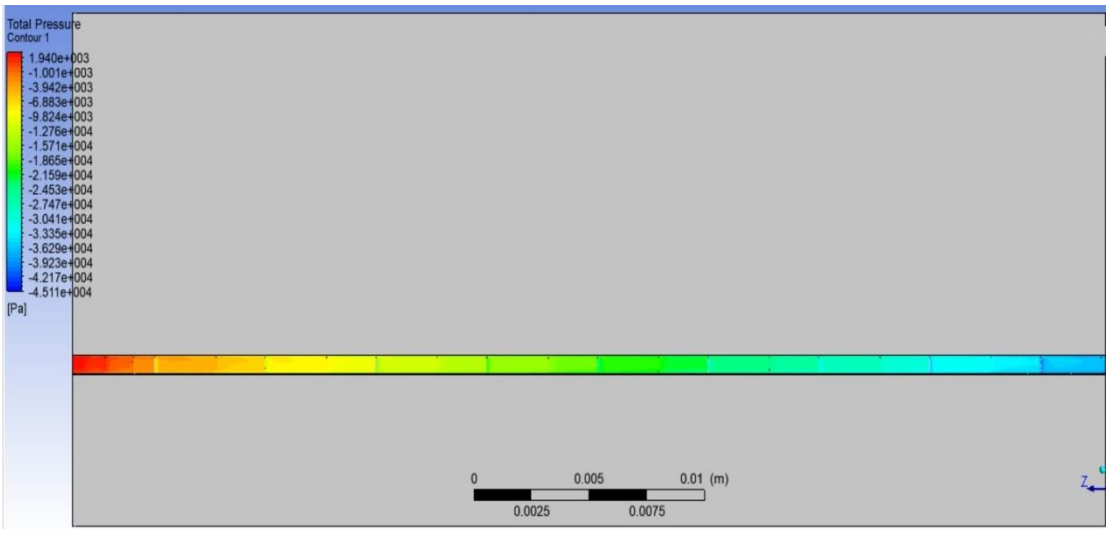

Fig 6.52: Contours of pressure at Re=790

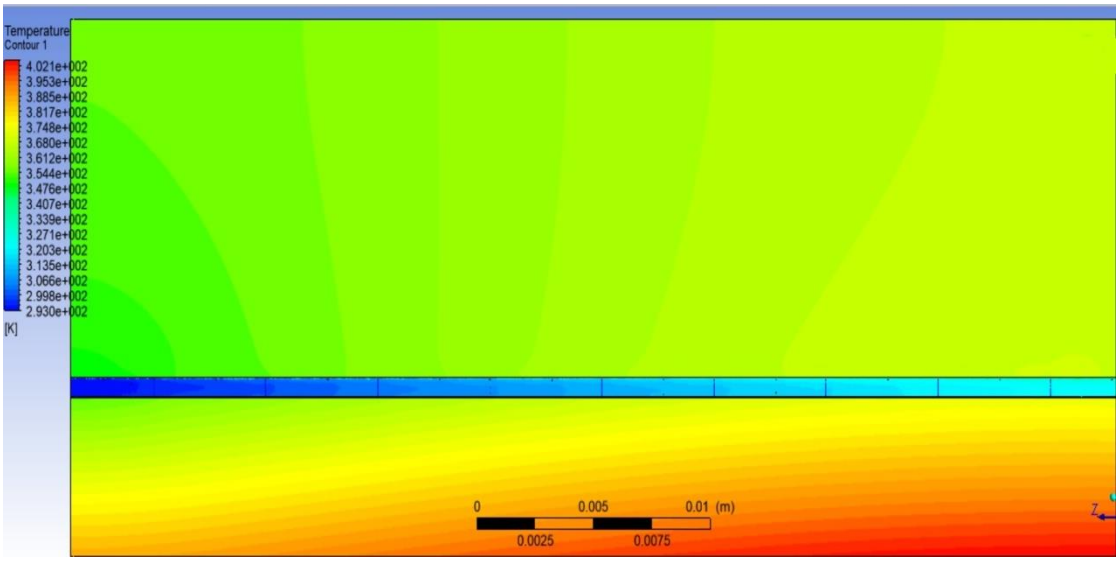

Fig 6.53: Contours of temperature of heat sink and water at Re=790

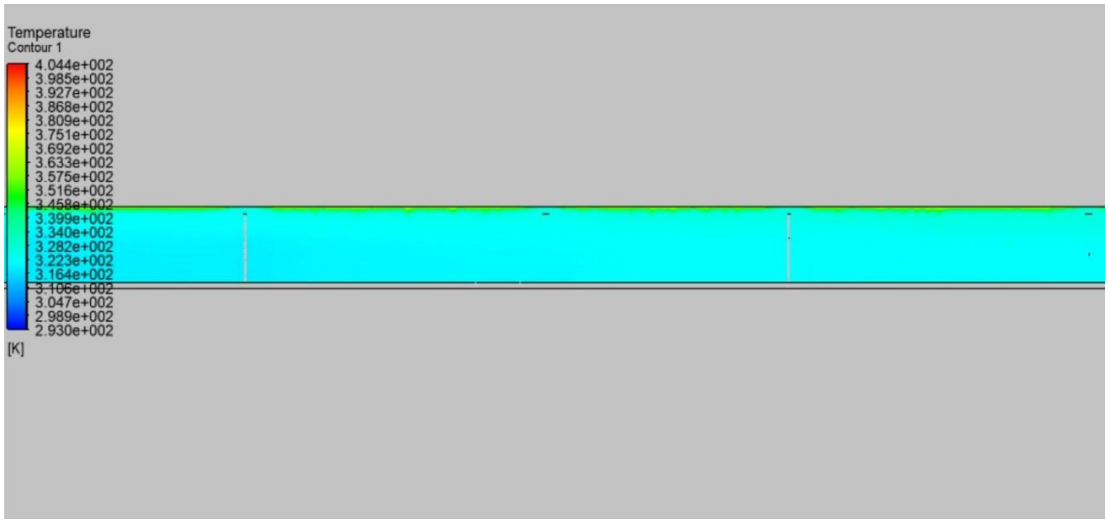

Figure 6.54: Contours of temperature at outlet at Re=790

(i) In the Figures 6.52 to 6.54, contours of temperature and pressure are shown for a single phase microchannel heat sink with pillars at Reynolds number 790.

(ii) In Figure 6.52, pressure penalty along the channel is 0.470 bar.

(iii) In Figure 6.54, outlet temperature of channel is 324.0 K

(iv) In Figure 6.53, the maximum temperature is at the base of the wall which is 404.4 K and the wall temperature seems to be increasing along the flow direction.

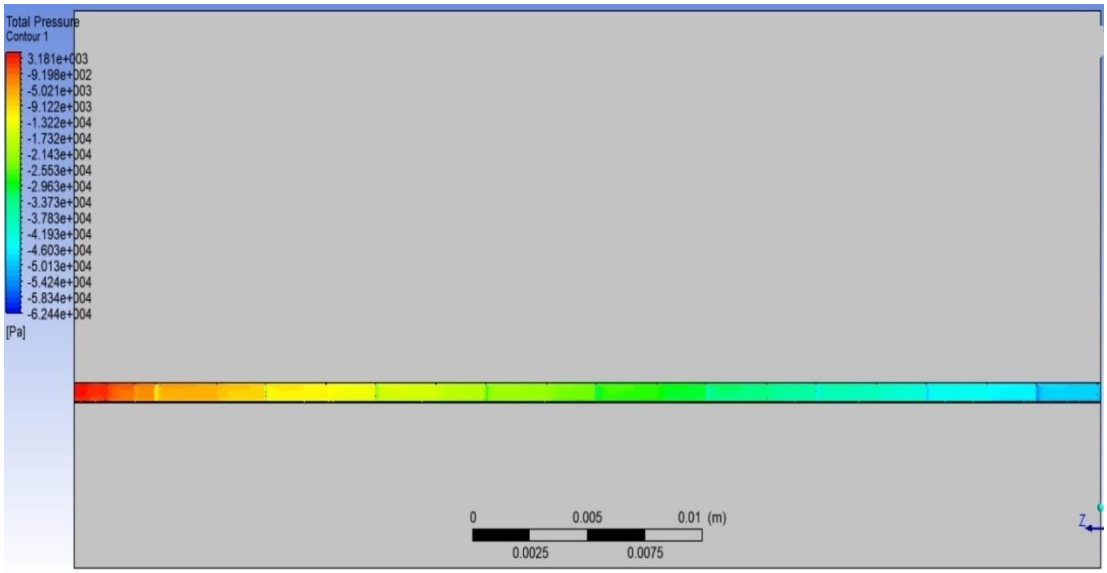

Fig 6.55: Contours of pressure at Re=990

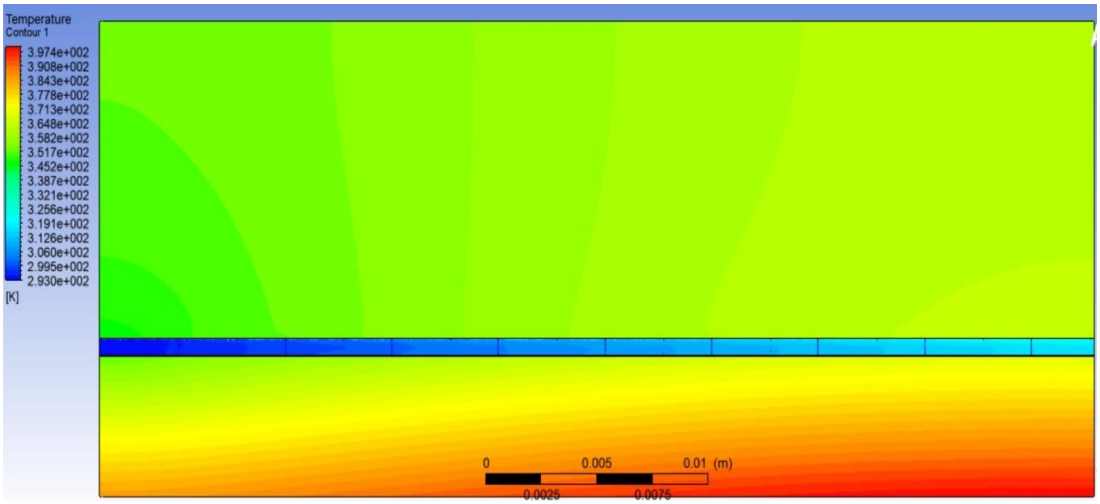

Fig 6.56: Contours of temperature of heat sink and water at Re=990

Figure 6.57: Contours of temperature at outlet at Re=990

(i) In the Figures 6.55 to 6.57, contours of temperature and pressure are shown for a single phase microchannel heat sink with pillars at Reynolds number 1190.

(ii) In Figure 6.55, pressure penalty along the channel is 0.660 bar.

(iii) In Figure 6.57, outlet temperature of channel is 321.0 K

(iv) In Figure 6.56, the maximum temperature is at the base of the wall which is 399.5 K and the wall temperature seems to be increasing along the flow direction.

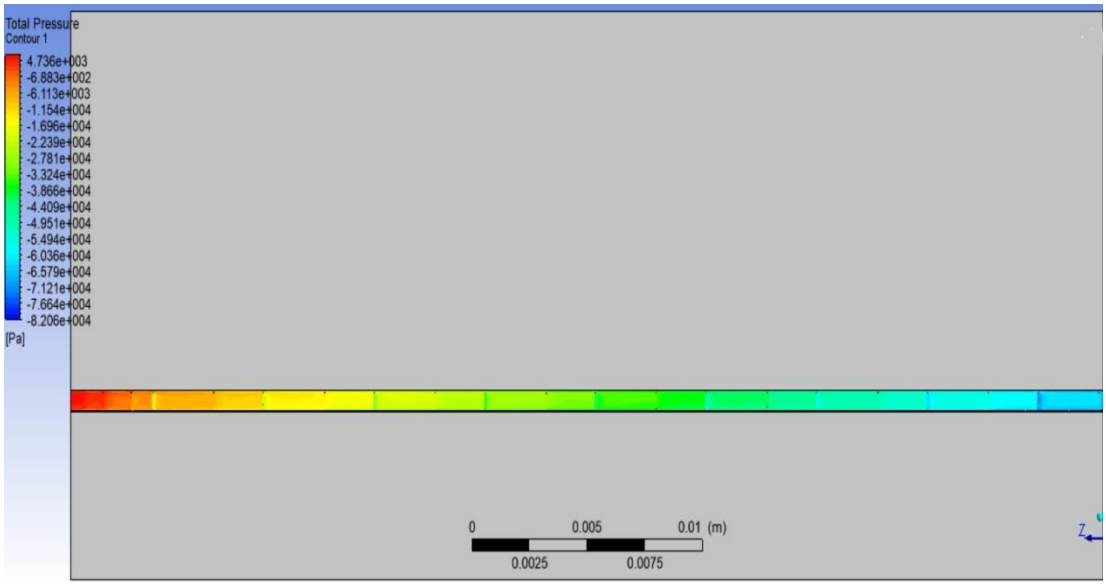

Fig 6.58: Contours of pressure at Re=1190

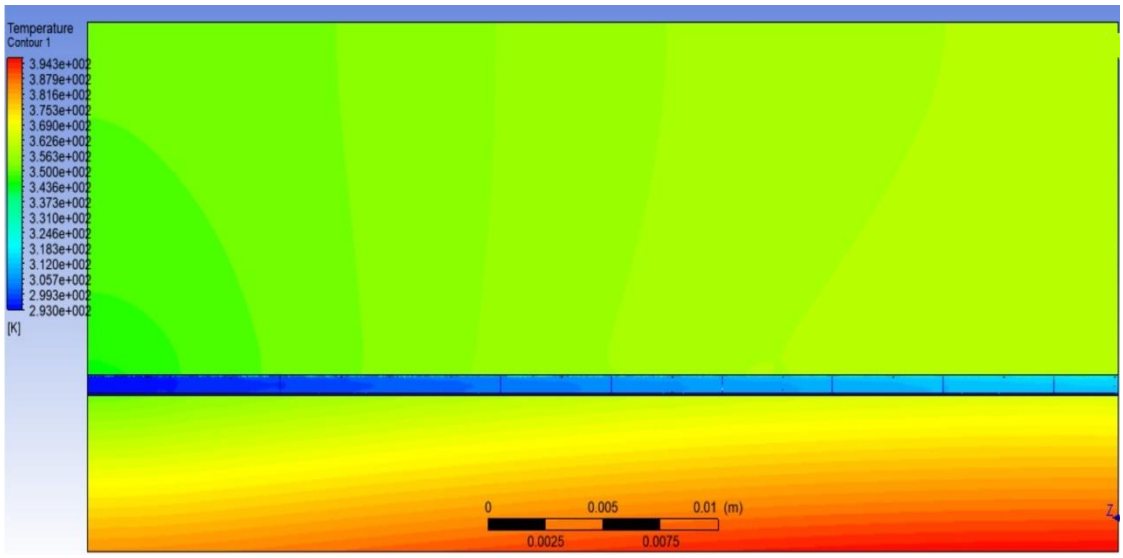

Fig 6.59: Contours of temperature of heat sink and water at Re=1190

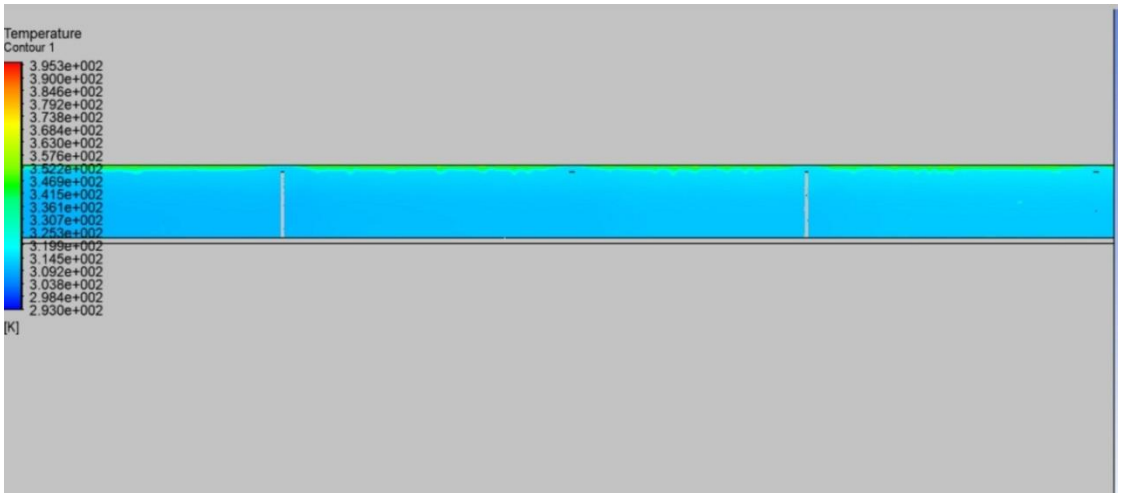

Figure 6.60: Contours of temperature at outlet at Re=1190

(i) In the Figures 6.58 to 6.60, contours of temperature and pressure are shown for a single phase microchannel heat sink with pillars at Reynolds number 1190.

(ii) In Figure 6.58, pressure penalty along the channel is 0.870 bar.

(iii) In Figure 6.60, outlet temperature of channel is 320.0 K

(iv) In Figure 6.59, the maximum temperature is at the base of the wall which is 395.0 K and the wall temperature seems to be increasing along the flow direction.

The pressure drop found out from the CFD analysis of rectangular microchannel heat sink with pillars from Figures 6.1, 6.4, 6.7, 6.10, 6.13 and has been tabulated corresponding to a heat flux of 100 W/cm^2 with varying Reynolds number.

Table 13: Pressure drop for heat flux=100W/cm^2

Reynolds number	Pressure drop from CFD (bar)
390	0.18
590	0.316
790	0.48
990	0.67
1190	0.89

The temperature rise found out from the CFD analysis of rectangular microchannel heat sink with pillars from Figures 6.3, 6.6, 6.9, 6.12, 6.15 and has been tabulated corresponding to a heat flux of 100 W/cm^2 with varying Reynolds number.

Table 14: Temperature rise for heat flux=100W/cm^2

Reynolds number	Temperature rise from CFD (K)
390	30.2
590	19
790	15
990	14.2
1190	9.2

The pressure drop found out from the CFD analysis of rectangular microchannel heat sink with pillars from Figures 6.16, 6.19, 6.22, 6.25, 6.28 and has been tabulated corresponding to a heat flux of 200 W/cm^2 with varying Reynolds number.

Table 15: Pressure drop for heat flux=200W/cm^2

Reynolds number	Pressure drop from CFD (bar)
390	0.17
590	0.306
790	0.45
990	0.65
1190	0.86

The temperature rise found out from the CFD analysis of rectangular microchannel heat sink with pillars from Figures 6.18, 6.21, 6.24, 6.27, 6.30 and has been tabulated corresponding to a heat flux of 200 W/cm^2 with varying Reynolds number

Table 16: Temperature rise for heat flux=200W/cm^2

Reynolds number	Temperature rise from CFD (K)
390	50
590	39
790	27
990	25.3
1190	24

The pressure drop found out from the CFD analysis of rectangular microchannel heat sink with pillars from Figures 6.31, 6.34, 6.37, 6.40, and 6.43 has been tabulated corresponding to a heat flux of 125 W/cm^2 with varying Reynolds number.

Table 17: Pressure drop for heat flux=125W/cm^2

Reynolds number	Pressure drop from CFD (bar)
390	0.18
590	0.3
790	0.48
990	0.67
1190	0.87

The temperature rise found out from the CFD analysis of rectangular microchannel heat sink with pillars from Figures 6.33, 6.36, 6.39, 6.42 and 6.45 has been tabulated corresponding to a heat flux of 125 W/cm^2 with varying Reynolds number.

Table 18: Temperature rise for heat flux=125W/cm^2

Reynolds number	Temperature rise from CFD (K)
390	33
590	25
790	20
990	16
1190	15

The pressure drop found out from the CFD analysis of rectangular microchannel heat sink with pillars from Figures 6.46, 6.49, 6.52, 6.55 and 6.58 has been tabulated corresponding to a heat flux of 225 W/cm^2 with varying Reynolds number.

Table 19: Pressure drop for heat flux=225W/cm^2

Reynolds number	Pressure drop from CFD (bar)
390	0.18
590	0.309
790	0.47
990	0.66
1190	0.87

The temperature rise found out from the CFD analysis of rectangular microchannel heat sink with pillars from Figures 6.48, 6.51, 6.54, 6.57 and 6.60 has been tabulated corresponding to a heat flux of 125 W/cm^2 with varying Reynolds number.

Table 20: Temperature rise for heat flux=225W/cm^2

Reynolds number	Temperature rise from CFD (K)
390	55
590	45
790	31
990	28
1190	27

CHAPTER 7

CONCLUSIONS

7.1 Conclusion

Based on the study done on straight rectangular microchannel heat sink and microchannel heat sink with pillars, there are numerous conclusions which can be drawn:

(i) The rise in temperature in microchannel with pillars was found out to be more as compared to microcahnnel without pillars.

(ii) As far as the thermal performance is concerned, the microchannel heat sink with pillars was found to be better than straight rectangular microchannel heat sink.

(iii) The microchannel heat sink with pillars suffered losses with respect to pressure penalty due to the presence of pillars along the flow

(iv) Also the presence of pillars brought non uniformities in temperature.

(v) As the bottom heat flux is increased (heat flux taken in this study were 100 W/cm^2, 125 W/cm^2, 200 W/cm^2, 225 W/cm^2 the outlet temperature of water is also getting increased

(vi) As the bottom heat flux is increasing the pressure losses are decreasing along the flow.

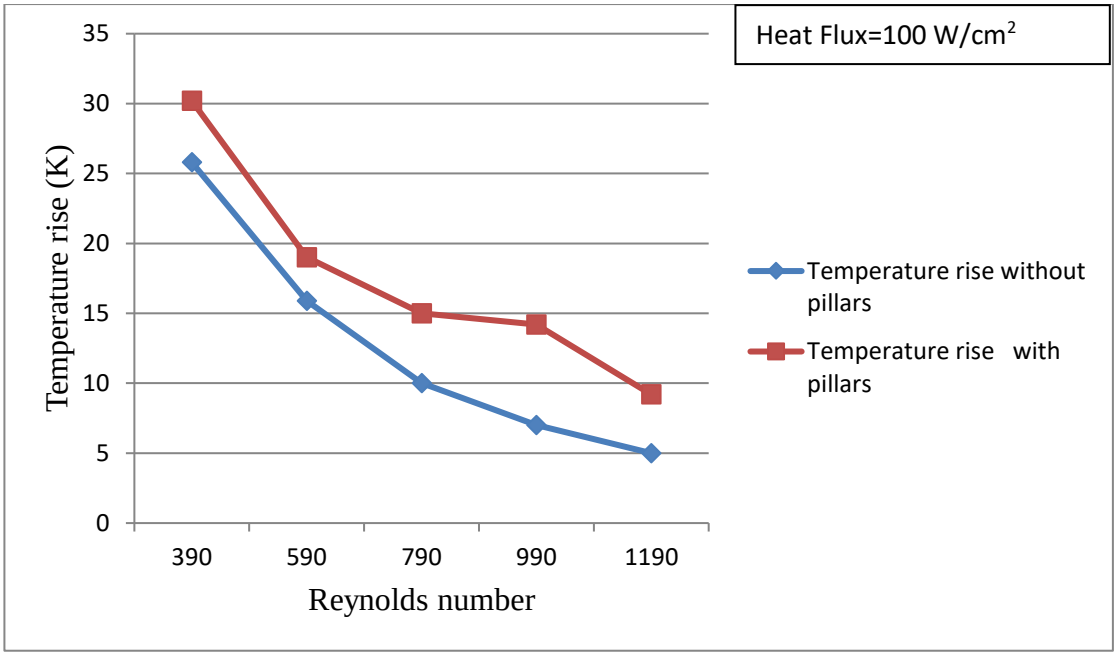

Fig 7.1: Comparison of temperature contours between microchannel heat sink without pillars and with pillars at heat flux of 100 W/cm^2

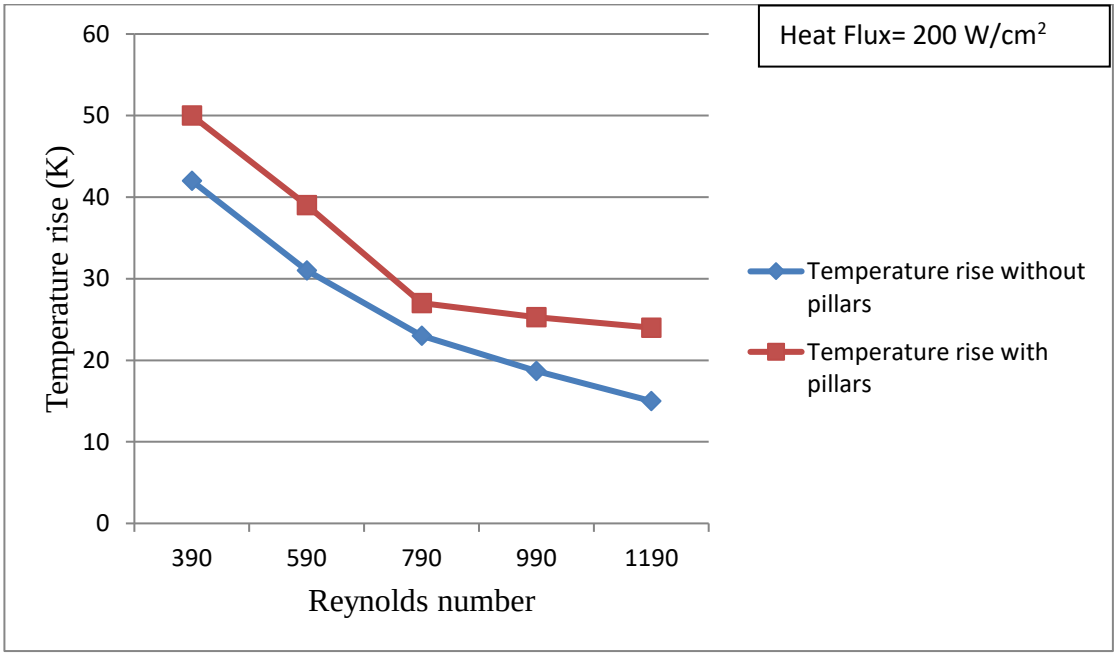

Fig 7.2: Comparison of temperature contours between microchannel heat sink without pillars and with pillars at heat flux of 200 W/cm^2

From Figure 7.1 and 7.2 it is concluded that the microchannel heat sink with pillars has greater temperature rise than simple heat sink without pillars for same values of

heat flux. Although there are more pressure losses but that is compensated by greater values of heat transfer. Thus the overall performance of heat sink with pillars was better than the heat sink without pillars.

7.2Future Scope

(i) Fluids having better thermo physical properties than water can be taken as coolant.

(ii) Nano fluids can be analysed.

(iii) Better shapes other than cylindrical can be analysed.

(iv) Two phase with boiling microchannel heat sink has a great scope. It can be improved by installing jet impingement with direction vectoring.

References

[1] Peng, X. F., & Peterson, G. P. (1996). Convective heat transfer and flow friction for water flow in microchannel structures. International journal of heat and mass transfer, 39(12), 2599-2608.

[2] Anderson J.D., Computational Fluid Dynamic: The Basics with Applications, McGraw-Hill, New York, 1995.

[3] Incropera, DeWitt, Bergman, Lavine, Introduction to Heat transfer, fifth ed., Wiley, New York, 2007.

[4] Liu, D., & Garimella, S. V. (2003, January). Analysis and optimization of the thermal performance of microchannel heat sinks. In ASME 2003 International Electronic Packaging Technical Conference and Exhibition (pp. 557-565). American Society of Mechanical Engineers

[5] Khan, W. A., Culham, J. R., & Yovanovich, M. M. (2005). Optimization of pin-fin heat sinks using entropy generation minimization. IEEE Transactions on Components and Packaging Technologies, 28(2), 247-254.

[6] Naqiuddin, N. H., Saw, L. H., Yew, M. C., Yew, M. K., & Yusof, F. (2017). Numerical study of the geometrically graded micro-channel heat sink for high heat flux application. Energy Procedia, 142, 4016-4021.

[7] Deng, D., Wan, W., Tang, Y., Shao, H., & Huang, Y. (2015). Experimental and numerical study of thermal enhancement in reentrant copper microchannels. International Journal of Heat and Mass Transfer, *91*, 656-670.

[8] CFX-15.0, Solver Theory (2014) ANSYS Inc.

[9] Naqiuddin, N. H., Saw, L. H., Yew, M. C., Yew, M. K., & Yusof, F. (2017). Numerical study of the geometrically graded micro-channel heat sink for high heat flux application. Energy Procedia, 142, 4016-4021.

[10] Vafai, K., & Zhu, L. (1999). Analysis of two-layered micro-channel heat sink concept in electronic cooling. International Journal of Heat and Mass Transfer, 42(12), 2287-2297.

[11] Khan, J. A., Morshed, A. M., & Fang, R. (2014). Towards ultra-compact high heat flux microchannel heat sink. Procedia Engineering, 90, 11-24

[12] Ali, M. Y., Yang, F., Fang, R., Li, C., & Khan, J. (2011, January). Effect of 1D Cu nanostructures on heat transfer characteristics of single phase microchannel

heat sink. In ASME/JSME 2011 8th Thermal Engineering Joint Conference (pp. T10128-T10128). American Society of Mechanical Engineers.

[13] Sung, M. K., & Mudawar, I. (2008). Single-phase hybrid micro-channel/micro-jet impingement cooling. International Journal of Heat and Mass Transfer, 51(17-18), 4342-4352.

[14] Husain, A., Ariz, M., Al-Rawahi, N. Z., & Ansari, M. Z. (2016). Thermal performance analysis of a hybrid micro-channel,-pillar and-jet impingement heat sink. Applied Thermal Engineering, 102, 989-1000.

[15] Armellini, A., Casarsa, L., & Giannattasio, P. (2009). Separated flow structures around a cylindrical obstacle in a narrow channel. Experimental Thermal and Fluid Science, 33(4), 604-619.

[16] Meis, M., Varas, F., Velázquez, A., & Vega, J. M. (2010). Heat transfer enhancement in micro-channels caused by vortex promoters. International Journal of Heat and Mass Transfer, 53(1-3), 29-40.

[17] Wang, Y., Houshmand, F., Elcock, D., & Peles, Y. (2013). Convective heat transfer and mixing enhancement in a microchannel with a pillar. International Journal of Heat and Mass Transfer, 62, 553-561.

[18] Dixit, P., Lin, N., Miao, J., Wong, W. K., & Choon, T. K. (2008). Silicon nanopillars based 3D stacked microchannel heat sinks concept for enhanced heat dissipation applications in MEMS packaging. Sensors and Actuators A: Physical, 141(2), 685-694

[19] Yao, J., Yao, Y., Mason, P. J., & Patel, M. K. (2006, September). Numerical simulation of heat transfer in rectangular microchannel. In European Conference on Computational Fluid Dynamics ECCOMAS CFD, TU Delft, Netherlands

[20] Khameneh, P. M., Mirzaie, I., Pourmahmoud, N., Majidyfar, S., Azizi, S. H., & Andalibi, M. R. (2012). A numerical study of single-phase forced convective heat transfer with flow friction in microchannels. International Journal of Engineering, 25(1), 79-87

[21] Jung, J., Kuo, C. J., Peles, Y., & Amitay, M. (2012). The flow field around a micropillar confined in a microchannel. International Journal of Heat and Fluid Flow, 36, 118-132

[22] Qu, W., & Mudawar, I. (2002). Experimental and numerical study of pressure

drop and heat transfer in a single-phase micro-channel heat sink. International Journal of Heat and Mass Transfer, 45(12), 2549-2565.